© 2014 Prathiba Duvvuri

CORRELATION FOR MEASURED MOLD HEAT FLUX AND CON1D SIMULATIONS FOR FEASIBLE OPERATING CONDITIONS IN THIN-SLAB CONTINUOUS CASTING

BY

PRATHIBA DUVVURI

THESIS

Submitted in partial fulfillment of the requirements
for the degree of Master of Science in Mechanical Engineering
in the Graduate College of the
University of Illinois at Urbana-Champaign, 2014

Urbana, Illinois

Adviser:
Professor Brian G. Thomas

ABSTRACT

In steel continuous casting, controlling heat flux from top of the mold to caster exit is very essential for the production of high quality slabs in a safe environment. Cooling in steel continuous casting comprises primary cooling in mold followed by secondary cooling in spray cooling zone. In this work, various parameters affecting heat flux are studied, first in mold from plant measurements and second in spray cooling zone based on simulations from the numerical model CON1D.

Heat flux in the continuous casting mold is critical to strand surface quality and solidification of the shell. Two years of plant measurements for the thin-slab caster at Nucor Decatur Steel mill and one year of measurements for the thin-slab caster at Nucor Tuscaloosa Steel mill are analyzed to relate average mold heat flux with casting conditions, including casting speed (most important), steel grade, mold powder properties, slab width, superheat, mold level deviation and mold plate thickness. Performing multiple regression analysis, different equations to predict mold heat flux are presented and discussed. The best model based on the combined measurements of both the casters fits better for both the plants than previous equations in the literature.

Secondary cooling of the strand after the mold is used to regulate strand surface temperature profile and metallurgical length. Control of heat removal is critical for the production of high quality slabs without defects and to achieve full solidification in desired region of the machine. To accomplish these, two constraints are considered in this work: First, controlling metallurgical length between straightener and end of containment to avoid stress related cracks and whales respectively; Secondly, to regulate surface temperature profile to avoid unbending in the temperature range of the ductility trough. In this work, using the heat-transfer model CON1D, feasible windows of operation like range of casting speeds and combination of critical speed and superheat satisfying the given constraints are determined for a thin-slab caster at Nucor Decatur steel mill in Alabama. The procedure is repeated for different compositions of steel with different superheats. The prior knowledge of determined feasible windows of operation is very helpful for production of high quality slabs without defects in a safe environment.

For my parents and sisters who have supported me always

ACKNOWLEDGEMENTS

Foremost, I would like to express my sincere gratitude to my research advisor, Professor Brian Thomas for his support, guidance and encouragement throughout this work. His advice, encouragement and feedback have helped me evolve as a researcher and I remain forever grateful for the opportunity to work with him.

I acknowledge financial support from Continuous Casting Consortium at the University of Illinois at Urbana-Champaign. Special thanks to Ron O'Malley, Bob Williams, Neal Ross, Daniel Green and others at Nucor Steel mills for providing valuable discussions and access for plant measurements.

I have been fortunate to have several exceptional people as my colleagues and friends at UIUC. The members of the Metals Processing Simulation Laboratory Bryan Petrus, Lance Hibbeler, Seong-Mook Cho, Rui Liu, Kai Jin, Kun Xu, Younghui Li, A.S.M Jonayat, Mathew Zappulla, Hyunjin Yang and, Aravind Murli have contributed in in their own unique ways to my time here. I thank them, and my other close friends at UIUC for making this an extremely memorable experience. And very special thanks to Bryan Petrus for very valuable discussions and guidance throughout this project.

And finally, my deepest thanks to my parents and sisters, who mean the most to me. Their sacrifices for my education and career are intangible. To them I owe everything I am today.

TABLE OF CONTENTS

LIST OF FIGURES…… vii

LIST OF TABLES…… xi

CHAPTER 1: INTRODUCTION 1

CHAPTER 2: CORRELATION FOR MOLD HEAT FLUX MEASURED IN THIN SLAB CASTING MOLDS 3

2.1. Introduction 3

2.2. Methodology 6

2.2.1. Data extraction 6

2.2.2. Data preprocessing 7

2.2.3. Model development 12

2.2.4. Model evaluation 15

2.2.5. Model verification 16

2.3. Results and discussion 18

2.3.1. Influence of individual variables 20

2.3.2. Model development and evaluation 34

2.4. Conclusions 40

CHAPTER 3: FEASIBLE OPERATING CONDITIONS IN SLAB CONTINUOUS CASTING USING CON1D 41

3.1. Introduction 41

3.2. Methodology 43

3.2.1. Continuous casting model 43

3.2.2. Governing Equation 43

3.2.3. Analytical solution 48

3.2.4. CON1D 49

3.2.5. Validation of CON1D with analytical solution and plant results 53

3.2.6. Thin slab caster at Nucor Decatur 57
3.2.7. Procedure 59
3.3. Results and Discussion 61
3.3.1. Feasible range of casting speeds 61
3.3.2. Critical casting speeds for critical super heats 64
3.3.3. Investigating feasible secondary water spray patterns 66
3.4. Conclusions 72
CHAPTER 4: CONCLUSIONS AND FUTURE WORK 73
REFERENCES 75
APPENDIX A: MATLAB CODE FOR REGRESSION ANALYSIS 81
APPENDIX B: SIGNIFICANT DIGITS OF THE FITTING PARAMETERS FROM REGRESSION ANALYSIS 93
APPENDIX C: ANALYTICAL SOLUTION OF THE CON1D GOVERNING EQUATION 94

LIST OF FIGURES

Figure 1.1 Schematic of continuous casting of steel……. 1

Figure 2.1 Box plots and density plots presenting data distribution of casting variables for fixed face of Decatur caster for two years …….. 9

Figure 2.2 Box plots and density plots presenting data distribution of casting variables for fixed face of Tuscaloosa caster for a year …….. 10

Figure 2.3 Increase in heat flux with water flow rate…….. 17

Figure 2.4 Variation in heat flux with rise in water temperature……. 17

Figure 2.5 Variation in heat flux with mold width……... 17

Figure 2.6 Regression with only water flow rate as a variable. AIC = -3730…….. 17

Figure 2.7 Regression with water flow rate and rise in temperature as variables. AIC = -3920……. 17

Figure 2.8 Regression with all 3 variables. AIC = -14337. Perfect match of predicted heat flux with actual heat flux……. 17

Figure 2.9 Total of average heat flux on two narrow faces versus total of average heat flux on two wide faces of Decatur caster…….. 18

Figure 2.10 Comparison of heat flux between loose and fixed sides of wide face of Decatur caster…… 19

Figure 2.11 Comparison of heat flux between loose and fixed sides of wide face of Tuscaloosa caster…….. 19

Figure 2.12 Average heat flux plotted against mold width after applying primary filters……. 20

Figure 2.13 Variation of casting speed with mold width after applying primary filters.. 20

Figure 2.14 Variation of heat flux with mold with after applying secondary filters…. 20

Figure 2.15 Increase in mold average heat flux with increase in casting speed for Decatur caster…… 22

Figure 2.16 Increase in mold average heat flux with increase in casting speed for Tuscaloosa caster…….. 22

Figure 2.17 Effect of carbon on average heat flux at Decatur caster……... 23

Figure 2.18 Effect of carbon on average heat flux at Tuscaloosa caster…….. 24

Figure 2.19 Average heat flux decreases as break point temperature of mold powder increases at Decatur caster…… 25

Figure 2.20 Average heat flux decreases as break point temperature of mold powder increases for Tuscaloosa caster……. 25

Figure 2.21 Variation of heat flux with viscosity of mold powder for Decatur caster… 26

Figure 2.22 Variation of heat flux with viscosity of mold powder for Tuscaloosa caster……. 26

Figure 2.23 Influence of mold width on heat flux for Decatur caster…….. 27

Figure 2.24 Influence of mold width on heat flux for Tuscaloosa caster…… 27

Figure 2.25 Effect of super heat on heat flux for Decatur caster……. 29

Figure 2.26 Effect of super heat on heat flux for Tuscaloosa caster…… 29

Figure 2.27 Variation of heat flux with mold level standard deviations at Nucor caster 30

Figure 2.28 Variation of heat flux with average mold level standard deviations at Tuscaloosa caster…….. 31

Figure 2.29 Little effect of mold plate thickness on mold heat flux at Decatur caster… 32

Figure 2.30 Little effect of mold plate thickness on mold heat flux at Tuscaloosa caster……..……... 32

Figure 2.31. Slight decrease in heat flux with heats on mold of campaign 1……... 33

Figure 2.32 Effect not clearly seen for campaign 2……. 33

Figure 2.33 Slight decrease in heat flux with heats on mold of campaign 3…….……... 33

Figure 2.34 Slight decrease in heat flux with heats on mold of campaign 4….……... 33

Figure 2.35 Slight decrease in heat flux with heats on mold of campaign 1…….……... 33

Figure 2.36 Effect not clearly seen for campaign 2……. 33

Figure 2.37 Slight decrease in heat flux with heats on mold of campaign 3……... 33

Figure 2.38 Slight decrease in heat flux with heats on mold of campaign 4….……... 33

Figure 2.39 RSS measure of developed models with varying number of casting variables on Nucor database…….. 36

Figure 2.40 Performance of different predicting equations on Decatur caster…….…… 38

Figure 2.41 Performance of different predicting equations on Tuscaloosa caster…… 39

Figure 3.1 Control volume for heat balance……. 43

Figure 3.2 Simulation domain: Solidifying slice moving along the length of the caster from meniscus to the torch cut off point……... 50

Figure 3.3 Schematic of heat transfer in spray zones…… 51

Figure 3.4 Validation of CON1D solution with analytical solution: Surface temperature of 1000°C is given as input……... 55

Figure 3.5 Validation of CON1D solution with analytical solution: Heat flux for a surface temperature of 1000°C as input…… 55

Figure 3.6 Validation of CON1D solution with analytical solution: Shell thickness of strand as output……. 56

Figure 3.7 2004 whale case: CON1D predicting metallurgical length beyond the end of caster…… 57

Figure 3.8 2006 whale case: CON1D predicting metallurgical length much beyond the end of caster…….. 57

Figure 3.9 Schematic of Nucor Decatur caster…… …… 58

Figure 3.10 Profiles at limits of feasible casting speed range of 2.4 to 4.0 m/min with constraint 1 (metallurgical length in the desired range)…… 62

Figure 3.11 Casting speed can be varied from 3.75 to 2.45 m/min satisfying 2 constraints……. 63

Figure 3.12 Range of casting speeds for low, peritectic and high carbon steels…….. 64

Figure 3.13 Maximum casting speed at different superheats satisfying given constraints……. 65

Figure 3.14 At a given casting speed, higher pour temperatures can be employed for high carbon steels compared to low carbon steels…… 66

Figure 3.15 Two methods to change spray patterns in the secondary cooling zones…... 67

Figure 3.16 Caster profiles with spray pattern 1 at a casting speed of 3.3 m/min ……... 68

Figure 3.17 Caster profiles with spray pattern 1 modified using Method 1, with minimum water flow rate in zone 2 ……. 68

Figure 3.18 Caster profiles with spray pattern 1 modified using Method 1, with maximum water flow rate in zone 2…….. 69

Figure 3.19 Caster profiles with spray pattern 1 modified using Method 2, with water flow rate in zone 2 as 40% of that of standard in zone 2…….. 70

Figure 3.20 Caster profiles with spray pattern 1 modified using Method 2, with minimum water flow rate in zone 2…….. 70

Figure 3.21 Caster profiles with spray pattern 1 modified using Method 2, with maximum water flow rate in zone 2…….. 71

Figure 3.22 Caster profiles with spray pattern 1 modified using Method 2, with 200% of maximum water flow rate in zone 2……. 71

LIST OF TABLES

Table I Primary filters for casting variables: Decatur caster……..….... 8

Table II Decatur caster: Operating conditions and secondary filters for casting variables…… 11

Table III Tuscaloosa caster: Operating conditions and secondary filters for casting variables…… 11

Table IV Mold powder properties at Decatur Caster…….…….. 12

Table V Mold powder properties at Tuscaloosa Caster…….…….. 12

Table VI Different equations with statistical estimates*…….……. 34

Table VII Material properties and process dimensions for scaling…….. 47

Table VIII Input parameters for validation of CON1D solution with analytical solution…….. 54

Table IX Different compositions considered in the study…… 60

Table X Optimum water flow rates in secondary cooling zone……... 63

Table XI Spray pattern 1 for a casting speed of 3.3 m/min at Nucor Decatur caster….. 67

CHAPTER 1: INTRODUCTION

Steel is extensively used in the construction of roads, railways, buildings, and other infrastructure which reflect the economic status of a country. It is known for its properties like high tensile strength and yield strength, good durability, great formability and low cost. Steel consumption expanded extensively with the addition of other alloy elements to get desired properties and with the development of efficient production methods.

Continuous casting refers to the process of solidification of hot molten liquid on a continuous basis. Owing to its quality, productivity and cost effectiveness compared to that of traditional conventional casting, continuous casting is being extensively employed in many metal production processes[1]. Especially, this has revolutionized the steel production.

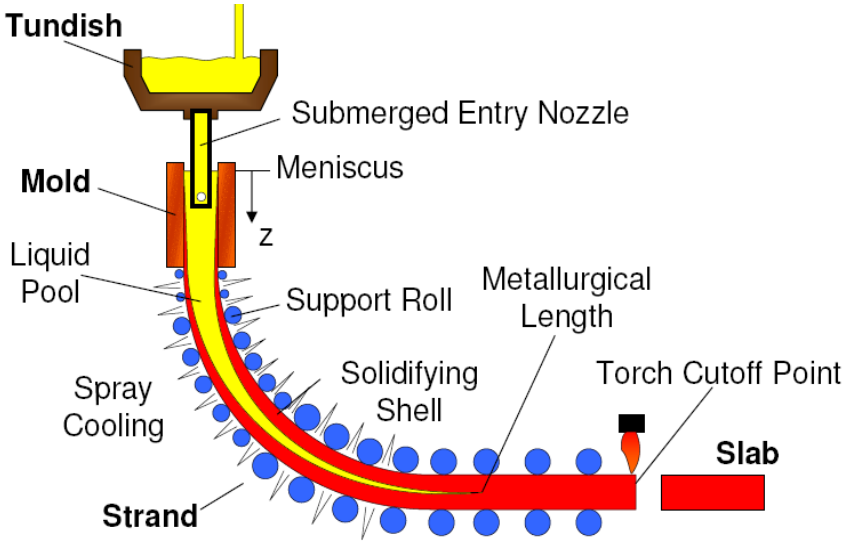

Figure 1.1 Schematic of continuous casting of steel

The schematic of steel continuous casting process is shown in Figure 1.1. Molten steel from tundish is poured into vertically oscillating, bottom-less copper mold through submerged entry nozzle. A thin solid shell withstanding the ferrostatic pressure of the inner liquid steel starts developing against the water cooled walls of the mold and this comprises primary cooling. Then the strand at the mold exit is drawn and supported by a series of power driven and supporting rolls in the water spray cooling zone which comprises secondary cooling.

Both primary cooling and secondary cooling play a vital role in determining strand surface quality, casting productivity and operating safety in preventing whales and breakouts. Thus

heat flux is critical which determines solidification rate, formation of grain structure, properties of steel, quality of steel etc., Heat flux is influenced by a number of factors like - mold design and spray zone design down the caster; operating conditions like casting speed, spray water flow rate; casting conditions like steel composition, mold powder properties, etc.,

In the first part of this work, as Chapter 2, mold heat transfer is studied from plant measurements from different thin slab casters. Most of the previous studies on mold heat transfer are analytical and computational. Correlation of mold heat transfer from actual measurements helps in better understanding of the influence of various casting conditions considered in the study. This knowledge helps in predetermining the casting conditions for a desired heat flux profile.

In the second part which comprises Chapter 3, well-known validated CON1D model is employed to determine the feasible operating windows of casting speed and super heat by controlling water sprays in the secondary cooling zone. In case of high demand of steel, for a given caster, only certain maximum speed can be achieved based on its design. Also, in case of very low demand, plants choose to operate at certain low speeds instead of completely stopping and restarting the caster owing to startup difficulties and time consumption. In these cases, predetermining the feasible operating windows for a given caster design can be very helpful to regulate the operating conditions for the optimum production of high quality slabs in a safe environment. Further, the feasibility of changing the standard spray patterns for satisfying the constraints is investigated.

As steel continuous casting is a complex process with multi-coupled phenomena, understanding the influence of various casting variables and process parameters on heat flux is critical for optimizing the casting process for production of high quality slabs in safe surroundings. The objective of controlling heat flux is achieved in this work by analyzing mold heat flux from plant measurements and spray secondary cooling from CON1D numerical simulations.

CHAPTER 2: CORRELATION FOR MOLD HEAT FLUX MEASURED IN THIN SLAB CASTING MOLDS

2.1. Introduction

Maintaining appropriate heat transfer in the steel continuous casting mold is critical to strand surface quality [2-14], mold life [6, 15-18], casting productivity [3, 14-16] and operating safety in preventing breakouts [8, 14, 19-23].

Owing to its importance, previous studies focused on investigating the effect of various casting variables on mold behavior and its influence on quality, safety etc. Mahapatra et al [2, 3] analyzed the influence of casting speed, steel carbon content, cooling water configuration, depth of submerged entry nozzle, mold flux and copper plate thickness at meniscus on mold heat flux profile and quality of slabs from oscillation mark studies. Studies by Billany et al [4] and Hiraki et al [5] attributed surface cracking of slabs to the variations of mold heat transfer primarily influenced by mold powder properties. Previous work [7, 9-11, 14, 24] investigated the effect of mold powder properties, superheat and oscillation configurations on characteristics of oscillation marks and hooks which influence the surface quality of slabs using a combination of mathematical models and plant measurements. Bryant Ho [25] quantified the effect of different process variables on mold heat transfer using interfacial heat transfer model. Kumar et. al. [13] developed strategies for detection of defect deformations based on measurements of thermocouples installed in the mold wall and level fluctuations for billet continuous casting. Ya Meng et al [14] analyzed the effect of casting speed, lubrication, mold taper and carried out crack formation and breakout analysis based on mold heat flux profiles using the Con1D model [26]. Santillana et al [27] studied the effect of casting powder and mold plate thickness on mold heat transfer in a thin slab caster, using plant measurements and the CON1D model to simulate temperature in the strand and mold.

As the mold is a critical component whose surface quality and temperature distribution determine the quality of slabs, some researchers investigated various mold designs and optimized operating conditions to enhance mold life [6, 15-18]. Peng et al [15] suggested uniform distribution of temperature with modified mold design in terms of cooling water channels configuration and coating layers to increase life of the mold, productivity as well as quality of slabs. Park et al [18] investigated the formation of surface cracks on mold face of a

thin-slab caster using metallographic studies and mathematical models and suggested ways to avoid cracks to improve mold life.

As breakouts impose a serious safety concern in addition to loss of production time and cost, detection of breakouts are proposed and investigated from mold instrumentation based on temperature measurements across the mold profile [8, 13, 19-23]. Emling et al [19] proposed that breakouts can be predicted if total mold heat removal is less than the minimum heat criterion for adequate shell thickness and suggested need for alternate techniques in view of insufficient response time. Xia et al [8] suggested that breakouts can be detected based on variations of mold integral heat flux and temperature profile in the copper plates. Jin et al [21] developed slab caster real time breakout alarm system based on artificial intelligence and mathematical models.

Considerable research on mold heat transfer has been based on computational modeling and numerical simulations with actual plant measurements employed at times for validation and calibration. Brimacombe et al [28-31]introduced advanced computational models to investigate heat transfer and solidification in the mold. Many relationships [32-37] to quantify mold heat transfer are based on plant trials at different plants, and are expressed as a function of residence time, t, spent in the mold, defined as casting speed divided by working mold length.

$$Q(MW/m^2) = At^n \tag{1}$$

where Q is the average mold heat flux, and A is an empirical constant. This equation can be rewritten as

$$Q(MW/m^2) = k \cdot V_c(m/\min)^n \tag{2}$$

Here $k = A.Z_M^{-n}$ where Z_M is working mold length. In previous work, n is reported from 0.33 [36] to 0.6 [33] with typical value of 0.5.

Based on measurements, Li et al[36] developed an empirical formula for average heat flux as a function of residence time that approximated many previous plant measurements, and differentiated it to quantify instantaneous heat flux down the mold length. Based on casting

speed measurements for a 700mm mold, Lorento [37] found k of 1.4 MW/m^2 $min^{-0.5}$ $m^{-0.5}$ and n of 0.5.

However, with improvements in mold instrumentation and data collection, plant measurements can be extensively used to investigate these phenomena in actual operation [8, 9, 23, 38]. Cicutti et al [23] developed an equation to predict mold heat flux (averaged over the hot face) as a function of casting speed, steel composition and mold powder properties by performing multiple regression of database with 2000 heats collected from a conventional slab caster producing low and medium carbon steels. Xia et al [8] investigated the dependence of integral heat flux on speed, steel composition and powder properties, and used the results for quality control and breakout analysis. Hecht et al [9] studied the effect of super heat, oscillation mark depth and mold powder consumption in addition to the effect of steel composition on mold heat removal, and investigated surface quality of crack sensitive steel grades as a function of mold heat flux on a 400 mm thick slab caster. Thin slab casters with a different heat flux profile from that of conventional slab casters [3, 9, 23] received relatively less attention. Park et al [18]and Wen Yang et al [38] studied the effect of casting speed, super heat and mold level fluctuations on a CSP thin slab caster.

To analyze large datasets of plant measurements, data analysis techniques are now available to identify relationships between process variables and to develop models for predicting process outcomes. In continuous casting of steel, there are significant opportunities for comprehensive study of plant measurements of the wide range of casting variables and their relationship to safety, quality, and production goals. This work applies fundamental data analysis methods to predict mold heat flux in a thin slab caster as a function of casting conditions, based on extensive plant measurements of over 2 years at two different steel plants. The influence of each of the casting variables on mold heat flux is analyzed for individual casters. Combining the measurements of both the castes, different empirical equations to predict mold heat flux are developed performing nonlinear multiple regression analysis. Based on statistical analysis, the models are evaluated on individual casters and compared with a previous equation in the literature. The best models are presented, and can be applied to predict mold heat transfer of other casters to understand and improve the continuous casting process.

2.2. Methodology

The present work investigates mold heat transfer in steel continuous casting based on two years of extensive plant measurements on two thin slab casters at Nucor Steel, in Decatur, AL and one year of data at Nucor Tuscaloosa, AL. The Nucor Decatur steel mill is a thin slab caster with a slab thickness of 90 mm, and working mold length of ~850.0 mm. The Nucor Tuscaloosa slab caster is 136.1 mm thick and has a working mold length of ~ 812.8 mm. Large data bases of measurements are maintained for every heat of steel cast in both casters, most recorded every 5 seconds.

The goal of the present work is to utilize these databases to investigate the relationships between various process variables and heat transfer in slab-casting molds. First, the effect of individual casting conditions on mold heat flux are studied by selectively filtering the data to maintain constant casting conditions. Then, a model to predict mold heat flux as a function of casting variables is developed using nonlinear multiple regression. This is accomplished in four steps: data extraction, data pre-processing, model development, and evaluating the models.

2.2.1. Data extraction

Since the molds of continuous casters are constantly cooled by water, the spatially-averaged heat flux extracted from a mold hot face (hereafter simply called mold heat flux) at a given time can be calculated from measurements of the volumetric flow rate and temperature rise of the cooling water as

$$Q = \frac{G \cdot \rho_w \cdot C_w \cdot \Delta T}{10^6 \cdot 60 \cdot W \cdot Z} = \frac{6.794 \cdot 10^{-5} \cdot G \cdot \Delta T}{W \cdot Z} \tag{3}$$

where Q is the heat flux (MW/m^2), G is the flow rate (l/min), ρ_w is the density (kg/l), C_w is the specific heat capacity (J/kg °C), and ΔT is the temperature rise (°C) of the cooling water for a mold face with working (i.e. in contact with steel) length Z (m) and strand width W (m).

Measurement data at the Nucor mills is stored in the Level II database. Different process variables pertaining to a particular heat are stored in different tables: composition in one table;

mold powder properties in another table; superheat and time of measurement in a third table etc,. Structured Query Language (SQL) is employed to extract the required data, which is located in different tables of the database. The query utilizes appropriate candidate keys (primary columns such as heat number) to cross-reference the data from the different tables and to reduce the run time.

This work analyzed 16,000 heats for over 2 years at the Decatur caster and 9,000 heats over an year at the Tuscaloosa caster, covering a wide range of operating conditions. A heat at these steel mills typically takes ~50 minutes to cast. To characterize the measurements of casting conditions during each heat, the measured data were averaged over a 10 minute interval, starting 20 minutes after ladle open so as to exclude transient effects during ladle changes. Heats that did not last this long, for example due to a breakout occurring or mold changes, were not included. Data at every 5 seconds were extracted using SQL code and the average, maximum, and minimum of the 120 measurements over the 10 minute interval were computed and saved. In addition, the standard deviation was calculated for the mold level. The mold powder properties are reported by plant metallurgists, including the breakpoint temperature (which is considered a measure of the crystallization or melting temperature), and the viscosity. The final version of the query contains 150 lines of SQL code and takes less than 50 seconds to collect 2 years of Decatur data.

2.2.2. Data preprocessing

Pre-processing is a very crucial step in data modeling, in order to remove incomplete, noisy and inconsistent data that would distort the final model. To restrict the study to heats with steady casting conditions and reliable measurements, “primary filters” were applied, which required each selected heat to satisfy the conditions summarized in Table I for Decatur and

Tuscaloosa casters. In the table, "variation" is the difference between the maximum and minimum measured value during the 10 minute interval selected for each heat.

Table I Primary filters for casting variables: Decatur caster

Casting variable	Filter criterion	Decatur caster Remaining heats (of 14135 total)	Tuscaloosa caster Remaining heats (of 9729 total)
Constant casting speed	variation in $V_c \leq 2$ mm/s	13137	8060
Mold powder type	excluding trial powders	13125	7981
Constant mold width	variation in $W \leq 1$ mm	10723	6173
Realistic super heat	$0 \leq s \leq 50$ °C	10558	5704
Realistic mold level standard deviation	$l \leq 3$ mm	10556	5704

- Width Variation ≤ 10 mm is considered for Tuscaloosa caster to study more heats

Box plots and histograms depicting density of measurements for the collected data are shown in Figure 2.1 for Decatur caster and Figure 2.2 for Tuscaloosa caster, to visualize the distribution of values for each variable. To investigate the influence of each casting condition individually, by keeping the other conditions as constant as possible, a secondary filter is applied to every variable except for the one under investigation. A good secondary filter for a given variable (when not under individual investigation) should contain a large number of heats, with all measurements falling within a narrow range.

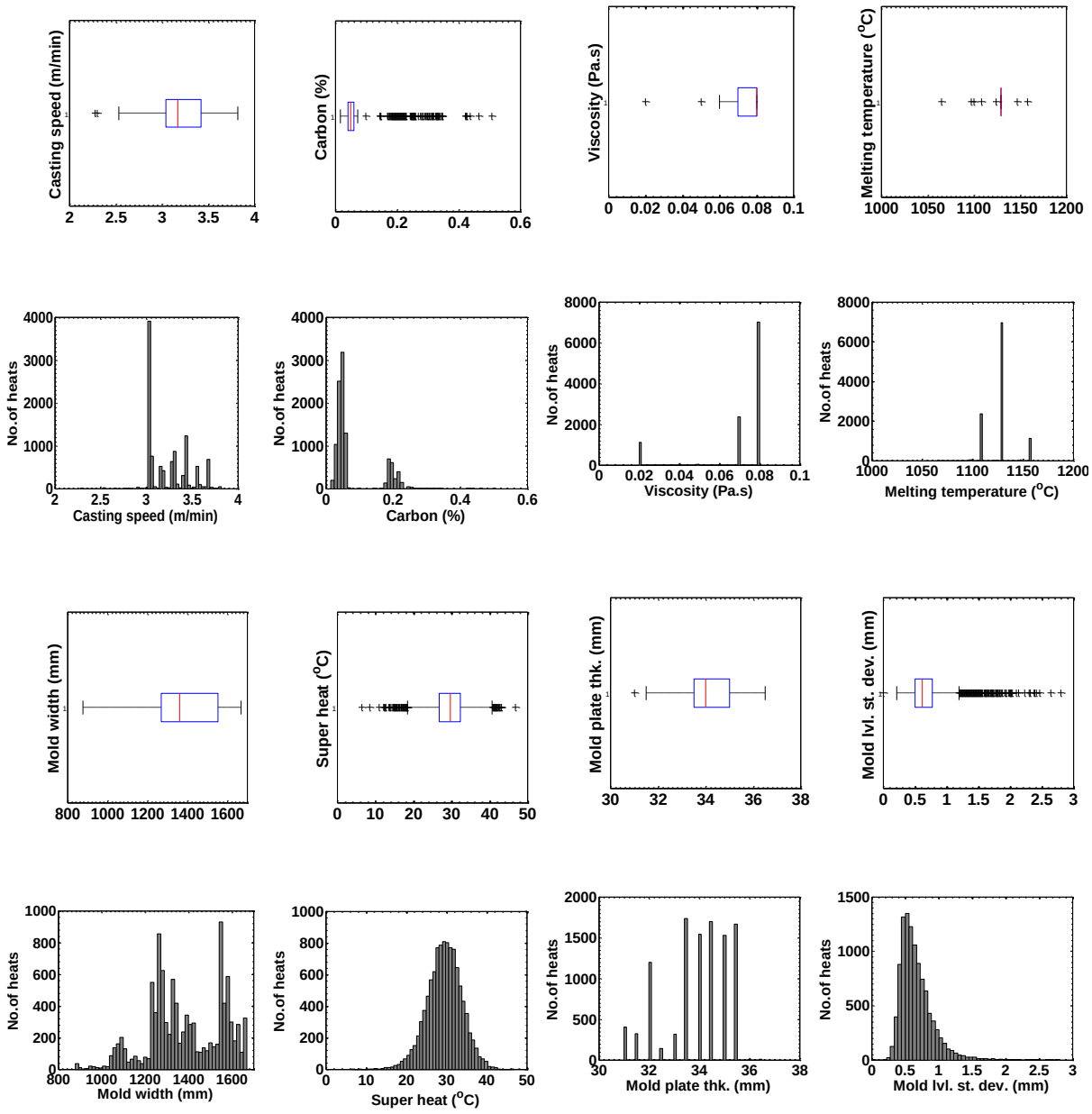

Figure 2.1. Box plots and density plots presenting data distribution of casting variables for fixed face of Decatur caster for two years

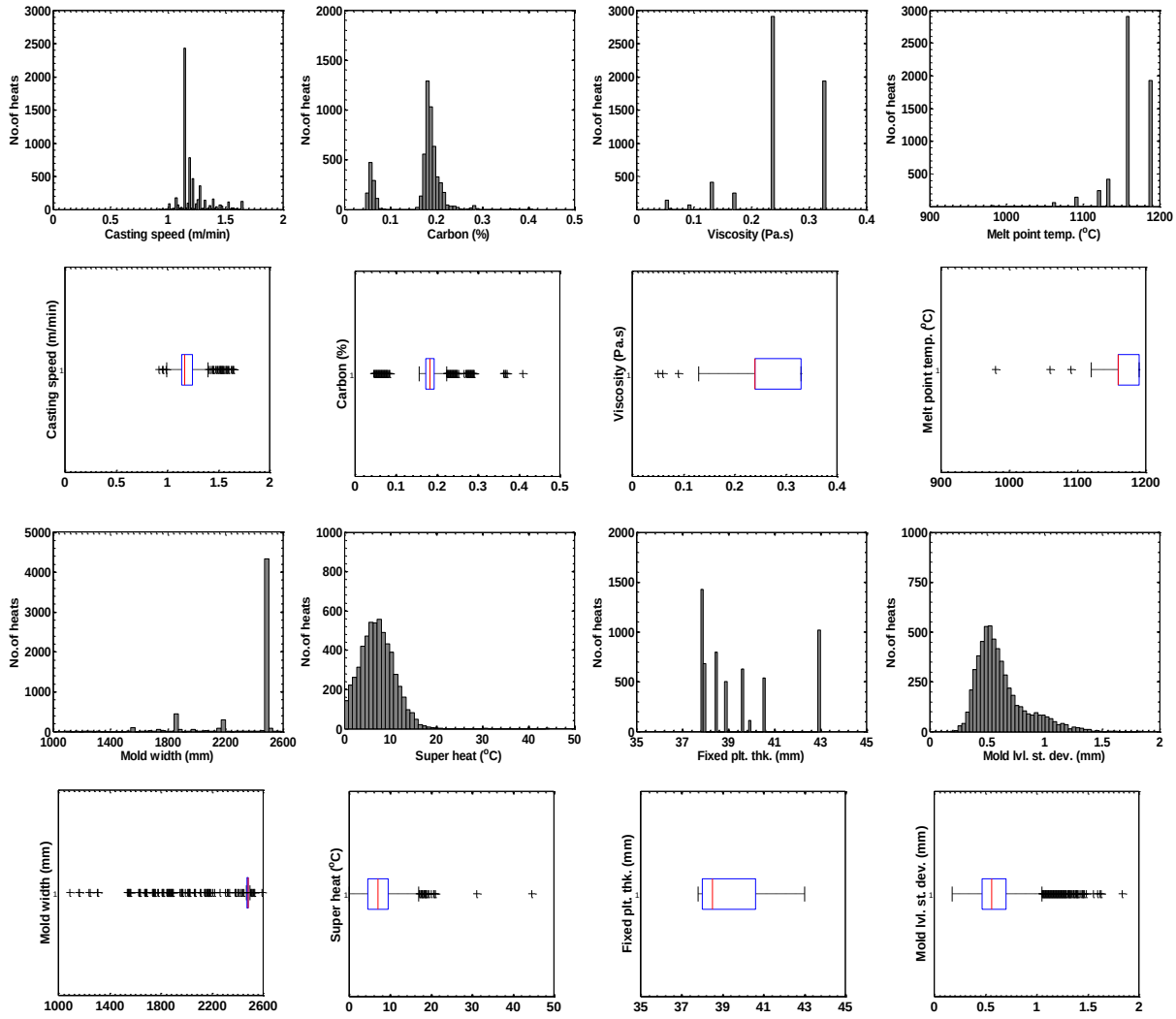

Figure 2.2. Box plots and density plots presenting data distribution of casting variables for fixed face of Tuscaloosa caster for a year

The secondary filters used in this work are given in Table II for the Decatur caster and Table III for Tuscaloosa. The properties of the casting powders are tabulated in Tables IV and V for Decatur and Tuscaloosa respectively.

Table II. Decatur caster: Operating conditions and secondary filters for casting variables

Casting variable	Measurement range (after primary filters)	Range for secondary filter
Casting speed (m/min)	2.27 - 3.71	3.02 - 3.05
Carbon percent (%)	0.015 - 0.507	0.035 - 0.055
Mold powder	see Table VI	D4
Mold width (mm)	878 - 1669	1540 - 1590
Super heat (°C)	6.0 – 47.0	27.0 – 33.0
Mold plate thickness (mm)	31.0 - 36.5	33.0 – 34.0
Mold level standard deviation (mm)	0.00 - 2.80	0.45 - 0.62

Table III. Tuscaloosa caster: Operating conditions and secondary filters for casting variables

Casting variable	Measurement range (after primary filters)	Range for secondary filter
Casting speed (m/min)	0.92 - 1.65	1.14 - 1.15
Carbon percent (%)	0.046 - 0.410	0.177 - 0.191
Mold powder	See Table V	T4
Mold width (mm)	1091 - 2591	2470 - 2500
Super heat (°C)	0.0 – 45.0	5.0 – 8.0
Mold plate thickness (mm)	37.8 - 43	42.5 - 43.5
Mold level standard deviation (mm)	0.18 - 1.84	0.48 - 0.54

Table IV Mold powder properties at Decatur Caster

		Viscosity (Pa-s)	Break point temperature (°C)
D1	1.09	0.07	1108
T42	1.09	0.06	1124
D3	1.05	0.08	1147
D4	1.00	0.08	1129
D5	1.33	0.02	1158
D6	1.25	0.04	1127
D7	1.25	0.04	1128

Table V. Mold powder properties at Tuscaloosa Caster

		Viscosity (Pa-s)	Break point temperature (°C)
T1	1.05	0.05	1143
T2	0.94	0.06	1083
T3	1.23	0.13	1216
T4	1.2	0.24	1194
T5	1.25	0.21	1205
T6	1.05	0.05	1147
T7	0.83	0.09	1067

*Viscosities of mold powder are calculated at 1300°C

2.2.3. Model development

The model development step starts by assuming a general structure for equations to predict mold heat flux as a function of casting variables. In general, the data analysis tools can determine parameters for the model that best fit the measurements, but not the structure of the

model. For this work, the structure was partly based on an equation developed by Cicutti [23], stated in the literature:

$$Q = 4.63 \cdot 10^6 \cdot \mu^{-0.09} \cdot T_{Flow}^{-1.19} \cdot V_c^{0.47} \cdot \left(1 - 0.152 \cdot \exp\left(-\left(\frac{0.107 - \%C}{0.027} \right)^2 \right) \right) \quad (4)$$

where Q is the mold heat flux (kW/m^2), μ is the mold slag viscosity (Pa-s), T_{Flow} is the "melting temperature" of the powder (°C), V_c is the casting speed (m/min), and %C is the carbon amount (weight %). The expression inside parentheses accounts for the known drop in mold heat flux for peritectic steels. The predicted drop in heat flux is a bell-shaped (Gaussian) curve over Carbon content. The bell curve has a minimum at 0.107 weight % Carbon, where it subtracts a fraction of 0.152 (15.2 %) of the heat flux relative to a non-peritectic steel under the same conditions. The value 0.027 controls the width of the heat flux drop.

The current work extends the Cicutti equation to include other parameters according to the following structure:

$$Q = x_1 \cdot V_c^{x_2} \cdot \mu^{x_3} \cdot T_{break}^{x_4} \cdot W^{x_5} \cdot s^{x_6} \cdot t^{x_7} \cdot l^{x_8} \left(1 - 0.152 \cdot \exp\left(-x_9 \left(\frac{\left(\frac{C_A + C_B}{2} \right) - \%C}{C_B - C_A} \right)^2 \right) \right) \quad (5)$$

where Q is the predicted mold heat flux (MW/m^2). The fitting parameters x_i, i = 1, 2, .., 9 are chosen to best match the measurements. The variables, or measurements used as a basis for the prediction, are casting speed V_c (m/min), mold slag viscosity μ (Pa-s), break point temperature of the powder T_{break} (°C), width of the slab W (mm) , temperature superheat s (°C), thickness of the mold plate t (mm), standard deviation of the mold level l (mm), and carbon amount %C (weight %). Rather than using Cicutti's expression to incorporate the heat flux drop for peritectic steels, Equation 5 gives this drop as a function of %C, including the effects of other alloys from the relation of Blazek et al [39]. Specifically, C_A and C_B determine the range of peritectic steels depending upon the measured composition of each heat as follows.

$$C_A = 0.0896 + 0.0458Al - 0.0205Mn - 0.0077Si + 0.0223Al^2 - 0.0239Ni + 0.0106Mo + 0.0134V - 0.0032Cr + 0.00059Cr^2 + 0.0197W \quad (6)$$

$$C_B = 0.1967 + 0.0036Al - 0.0316Mn - 0.0103Si + 0.1411Al^2 + 0.05Al \cdot Si - 0.0401Ni + 0.03255Mo + 0.0603V + 0.0024Cr + 0.00142Cr^2 - 0.00059Cr \cdot Ni + 0.0266W \quad (7)$$

where Al , Mn , Si , etc., are the element weight percentages of the steel composition in each heat. Then, non-linear regression analysis is performed in MATLAB, as given in Appendix A, to find the best fit values for the parameters that minimize the error (specifically the sum of squares of the differences between each measured heat flux and the predicted value from Equation 5) comprising 9022 and 3531 heats respectively. Of the total heats remained from primary filters, more filters are applied like heats with unknown mold hot face thickness to Decatur caster and incredible mold powder property sources to Tuscaloosa caster to arrive at the above number of heats considered for regression analysis.

The minimization is performed using *fminsearch* function in MATLAB which employs the Nelder-Mead Simplex algorithm [40]. This function is sensitive to the initial guess. Therefore, to determine a good initial guess, a linear regression is first performed in Microsoft Excel, by taking the logarithm to make Equation 5 linear. Then, nonlinear regression is performed in MATLAB for 100 initial guesses randomly distributed in the neighborhood of the linear best fit.

Initially, the significance of each of the eight casting variables included in Equation 5 on mold heat flux is not clear. So, to find the best model, this analysis is performed with different combinations of casting variables. With eight variables, there are 256 different potential models, considering all possible combinations. Rather than test every combination, stepwise forward selection is used. Models are developed in a sequence, beginning with a simple model with only one, most-important, casting variable. In each subsequent model, the one new casting variable that results in least RSS error is added into the equation [41].

2.2.4. Model evaluation

Among the different models from this stepwise forward selection, the best model is selected, accounting both for accuracy and simplicity, based on two statistical measures: the residual sum of squares (RSS) and Akaike Information Criterion (AIC) [42].

The residual sum of squares (RSS) is a measure of discrepancy between the data and estimation model. It is the sum of squares of the differences between the observed and predicted values.

$$RSS = \sum_{i=1}^{n} (y_i - f(x_i))^2 \tag{8}$$

where y_i is the observed value and $f(x_i)$ is the model predicted value, and n is the total number of observations. A smaller RSS indicates a better fit.

The coefficient of determination (R^2) is the ratio of explained variation to the total variation of the data and expresses the goodness of fit of a regression as follows.

$$R^2 = 1 - \frac{\sum_{i=1}^{n} (y_i - f(x_i))^2}{\sum_{i=1}^{n} (y_i - \bar{y})^2}, \quad \bar{y} = \frac{1}{n} \sum_{i=1}^{n} y_i \tag{9}$$

R^2 always lies between 0 and 1, with 1 indicating a perfect prediction of all data, and 0 indicating extreme variability. In this work, it is only employed to examine the relationship between mold heat flux and individual casting variables.

It is always possible to decrease RSS by increasing the number of variables in the model, even if the variable does not really contribute to the accuracy of the prediction. Other statistical measures, such as AIC, which penalizes adding insignificant variables, are better for comparing different model structures.

The Akaike Information Criterion (AIC) is a measure of the relative quality of a statistical model. The AIC for a model is

$$AIC = -2L + 2k \tag{10}$$

where L is the maximum likelihood of the measured data occurring given the "best" possible set of parameters, and k is the number of parameters. Using RSS as a measurement of the total error, the maximum likelihood corresponds to the smallest possible RSS, i.e. with the best fit parameters. Using this minimum RSS, the maximum log-likelihood value can be calculated as

$$L = -\frac{n}{2}\ln\left(\frac{RSS}{n}\right) \tag{11}$$

AIC measures the trade-off between the goodness of fit and complexity of the model. A smaller AIC indicates a better model.

The models are developed for Decatur and Tuscaloosa casters individually and combining measurements of both casters and are treated as training data. The developed models are then tested on Decatur and Tuscaloosa casters. The performance of the optimum model to predict mold heat flux is then compared to the Cicutti prediction (Equation 4).

2.2.5. Model verification

Before developing a practical model with the complete database, the procedure for choosing best fit parameters described in the previous section is verified with a known equation, calculating the average heat flux for 1000 heats of Decatur caster assuming a mold heat flux model form:

$$Q = x_1 \cdot G^{x_2} \cdot \Delta T^{x_3} \cdot W^{x_4} \tag{12}$$

where G is the water flow rate (l/min), ΔT is the rise in water temperature (°C) , and W is the mold width (m).

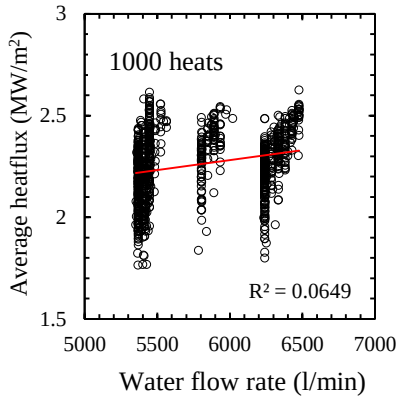

Figure 2.3. Increase in heat flux with water flow rate

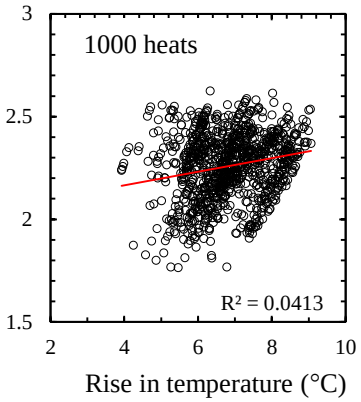

Figure 2.4. Variation in heat flux with rise in water temperature

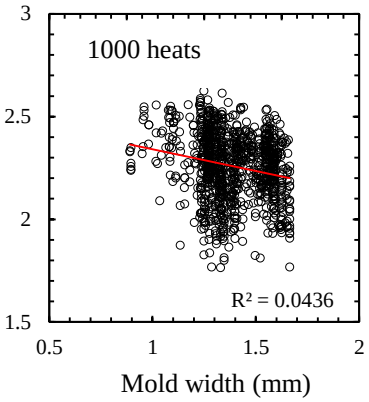

Figure 2.5. Variation in heat flux with mold width

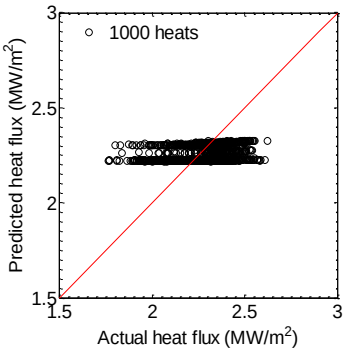

Figure 2.6. Regression with only water flow rate as a variable. AIC = -3730

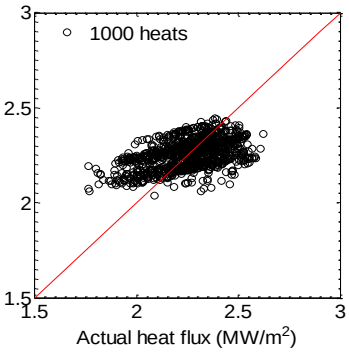

Figure 2.7. Regression with water flow rate and rise in temperature as variables. AIC = -3920

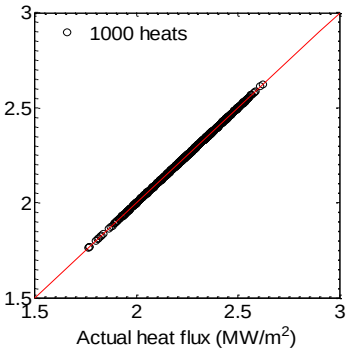

Figure 2.8. Regression with all 3 variables. AIC = -14337. Perfect match of predicted heat flux with actual heat flux

The influence of each of the above chosen variables on mold heat flux is shown in Figures 2.3-2.5. Regressions using only one (G), two (G and ΔT), and all three variables are shown in Figures 2.6-2.8 to illustrate the use of AIC in judging the model. With the addition of each variable, AIC drops indicating an improved model. There is only a moderate drop when the second variable is included, but a large drop when all three variables are included. This illustrates a problem in modelling nonlinear relationships, that it is difficult to separate the effects of the parameters. In addition, trends may appear weak and predictions poor if even one important and cross-correlated variable is missing from the model.

The best fit for x_i are $7.973 \cdot 10^{-5}$ ($\approx 6.794 \cdot 10^{-5} / 0.850$), 1, 1 and -1 respectively which exactly match those of the original equation (Equation 3), given the fixed working mold length of 850 mm. Thus, the procedure is reliable.

2.3. Results and discussion

For the Decatur caser, heat extraction from the four mold faces is compared in Figures 2.9 and 2.10. Figure 2.9 shows larger heat flux from the wide faces than the narrow faces, in agreement with previous studies [23, 38]. Figures 2.10 and 2.11 show that there is no significant difference in the heat flux extracted between fixed and loose wide faces at both Decatur and Tuscaloosa casters. Therefore, model development was performed using only the fixed face data, of both casters.

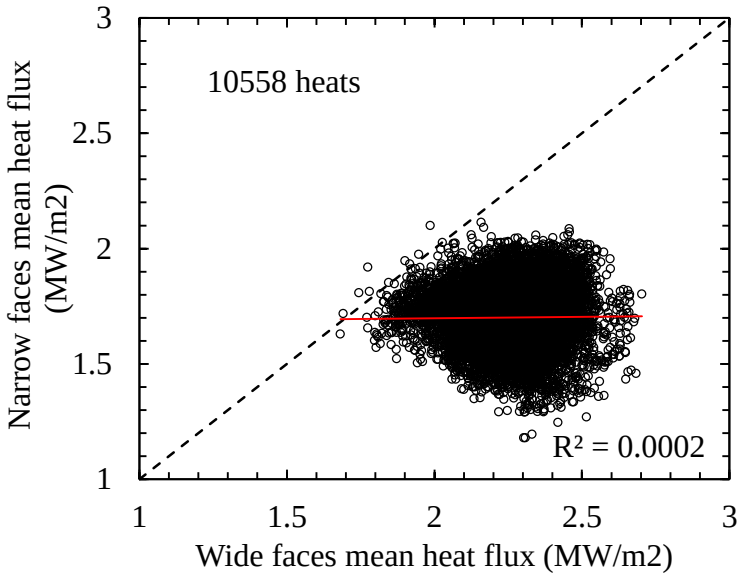

Figure 2.9. Total of average heat flux on two narrow faces versus total of average heat flux on two wide faces of Decatur caster

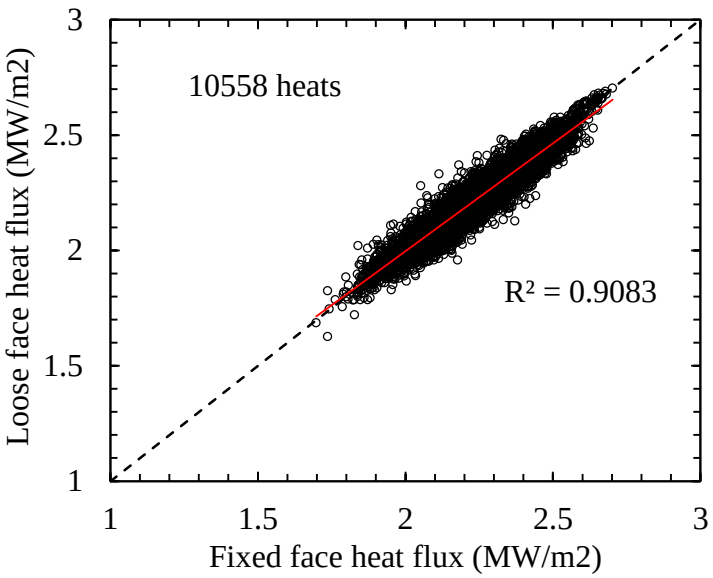

Figure 2.10. Comparison of heat flux between loose and fixed sides of wide face of Decatur caster

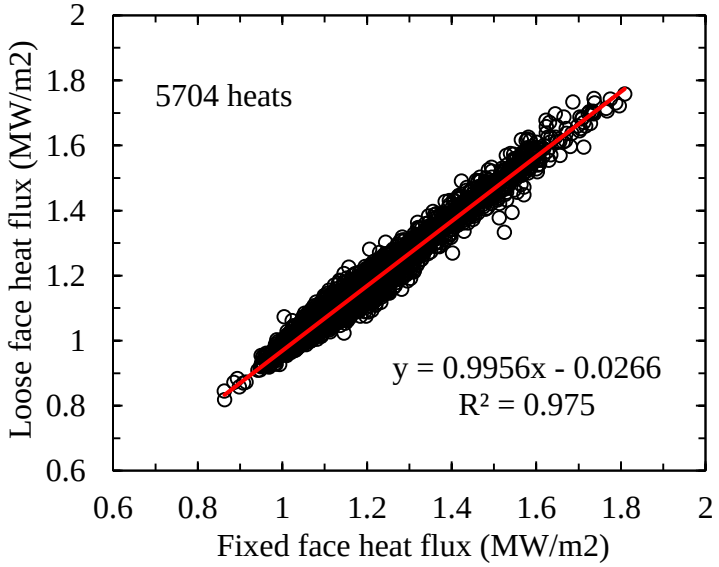

Figure 2.11. Comparison of heat flux between loose and fixed sides of wide face of Tuscaloosa caster

2.3.1. Influence of individual variables

In order to investigate the influence of each of the eight casting variables on mold heat flux, the effect of other casting parameters must be made as insignificant as possible. In the current work, this was done by applying appropriate secondary filters to make all variables, except the one under study, as constant as possible, as described in the methodology section.

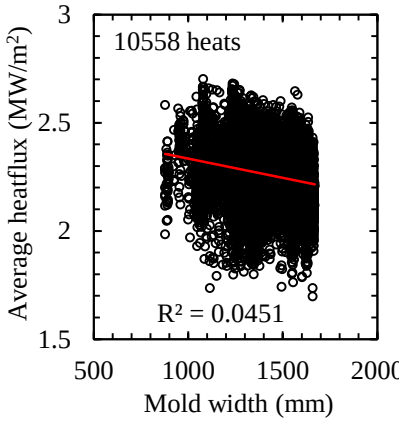

Figure 2.12. Average heat flux plotted against mold width after applying primary filters

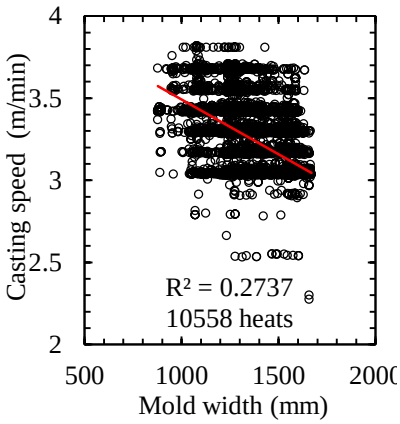

Figure 2.13. Variation of casting speed with mold width after applying primary filters

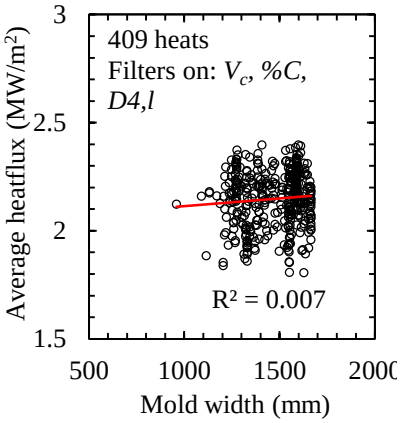

Figure 2.14. Variation of heat flux with mold with after applying secondary filters

An illustration of why this is important is provided in Figures 2.12-2.14 for heats from the Decatur caster. In Figure 2.12, the heat flux is plotted against mold width for every heat in the entire data set, with only primary filters applied to ensure reliable, steady measurements. The linear regression shows that heat flux tends to decrease with mold width. However, intuitively, with increasing mold width, low heat flux at the corners becomes less important as high heat flux at the region of good contact over the rest of the wide face becomes larger. Thus mold heat flux is expected to increase with increase in mold width, which is opposite of what is seen in the data. Figure 2.13 offers an explanation for this, showing a strong cross-correlation between casting speed and mold width. The common practice is to decrease casting speed as mold width increases to maintain constant throughput for quality reasons. Since heat flux has a stronger dependence on casting speed, this leads to a net decrease in heat flux with increasing mold width as seen in Figure 2.12. However, Figure 2.14 shows that, when secondary filters are

applied to make casting speed constant, there is a small positive correlation observed between heat flux and mold width, as expected.

There are other cross-correlations in the data, related to mold powders. Specific mold powders are selected for particular grades, and some mold powders are related in composition, leading to related properties (viscosity and break point). Also, there are only a small number of powders in the data set after primary filtering, so sparseness of data may also lead to false correlations. These are accounted for by studying measurements for only a single powder, using the secondary filters.

The influence of each of the casting variables on mold heat flux was first studied for each of the Decatur and Tuscaloosa casters individually.

2.3.1.1. Casting speed

Casting speed has the most significant influence on mold heat flux, as observed in Figure 2.15 for Decatur Caster and Figure 2.16 for Tuscaloosa caster, which is well known and investigated in many previous studies [3, 8, 9, 23, 27, 38, 43-46]. Mahapatra et al [3] observed that an increase in casting speed decreases depth of mold oscillation marks enhancing mold heat flux with a little effect on peritectic steels. As casting speed increases, the residence time of the steel in the mold decreases. This makes the solidifying steel shell thinner, causing steeper temperature gradients, leading to higher heat flux. This thus results in higher mold hot face temperature, a thinner slag layer and lower solid slag layer viscosity decreasing the slag resistance to heat flow. It is also observed that with increase in casting speed, the resistance to heat flow across the gap between the shell and mold decreases, owing to the drop in mold powder consumption (kg/m^2) [27]. Chow et al [46] showed that the effect of casting speed on mold heat transfer decreases at higher casting speeds and is dependent on carbon content. Studies have shown that mold heat transfer increases with casting speed from plant

measurements [8, 23, 38, 47] and mathematical models [43, 48]. In agreement with previous studies, mold heat flux is increasing with increase in casting speed for the thin slab caster.

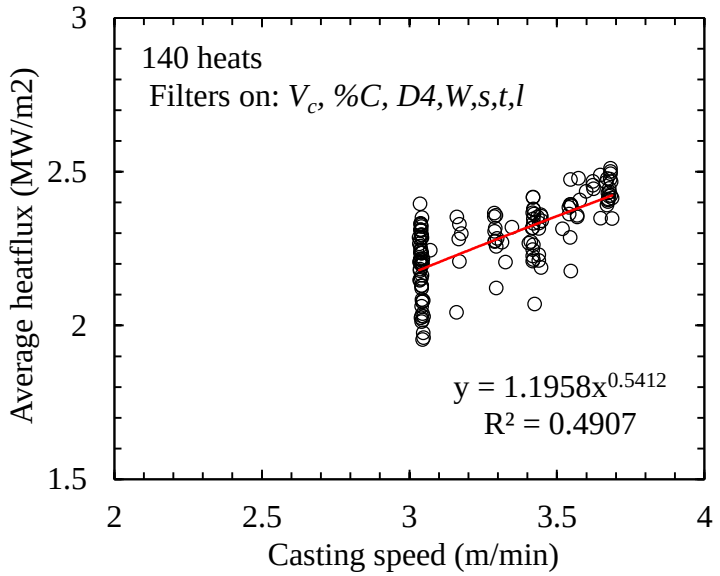

Figure 2.15. Increase in mold average heat flux with increase in casting speed for Decaturcaster

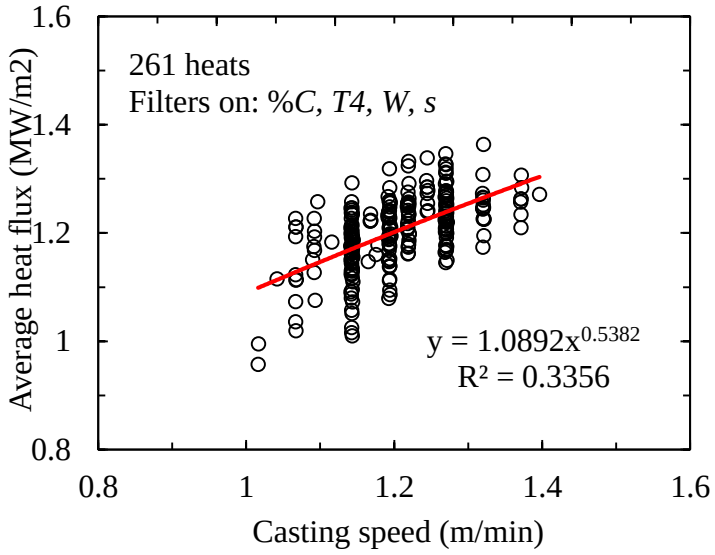

Figure 2.16. Increase in mold average heat flux with increase in casting speed for Tuscaloosa caster

2.3.1.2. Carbon content

Many studies evaluated the effect of carbon content on mold heat transfer [3, 8, 19, 23, 46, 47, 49, 50]. It is known that less heat is removed for peritectic steels around 0.1 % C compared to lower and higher carbon steels. This is because of the larger contraction of the steel during the peritectic phase change associated with shrinkages from δ to γ transformations which increases the gap between the shell and mold face resulting in lower heat flux. Chow et al [46] observed that this effect is more pronounced at meniscus region. Cicutti et al [23] quantified the effect of carbon while developing an equation for predicting mold heat flux. Xia et al and Hecht et al [8, 47] suggested considering equivalent carbon which included the composition of other alloy elements that influence peritectic phase transformations from plant measurements. However, the Nucor Decatur and Tuscaloosa mills does not cast peritectic steels. As shown in Figure 2.17 and Figure 2.18 for Decatur and Tuscaloosa casters, this effect cannot be observed from the data. For general application of the model to other casters, the term and variable (%C) accounting for this effect of steel composition was retained.

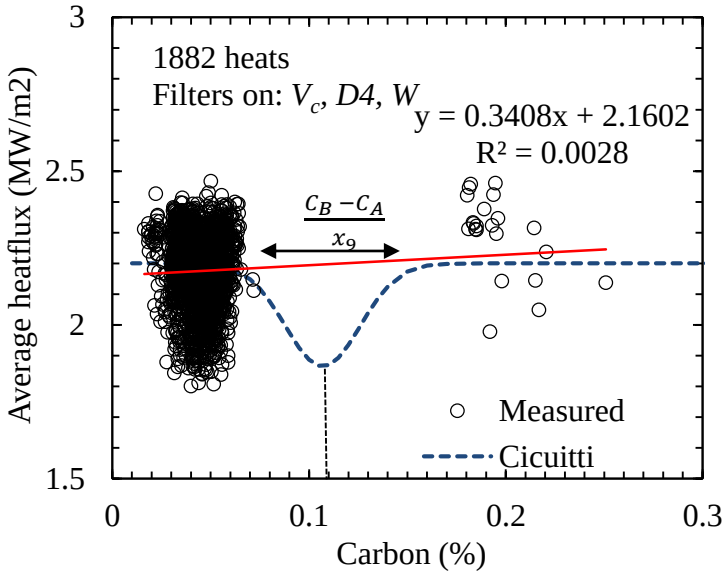

Figure 2.17. Effect of carbon on average heat flux at Decatur caster

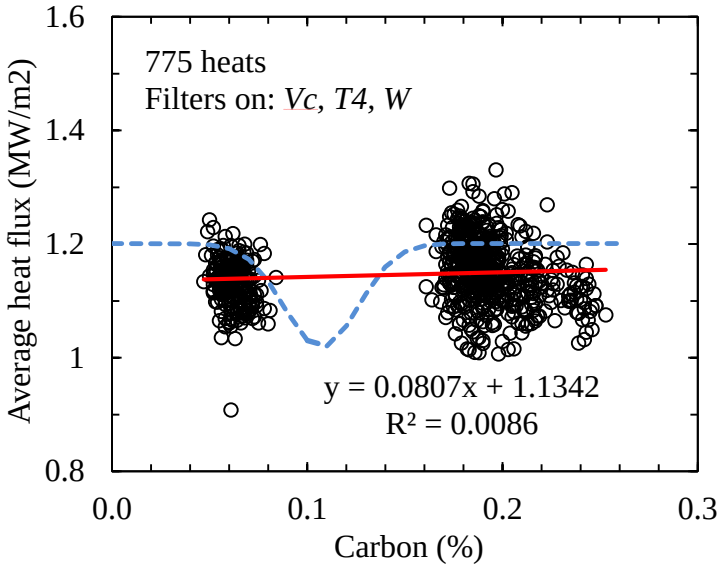

Figure 2.18. Effect of carbon on average heat flux at Tuscaloosa caster

2.3.1.3. Mold powder properties

Mold powder acts a lubrication layer between the strand and mold and thus the powder properties are known to have a significant influence on mold heat flux. Studies [3, 8, 10, 11, 14, 19, 23, 27, 47, 51] suggested viscosity and melting temperature of mold powder primarily influence the molten flux rate into the gap and thus the slag thickness and mold heat flux. Xia et al [8] investigated the mold heat flux from thermal conductivity of the mold powder based on its composition in addition to viscosity, melt temperature and basicity. In addition to the powder properties, Santillana et al [27] suggested that casting speed and hot face temperature influence the solid and liquid slag layer velocities and thickness which determine mold heat transfer. Lee et al [11] reported that powders with lower solidification temperature and viscosity facilitate easier steel flow and thus produce significantly less depth of oscillation marks and hooks which then determine the mold heat flux mold [3, 10, 11, 14].

In this work, the different mold slag properties are characterized by the viscosity and break point temperature. Figures 2.19 and 2.20 for both casters show that, as reported in the literature, higher break point temperature correlates with a lower heat flux. Liquid slag layer transfers heat more efficiently than solid slag layer sticking adjacent to the mold wall. Thus as

crystallization temperature increases, thickness of liquid slag layer decreases and solid slag layer thickness increases which increases the gap resistance and decreases the overall heat transfer across the slag layers.

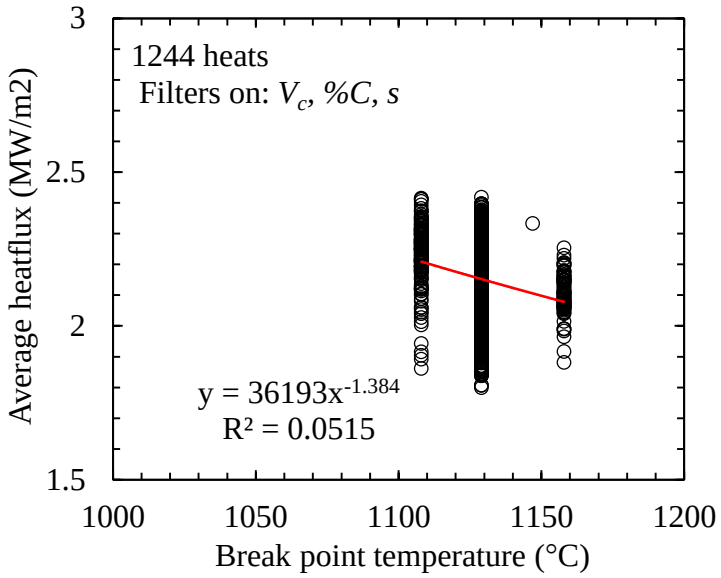

Figure 2.19. Average heat flux decreases as break point temperature of mold powder increases at Decatur caster

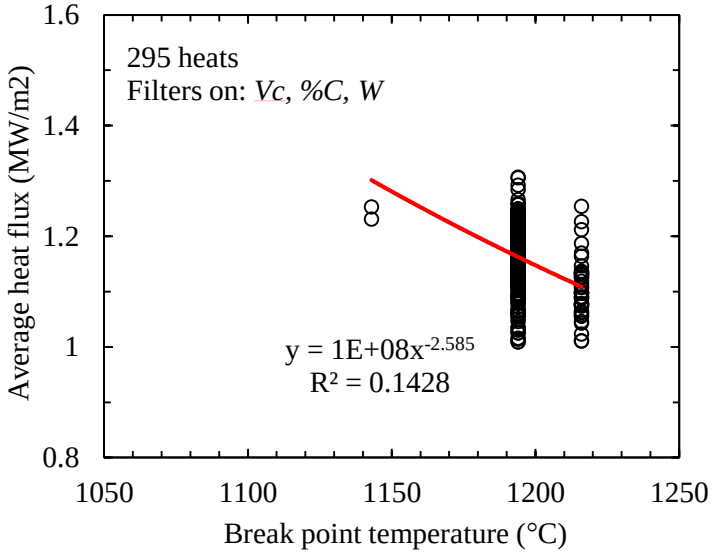

Figure 2.20. Average heat flux decreases as break point temperature of mold powder increases for Tuscaloosa caster

Figures 2.21 and 2.22 show a very slight effect of mold heat flux increasing with increasing slag viscosity. This disagrees with previously reported results that higher viscosity is related to lower heat flux. This is likely due to cross-correlations and the small data set for mold powders, as described previously.

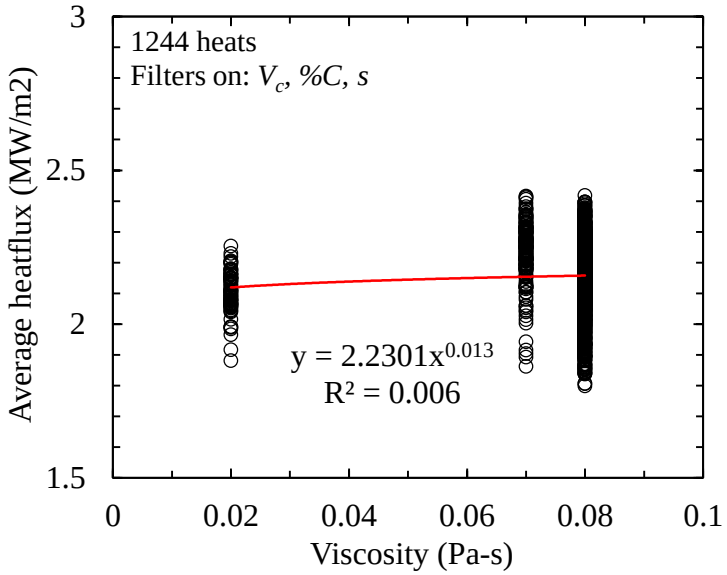

Figure 2.21. Variation of heat flux with viscosity of mold powder for Decatur caster

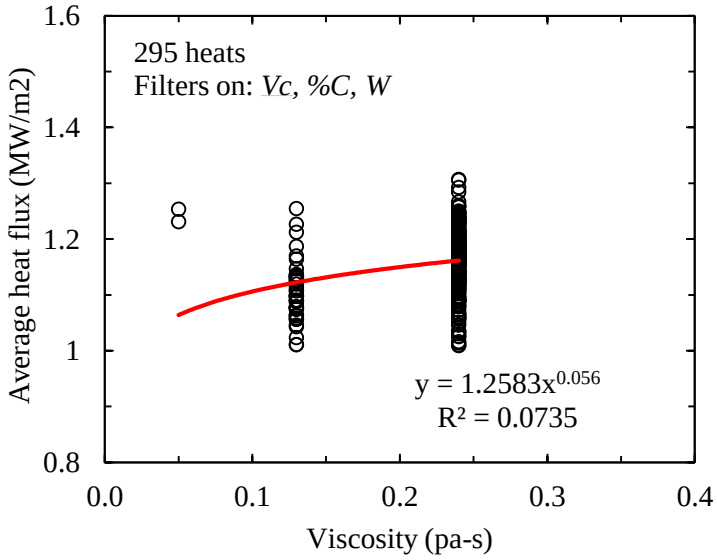

Figure 2.22. Variation of heat flux with viscosity of mold powder for Tuscaloosa caster

2.3.1.4. Mold width

Figures 2.23 and 2.24 for Decatur and Tuscaloosa casters shows a small increase in mold heat flux with increasing mold width. As discussed at the beginning of this section, this is likely due to the drop in heat flux at the mold corners becoming less important as the length of the region of good contact increases.

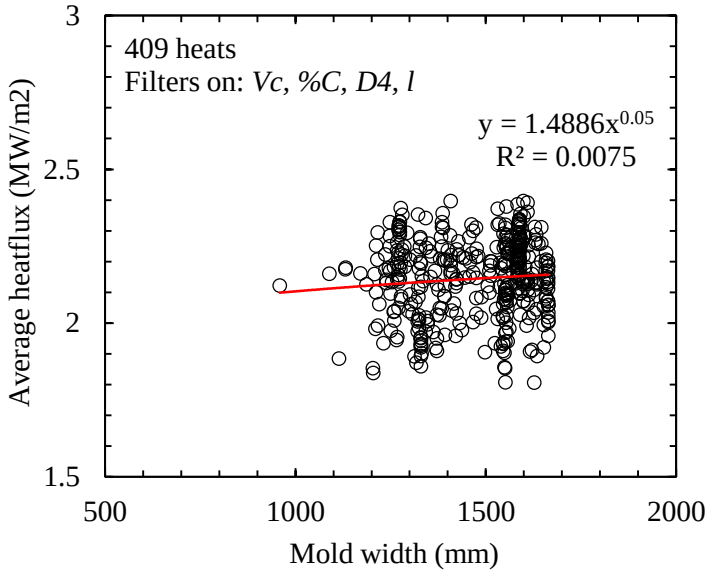

Figure 2.23. Influence of mold width on heat flux for Decatur caster

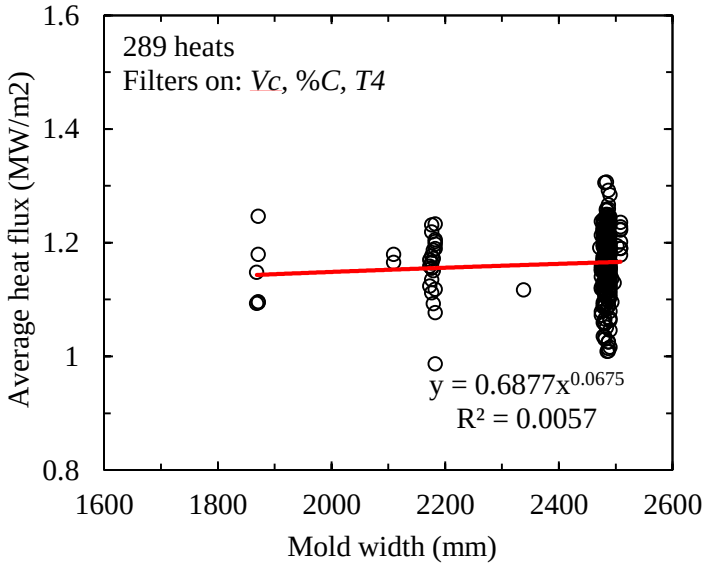

Figure 2.24. Influence of mold width on heat flux for Tuscaloosa caster

2.3.1.5. Superheat

Higher the superheat, higher the heat content of steel and thus higher the heat to be extracted across the mold to form the adequate shell thickness by the time strand exits the mold. Also, super heat at the meniscus is one of the factors that influence the formation of oscillation marks [7, 24] that determine the heat flow across the mold [3, 10, 11, 14]. Higher liquid temperatures at the top surface lessens meniscus freezing and hook formation, leading to shallower oscillation marks and less gap resistance thus enhancing mold heat flux.

For Decatur and Tuscaloosa casters, Figures 2.25 and 2.26 respectively show that mold heat flux increases slightly with increasing superheat of the incoming liquid steel, despite scatter and even after making other casting parameters as constant as possible to isolate their effect. This is in agreement with a previous study [9, 38] which showed little effect of superheat on mold heat flux. Superheat temperature is measured in the tundish which contains a mixture of batches of steel from ladle and may explain scatter. There might also be some loss of heat by the time the steel reaches the mold from tundish and this has to be accounted.

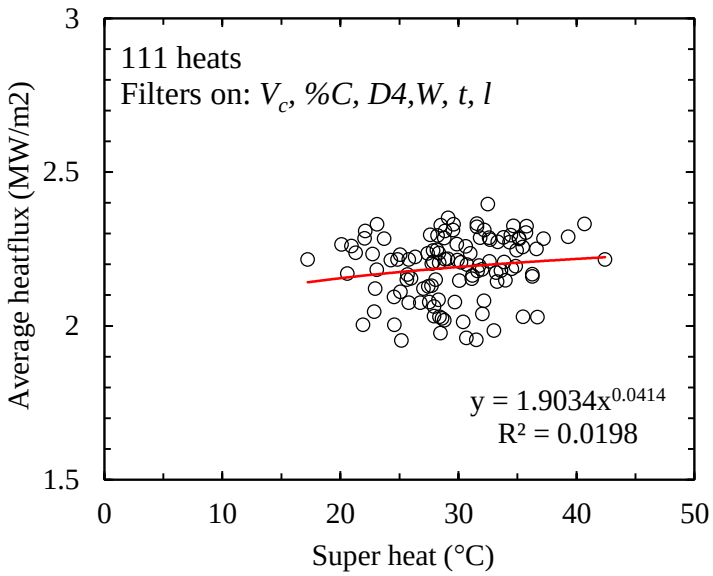

Figure 2.25. Effect of super heat on heat flux for Decatur caster

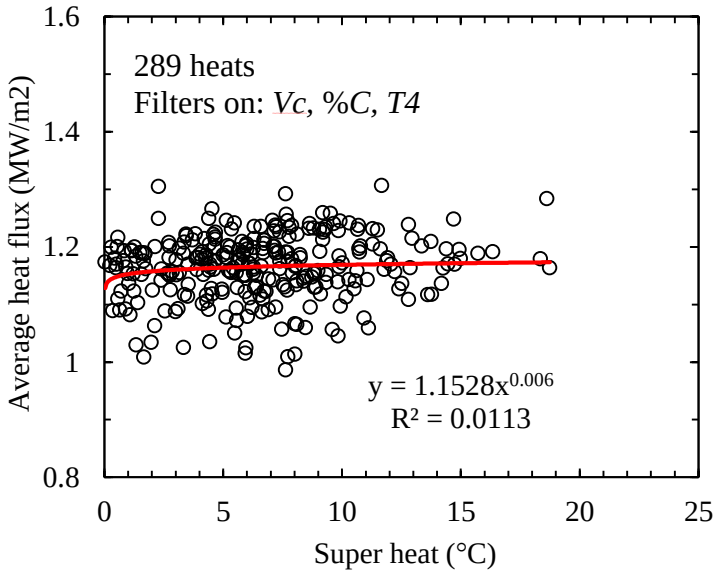

Figure 2.26. Effect of super heat on heat flux for Tuscaloosa caster

2.3.1.6. Mold level standard deviation

Like superheat, mold level fluctuations at the top surface of the meniscus influence the formation of oscillation marks that determine the heat flow across the mold[3, 10, 11, 14]. Higher mold level fluctuations result in deeper oscillation marks, increasing gap resistance, and thus reducing mold heat flux. Studies by Park et al [18] have shown that mold thermal response

is a good indication of metal level fluctuations, which are a potential source of cyclic thermal loading on the mold thus determining heat flux variations and mold life.

Figures 2.27 and 2.28 at Decatur and Tuscaloosa casters respectively show that increasing level fluctuations (as indicated by the standard deviation in mold level), have little effect on mold heat flux. This is in agreement with a previous study on a CSP thin slab caster [38]. Since mold level signals are recorded only at certain locations and not throughout the surface, the way they are recorded has a strong influence on analysis. As it is difficult to accurately quantify these recordings, in this work, standard deviation of mold level fluctuations is considered as a representation of level deviations. As the standard deviation is less than 1 mm, the deviation measurements appear to be filtered for the benefit of the mold level control system, before being stored in the database. This may be why the expected trend is not observed in the data.

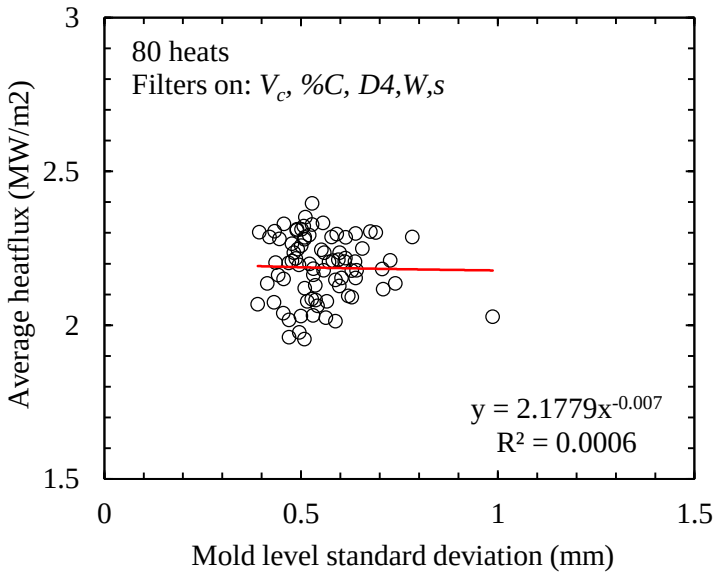

Figure 2.27. Variation of heat flux with mold level standard deviations at Nucor caster

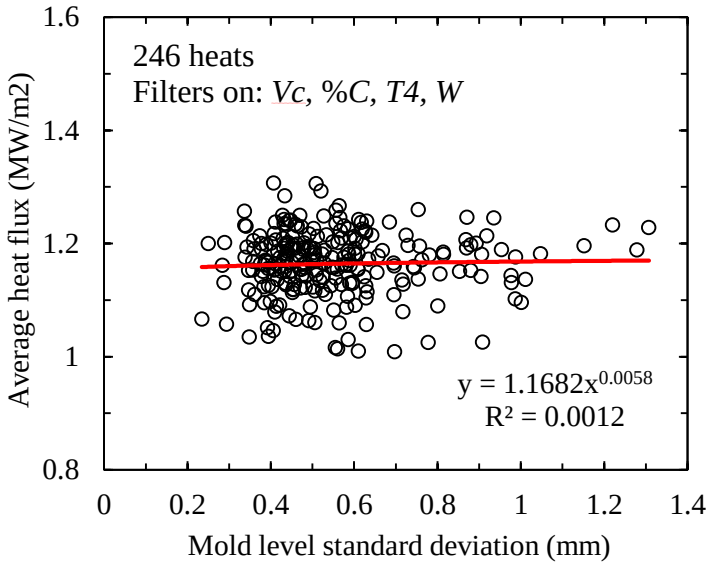

Figure 2.28. Variation of heat flux with average mold level standard deviations at Tuscaloosa caster

2.3.1.7. Mold plate thickness

It is expected that as mold plate thickness decreases, the resistance to heat flow decreases slightly, resulting in higher heat flux. Santillana et al [27] measured even higher than expected increase in mold heat flux as mold plate thickness decreases, owing to the decreased hot face temperature of the mold decreasing slag layer thickness and resistance to heat flow thus increasing heat flux. But as shown in Figures 2.29 and 2.30, there appears to be little correlation between heat flux and measured mold plate thickness in this data. The effect is confounded by possible cross correlations because water flow rate may be adjusted with mold plate thickness.

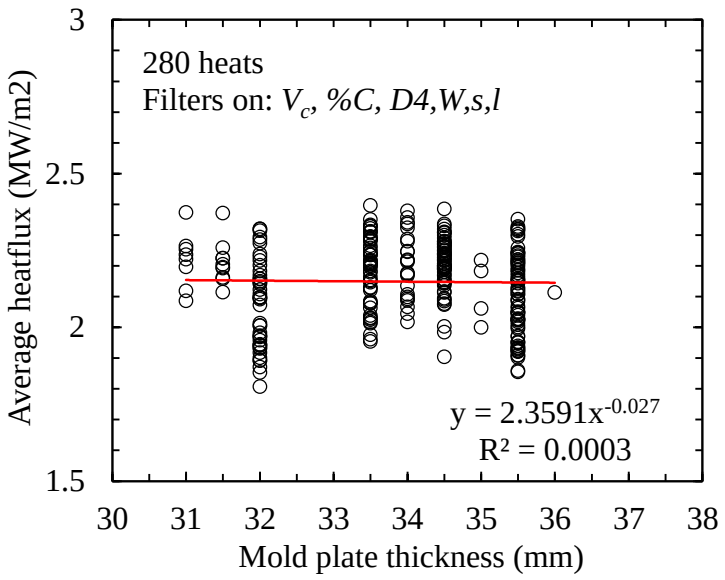

Figure 2.29. Little effect of mold plate thickness on mold heat flux at Decatur caster

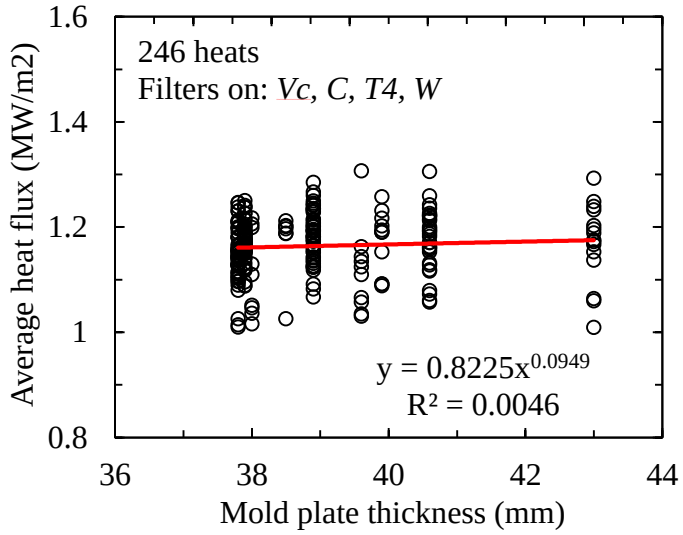

Figure 2.30. Little effect of mold plate thickness on mold heat flux at Tuscaloosa caster

In addition, plate thickness is measured only when the mold is changed, and therefore does not account for wear over the course of a campaign. As a proxy for this wear, Figures 2.31-2.34 for Decatur caster and Figures 2.35-2.38 for Tuscaloosa caster show mold heat flux over the four longest campaigns in the data set plotted against the number of heats cast using that mold, using secondary filters for speed, composition and mold powder to account for changing casting conditions. There is a weak negative relationship between mold heat flux and wear.

This is expected because with mold wear, surface roughness increases, gap resistance increases decreasing effective heat transfer.

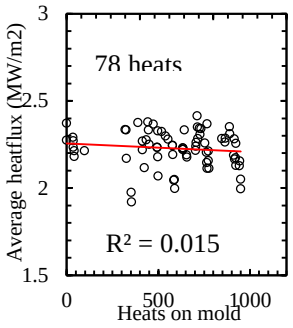

Figure 2.31. Slight decrease in heat flux with heats on mold of campaign 1

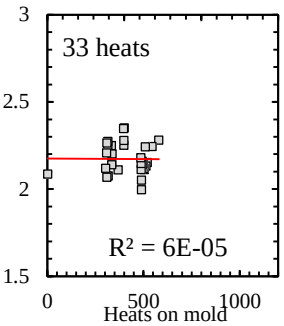

Figure 2.32. Effect not clearly seen for campaign 2

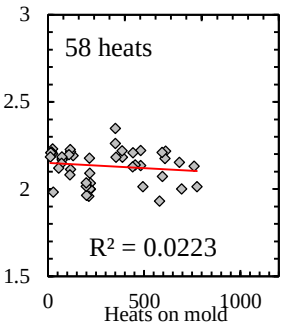

Figure 2.33. Slight decrease in heat flux with heats on mold of campaign 3

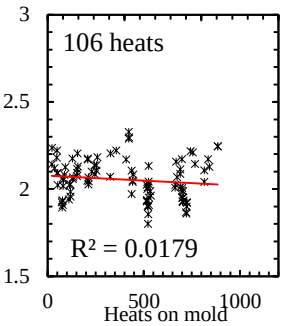

Figure 2.34. Slight decrease in heat flux with heats on mold of campaign 4

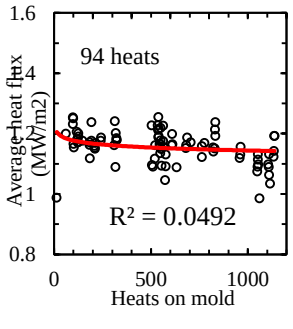

Figure 2.35. Slight decrease in heat flux with heats on mold of campaign 1

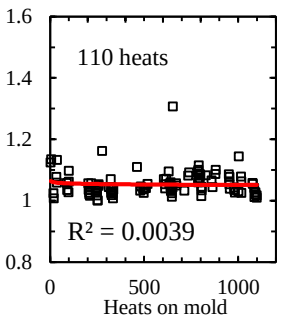

Figure 2.36. Effect not clearly seen for campaign 2

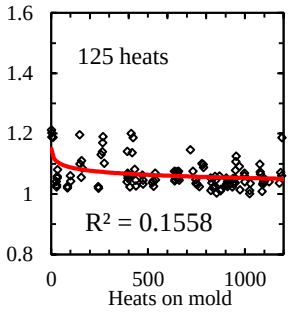

Figure 2.37. Slight decrease in heat flux with heats on mold of campaign 3

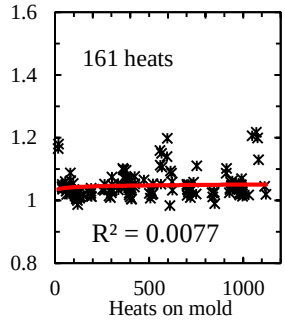

Figure 2.38. Slight decrease in heat flux with heats on mold of campaign 4

2.3.2. Model development and evaluation

The procedure described in the methodology section is performed to find best fit parameters for different combinations of casting variables based on the measurements of both Decatur and Tuscaloosa casters comprising 9022 and 3531 heats respectively. The results are summarized in Table VI.

Table VI Different equations with statistical estimates*

Equation	RSS	AIC
$Q = 1.059 \cdot V_c^{0.646}$	143.1	-56159
$Q = 1.247 \cdot V_c^{0.645} \cdot \left(1 - 0.152 \times exp\left(-0.115 \times \left(\frac{\frac{C_A + C_B}{2} - \%C}{(C_B - C_A)} \right)^2 \right) \right)$	143.0	-56162
$Q = 28.272 \cdot 10^3 \cdot V_c^{0.570} \cdot T_{break}^{-1.414} \cdot \left(1 - 0.152 \cdot \exp\left(-8.19 \cdot 10^{-9} \cdot \left(\frac{\frac{C_A + C_B}{2} - \%C}{(C_B - C_A)} \right)^2 \right) \right)$	123.4	-58018
$Q = 15.285 \cdot 10^3 \cdot V_c^{0.609} \cdot T_{break}^{-1.403} \cdot W^{0.068} \cdot \left(1 - 0.152 \cdot \exp\left(-1.68 \cdot 10^{-8} \cdot \left(\frac{\frac{C_A + C_B}{2} - \%C}{(C_B - C_A)} \right)^2 \right) \right)$	120.4	-58317
$Q = 37.594 \cdot 10^3 \cdot V_c^{0.590} \cdot T_{break}^{-1.529} \cdot W^{0.066} \cdot \mu^{-0.010} \cdot \left(1 - 0.152 \cdot \exp\left(1.77 \cdot 10^{-8} \cdot \left(\frac{\frac{C_A + C_B}{2} - \%C}{(C_B - C_A)} \right)^2 \right) \right)$	119.6	-58401
$Q = 39.263 \cdot 10^3 \cdot V_c^{0.588} \cdot T_{break}^{-1.529} \cdot W^{0.065} \cdot \mu^{-0.01} \cdot t^{-0.011} \cdot \left(1 - 0.152 \cdot \exp\left(1.85 \cdot 10^{-8} \cdot \left(\frac{\frac{C_A + C_B}{2} - \%C}{(C_B - C_A)} \right)^2 \right) \right)$	119.6	-58400

Table VI (cont.)

$Q = 35.262 \cdot 10^{3} \cdot V_c^{0.586} \cdot T_{break}^{-1.498} \cdot W^{0.061} \cdot \mu^{-0.008} \cdot t^{-0.032} \cdot l^{0.012} \cdot \left(1 - 0.152 \cdot \exp\left(-4.33 \cdot 10^{-4} \cdot \left(\frac{C_A + C_B}{2} - \%C \over (C_B - C_A)\right)^2\right)\right)$	123.0	-58047
$Q = 30.07 \cdot 10^{3} \cdot V_c^{0.591} \cdot T_{break}^{-1.492} \cdot W^{0.062} \cdot \mu^{-0.008} \cdot l^{0.012} \cdot t^{-0.003} \cdot s^{0.00} \left(1 - 0.152 \cdot \exp\left(-6.14 \cdot 10^{-2} \cdot \left(\frac{C_A + C_B}{2} - \%C \over (C_B - C_A)\right)^2\right)\right)$	132.2	-57141

*constants are rounded off to 3 decimal figures. Complete constant values are given in Appendix B

The successive models are developed through stepwise forward selection, meaning that the single variable that most decreases RSS is added to make the next model. The exception to this is the carbon term, as discussed below. RSS Error and AIC at each step illustrate the significance of the casting variable added.

As discussed in the individual effects section, some of these variables have strong cross-correlations with each other. These make it difficult for numerical techniques to converge to a unique set of best-fit parameters. There may be more than one set of best-fit parameters that give similar predictions. Therefore, including cross-correlated variables together, such as width and casting speed, may improve predictions of heat flux. However, it is difficult to extract conclusions about the underlying physics.

As seen above and in the literature, casting speed has a clear, strong influence on the average mold heat flux. Therefore, the first, simplest model is fitted with casting speed alone. Although the effect of carbon is not detectable with the current data set as peritectics are not cast at Nucor Decatur and Tuscaloosa mills, for general application of the model to other casters, the carbon term is important. Therefore, the second model included casting speed and the expression accounting for drop in heat flux for peritectic grades. RSS did not decrease and AIC increased from model 1 to model 2, due to the lack of data, but the peritectic expression is included in the remaining models for generality to other casters.

The remaining variables were added in stepwise order. A decrease in RSS and AIC with the addition of break point temperature, width, viscosity and mold level deviation in the respective order indicate their inclusion is significant. But the contribution of viscosity and mold level deviation is very small. In fact, though heat flux appeared to have little correlation with viscosity, as shown in Figures 2.21 and 2.22, model 5 shows that there is a weak decrease in heat flux as viscosity increases. Based on AIC, model 8 appears to be the best predictive model. RSS measure of performance of the new model equations based on Nucor database comprising 12553 heats is depicted in Figure 2.39.

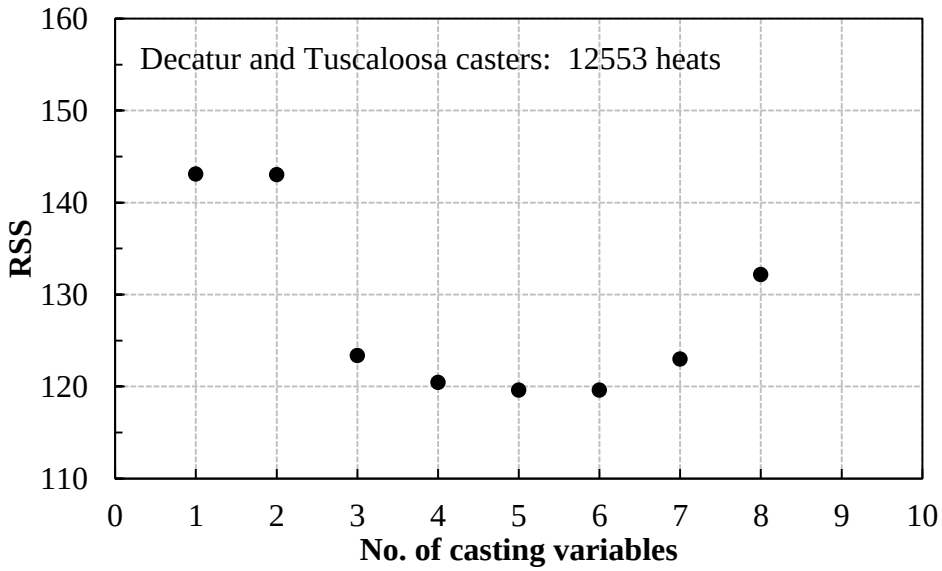

Figure 2.39. RSS measure of developed models with varying number of casting variables on Nucor database

There is no significant decrease in RSS on addition of mold plate thickness, mold level deviation, and superheat. The respective variables may not have significant effect on heat flux owing to the way they are included in the equation could need modification, or the measurements may be too inaccurate to discern the effect. For example, mold plate thickness is measured only at the start of a campaign, and whatever wear occurs during the campaign is not measured.

Thus, model 5, based on the RSS measure, is considered to be superior to the other equations with respect to simplicity and accuracy shown again as follows and will be referred to as Nucor equation.

$$Q = 37.594 \cdot 10^{3} \cdot V_c^{0.590} \cdot T_{break}^{-1.529} \cdot W^{0.066} \cdot \mu^{-0.010} \cdot \left(1 - 0.152 \cdot \exp\left(1.77 \cdot 10^{-8} \cdot \left(\frac{\frac{C_A + C_B}{2} - \%C}{(C_B - C_A)} \right)^2 \right) \right) \quad (13)$$

Similarly non-linear regression analysis is performed on Decatur and Tuscaloosa casters individually and corresponding best models, namely Decatur equation and Tuscaloosa equation are developed as follows

$$Q = 3.128 \cdot 10^{5} \cdot V_c^{0.620} \cdot T_{melt}^{-1.845} \cdot W^{0.072} \cdot \mu^{-0.017} \cdot \left(1 - 0.152 \cdot \exp\left(-0.021 \cdot \left(\frac{\frac{C_A + C_B}{2} - \%C}{(C_B - C_A)} \right)^2 \right) \right) \quad (14)$$

$$Q = 2.676 \cdot 10^{3} \cdot V_c^{0.740} \cdot T_{break}^{-1.188} \cdot W^{0.09} \cdot \mu^{-0.014} \cdot \left(1 - 0.152 \cdot \exp\left(2.37 \cdot 10^{-8} \cdot \left(\frac{\frac{C_A + C_B}{2} - \%C}{(C_B - C_A)} \right)^2 \right) \right) \quad (15)$$

The performance of three new equations along with Cicutti equation on Decatur and Tuscaloosa casters are shown in Figures 2.40 and 2.41 respectively. The individual equations solely developed on respective casters are predicting better compared to other equations. On Decatur caster, Tuscaloosa equation is overpredicting heat flux and Decatur equation is underpredicting heat flux on Tuscaloosa caster. Nucor equation is predicting almost same as Decatur and Tuscaloosa equations on both the casters. The Cicutti equation is seen to overpredict the heat transfer rate, which is similar to the performance of other equations [eg Lorento] based on measurements of thick slab casters. The Nucor equation is clearly predicting better than the Cicutti equation on both the casters and thus, Nucor equation, based on wider database of two casters is the recommended equation to apply on other casters.

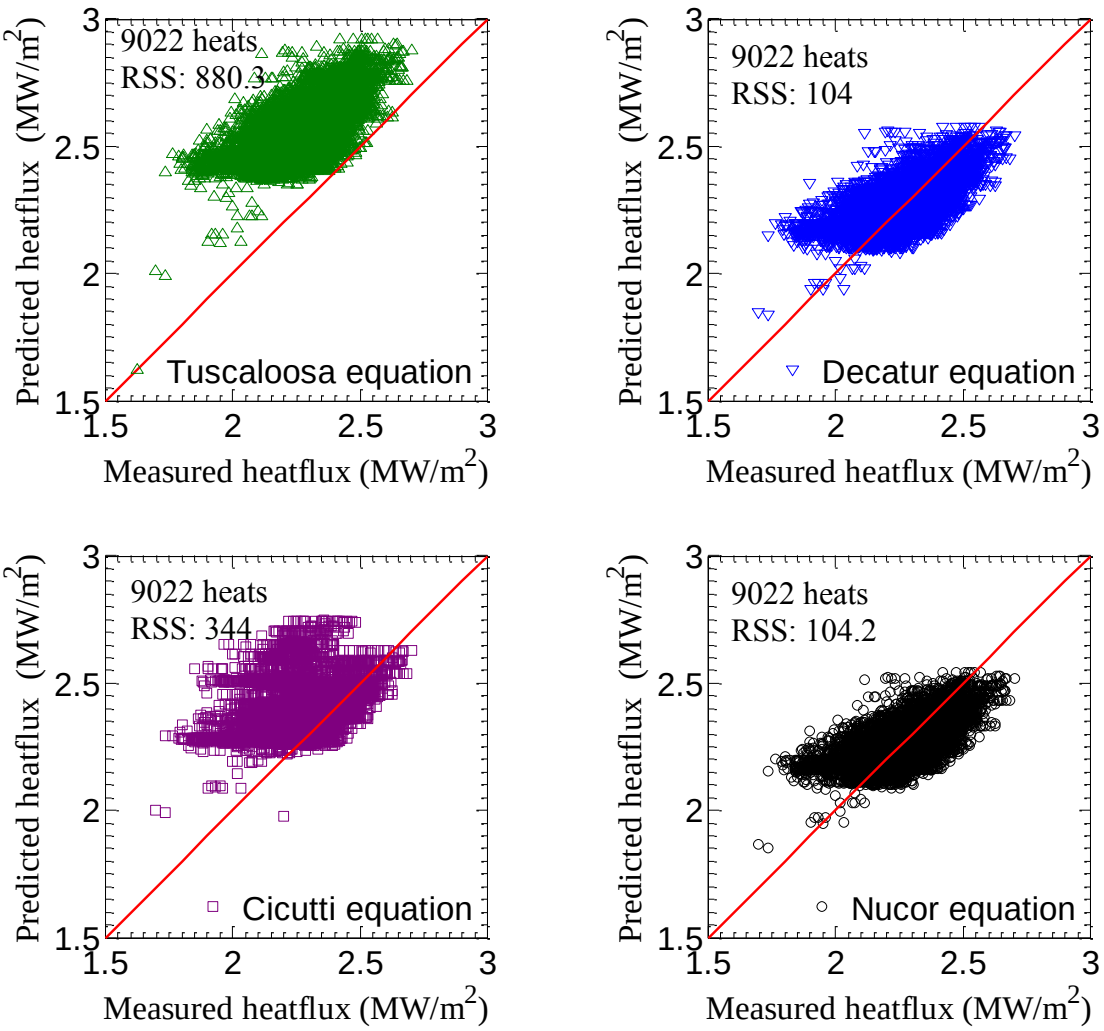

Figure 2.40. Performance of different predicting equations on Decatur caster

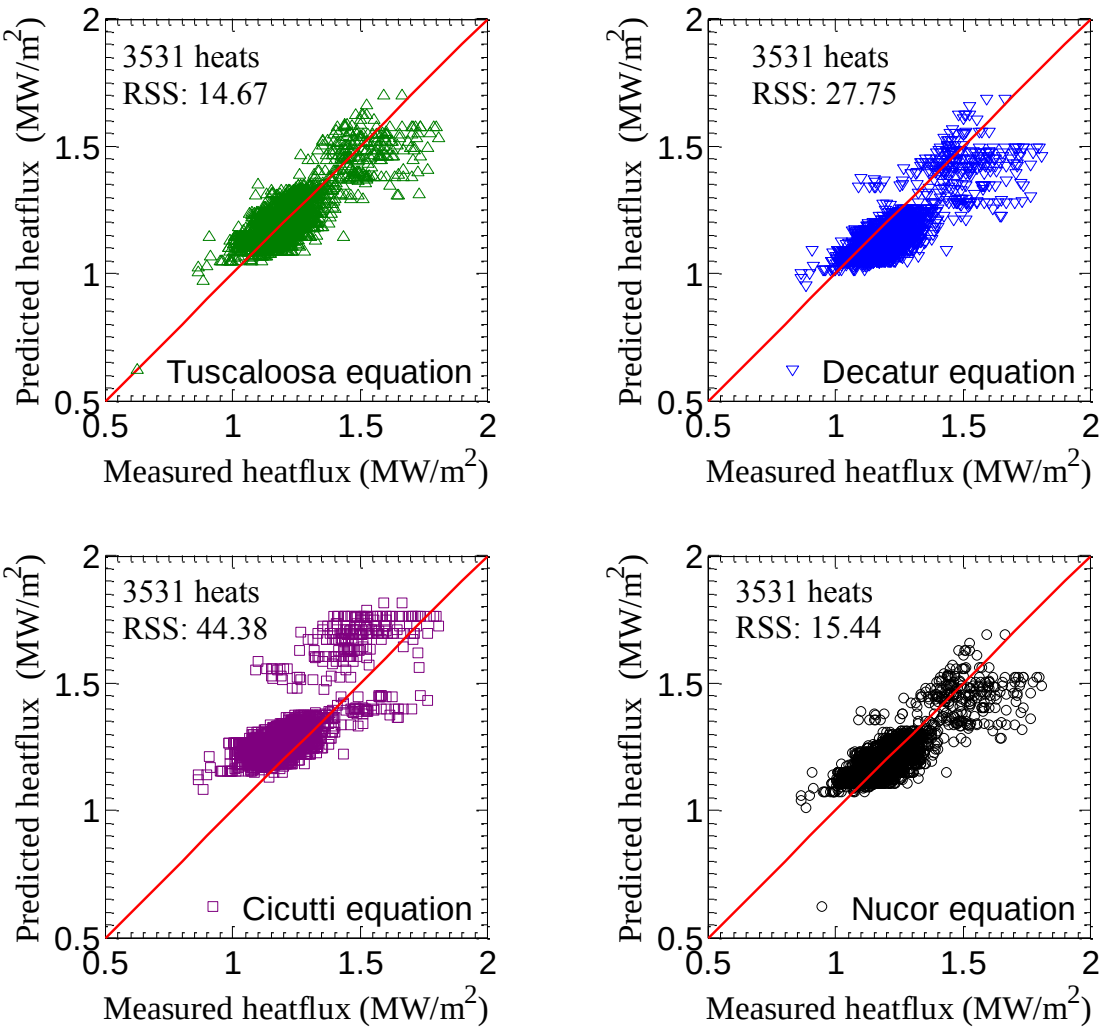

Figure 2.41 Performance of different predicting equations on Tuscaloosa caster

The scatter still shows that this equation has room for improvement. One possibility is that the model needs to account for other casting variables, like mold oscillation mark depth and frequency, which are not considered in the present work. Better selection of casting variables, the structure of the model, and the handling of codependent variables could also lead to better results.

2.4. Conclusions

The average mold heat flux over the wide face of a thin slab casting mold is investigated using measurements including eight casting variables from Nucor steel mills located in Decatur and Tuscaloosa. Of all the variables studied, casting speed has a clear, strong influence positively correlating with heat flux. The expected influence of carbon content is not observed because of a lack of data for peritectic steels. Individually, break point temperature of the mold powder, mold width and powder viscosity have a weaker effect, but was found through nonlinear multiple regression of the data. As mold powder properties differ between measurement methods and manufacturers and in addition, due to limited mold powder property, more work is needed on mold powder effect. Compared to break point temperature, viscosity of mold powder has a weaker effect. The effect of superheat, mold plate thickness, and mold level standard deviation are not evident in the data. Equations to predict mold heat flux as a function of casting variables are developed based on the measurements of each individual caster and both casters together. Owing to limited data with respect to steel composition and powder properties, recommended simple equation is the model with casting speed alone based on entire Nucor data. The best equation for both casters, Nucor equation as a function of 5 casting variables, matches better than Cicutti equation, a previous equation developed for a thick slab caster and is almost as good as the equations for the individual casters. The Nucor equation is expected to behave well on other casters, owing to its wide database of measurements from two different casters. The results of this paper also provide insights into mold thermal behavior, and the methodology can be readily extended to other casters and phenomena.

CHAPTER 3: FEASIBLE OPERATING CONDITIONS IN SLAB CONTINUOUS CASTING USING CON1D

3.1. Introduction

The process of continuous casting of steel is mainly governed by heat transfer and solidification, with primary cooling in the mold followed by secondary cooling using water sprays. Spray cooling plays a vital role in regulating the surface temperature of the strand, which governs formation of grain structure, properties of the steel such as ductility, and crack formation. Thus, accurate control of secondary cooling sprays is important for the production of high quality slabs [52, 53]. Spray cooling also affects the solidification rate and thus the distance from the meniscus to the final solidification point, called the "metallurgical length." Slab casters require roll support in order to prevent bulging and whale defects where liquid steel is present [54].Thus, spray cooling also affects productivity of the caster.

Many studies investigated the importance of secondary cooling in determining steel quality. Steel at elevated temperatures experiences two temperature zones of low ductility, one above 1340 °C that is responsible for hot tearing cracks and another from 700 °C and 900 °C which causes intergranular cracks, as reviewed in previous work [55-57]. Secondary cooling should be controlled to minimize severe temperature gradient fluctuations of the strand surface and uneven solidification that can cause cracks [58, 59]. Many have suggested optimization of secondary cooling to avoid cracks, especially on small radius casters and in the straightening section of the caster [59, 60] where surface strains are higher.

Owing to the importance of controlling metallurgical length to avoid stress related cracks, excessive bulging and whales, several previous studies have investigated factors affecting metallurgical length. Uehara et al [61] studied generation of internal cracks and slab internal bulging during straightening. Although spray cooling is important, metallurgical length depends mainly on casting speed. Metallurgical length increases in direct proportion with higher casting speeds. Thus, there are limits to [36] suggested that casting speed cannot be increased arbitrarily and reported the theoretical limits of shell thickness, casting speed and productivity using CON2D[62].

Many Mathematical and computational models have been developed and employed for understanding the continuous casting process and conducting parametric studies. Among them, CON1D is a model of heat transfer and solidification governing various complex phenomena

in continuous casting [14], [63] that has been calibrated and validated to predict metallurgical length CON1D [14] based on experimental plant measurements. Owing to its accuracy, CON1D has been widely employed by the steel industry for the design, implementation and control of continuous casting process for the production of high quality steel minimizing defects.

In order to avoid defects in a given caster, casting speed, spray cooling, and superheat should be controlled to avoid defects. In this work, CON1D is employed to determine feasible operating windows for these parameters in a thin slab caster at Nucor Steel in Decatur, Alabama, which satisfy several constraints. The first set of constraints is to avoid stress-related cracks, which occur during bending or straightening of a fully-solidified strand. To avoid this, the liquid core should extend beyond the exit of the straightener. In order to simultaneously avoid whale defects, the metallurgical length must be shorter than the end of containment by the roll supports. Thus, the metallurgical length is constrained to fall within a specific length range.

A second set of constraints is to avoid cracks on sensitive steel grades, so the steel strand should not be subjected to excessive strain and tensile stress while the surface temperature is within the range of the ductility trough (700°C - 900°C). To achieve this, the surface temperature should be kept either hotter or colder than the ductility trough, while in the "bender" and "straightener," which are the regions down the caster where the strand undergoes bending and unbending respectively, and generate high strains on the strand surface that may lead to transverse cracks. A simultaneous constraint is to avoid large temperature gradients, which exacerbate surface cracks, and especially to avoid surface reheating, which also can cause tensile stress on the solidification front, leading to internal hot tear cracks [58]. To achieve this additional requirement, efforts are made to maintain a decreasing temperature distribution down the caster, with minimal fluctuations.

This work determines the feasible range of casting speeds for three different grades of steel with carbon contents of 0.24% (High), 0.1011% (Peritectic) and 0.003% (Low) at a given superheat with optimum spray patterns in the secondary cooling zones. This work also determines the maximum casting speed and its corresponding critical super heat to satisfy the

quality constraints for the above grades. This work aims to provide useful insights in the determination of feasible windows of operation for a given caster, by controlling casting speed, super heat and secondary cooling spray patterns to optimize the process without compromising on quality and safety.

3.2. Methodology

3.2.1. Continuous casting model

This work applies the numerical model, CON1D to understand and optimize the process of continuous casting of steel.

3.2.2. Governing Equation

The process of continuous casting involves heat transfer and solidification, subject to surface cooling by convection and radiation. From the Law of conservation of energy for heat balance, "Rate of change of total energy of a thermodynamic system is equal to the sum of the rate of change of heat flow across the system, heat generated in the system, and deformation heating". Enthalpy term accounts for the latent heat evolution and heat capacity that depend on the temperature.

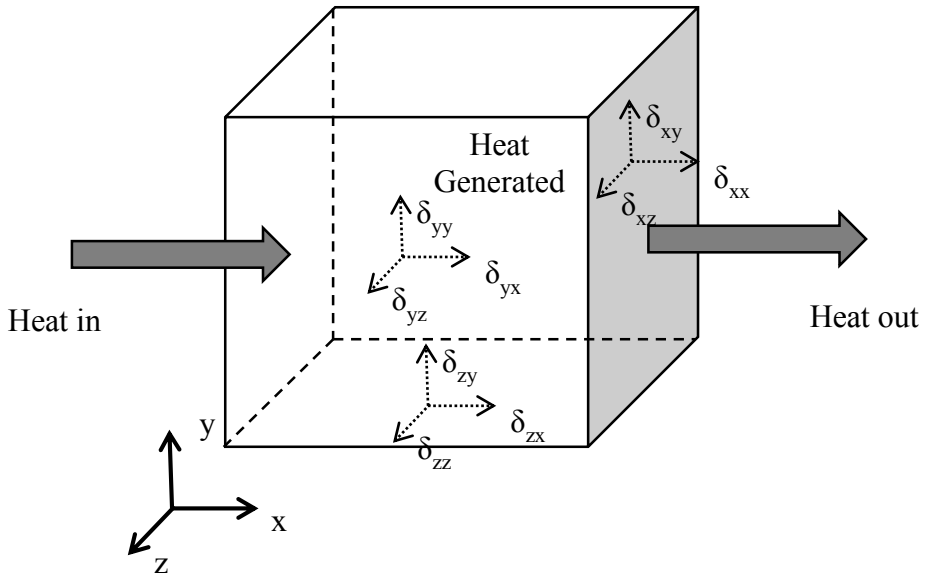

Figure 3.1 Control volume for heat balance

Thus the 3D transient heat conduction equation in finite control volume is as follows.

$$\rho \frac{DH}{Dt} = -\nabla \cdot q + \dot{Q} + \delta : D \tag{16}$$

Where ρ is density (kg/m^3), H is specific enthalpy (J/kg), t is time (s), q is heat flux (W/m^2), $\dot{\boldsymbol{Q}}$ is the internal heat generation (W/m^3) and $\boldsymbol{\delta}$: $\boldsymbol{D}$ is deformation heating, which is the double dot product of stress (N/m^2) and velocity gradients (1/s), containing a total of 9 terms in three Cartesian directions.

As enthalpy is a scalar quantity, its total derivative is considered as follows:

$$\frac{DH}{Dt} = \frac{\partial H}{\partial t} + V \cdot \nabla H \tag{17}$$

Where V is the velocity vector (m/s).

Considering a slice domain that moves at a constant velocity in the casting direction with no velocity gradient in other directions, the deformation heating term tends to zero as derivative of a constant is zero. Assuming there is no heat generation due to neutron bombardment or ohmic heating or electromagnetic field or chemical reactions, internal heat generation is negligible. Assuming heat transfer is governed by Fourier's Law of Heat conduction,

$$q = -k \nabla T \tag{18}$$

Where k is the thermal conductivity of steel (W/m-K) and T is temperature (°C), then

Equation (1) becomes:

$$\rho \left(\frac{\partial H}{\partial t} + V \cdot \nabla H \right) = \nabla \cdot (k \nabla T) \tag{19}$$

From the Enthalpy-temperature diagram for steel, enthalpy is comprised by super heat, latent heat during phase changes and transformations between ferrite and austenite, and sensible heat.

$$H = H_o + C_p\,(T - T_o) + H_f\,(1 - f_s) + H_{\gamma-\alpha}\,(1 - f_\alpha) \tag{20}$$

Here, H_o is the specific enthalpy at a reference Temperature, T_o (°C) and H_f, $H_{\gamma\text{-}\alpha}$ stands for specific enthalpy during phase change with a solid fraction of f_s and phase transformation from austenite to ferrite with a ferrite fraction of f_α respectively with a specific heat capacity, C_p(J/Kg-K) at a given temperature. Assuming, phase transformation term can be added to other term/ neglected. Thus equation [4] in Cartesian coordinate system can be written as,

$$\rho C_p\left(\frac{\partial T}{\partial t} + V_x\frac{\partial T}{\partial x} + V_y\frac{\partial T}{\partial y} + V_z\frac{\partial T}{\partial z}\right) = \frac{\partial}{\partial x}\left(k\frac{\partial T}{\partial x}\right) + \frac{\partial}{\partial y}\left(k\frac{\partial T}{\partial y}\right) + \frac{\partial}{\partial z}\left(k\frac{\partial T}{\partial z}\right) + \rho H_f\frac{\partial f_s}{\partial t} \tag{21}$$

Considering a Lagrangian frame of reference, where the slice moves along the caster in the direction of casting (z direction) at casting speed V_z with no velocity in x and y directions, implies $V_x = 0$ and $V_y = 0$.

$$\frac{\partial}{\partial x}\left(k\frac{\partial T}{\partial x}\right) = k\frac{\partial^2 T}{\partial x^2} + \frac{\partial k}{\partial T}\left(\frac{\partial T}{\partial x}\right)^2 \tag{22}$$

Assuming the product of variation of k with temperature and variation of temperature with y and z directions is negligible in y and z directions respectively, the governing equation is simplified as,

$$\rho C_p\frac{\partial T}{\partial t} = k\frac{\partial^2 T}{\partial x^2} + \frac{\partial k}{\partial T}\left(\frac{\partial T}{\partial x}\right)^2 + k\frac{\partial^2 T}{\partial y^2} + k\frac{\partial^2 T}{\partial z^2} + \rho H_f\frac{\partial f_s}{\partial t} \tag{23}$$

Scaling:

Scaling is performed on the governing equation by creating dimensionless variables for x, y, z, t and T as follows,

$$x^* = \frac{x}{L_x};\ y^* = \frac{y}{L_y};\ z^* = \frac{z}{L_z};\ t^* = \frac{t}{t_c};\ \theta = \frac{T - T_{min}}{T_{max} - T_{min}} \tag{24}$$

Where L_x is the thickness of the slab (m), L_y is the width of the slab (m), L_z is the length of the mold (m) and t_c is characteristic time (s).

$$\frac{\rho C_p \Delta T}{t_c}\frac{\partial \theta}{\partial t^*} = \frac{k\Delta T}{{L_x}^2}\frac{\partial^2 \theta}{\partial {x^*}^2} + \frac{k\Delta T}{{L_x}^2}\frac{\partial k \partial \theta}{\partial {x^*}^2} + \frac{k\Delta T}{{L_y}^2}\frac{\partial^2 \theta}{\partial {y^*}^2} + \frac{k\Delta T}{{L_z}^2}\frac{\partial^2 \theta}{\partial {z^*}^2} + \frac{\rho H_f \partial f_s}{\partial t} \tag{25}$$

Rearranging the terms after multiplying by $\frac{{L_z}^2}{k\Delta T}$

$$\frac{\rho C_p}{t_c}\frac{{L_z}^2}{k}\frac{\partial \theta}{\partial t^*} = \frac{{L_z}^2}{{L_x}^2}\frac{\partial^2 \theta}{\partial {x^*}^2} + \frac{{L_z}^2}{{L_x}^2}\frac{\partial k \partial \theta}{\partial {x^*}^2} + \frac{{L_z}^2}{{L_y}^2}\frac{\partial^2 \theta}{\partial {y^*}^2} + \frac{\partial^2 \theta}{\partial {z^*}^2} + \frac{{L_z}^2}{k\Delta T}\frac{\rho H_f \partial f_s}{\partial t^*} \tag{26}$$

With Thermal Diffusivity $\boldsymbol{\alpha} = \frac{\boldsymbol{k}}{\boldsymbol{\rho C_p}}$; Peclet Number $\boldsymbol{Pe_L} = \frac{{\boldsymbol{L_z}}^2}{\boldsymbol{\alpha t_c}}$; Stefan Number $\boldsymbol{Ste_L} = \frac{\boldsymbol{C_p \Delta T}}{\boldsymbol{H_f}}$, the governing equation becomes,

$$Pe_L\frac{\partial \theta}{\partial t^*} = \frac{{L_z}^2}{{L_x}^2}\frac{\partial^2 \theta}{\partial {x^*}^2} + \frac{{L_z}^2}{{L_x}^2}\frac{\partial k \partial \theta}{\partial {x^*}^2} + \frac{{L_z}^2}{{L_y}^2}\frac{\partial^2 \theta}{\partial {y^*}^2} + \frac{\partial^2 \theta}{\partial {z^*}^2} + \frac{Pe_L}{Ste_L}\frac{\partial f_s}{\partial t^*} \tag{27}$$

Substituting the material properties and process dimensions as in Table VII in the above equation,

$$9373.83\ \frac{\partial\theta}{\partial t^*} = 100\frac{\partial^2\theta}{\partial x^{*2}} + 100\frac{\partial k\partial\theta}{\partial x^{*2}} + 0.44\frac{\partial^2\theta}{\partial y^{*2}} + \frac{\partial^2\theta}{\partial z^{*2}} + 2206.28\frac{\partial f_s}{\partial t^*} \quad (28)$$

Table VII Material properties and process dimensions for scaling

Property	Value
Melting temperature, T_m	1550 ^{o}C
Atmospheric temperature, T_{atm}	35 ^{o}C
Casting speed, V_c	0.05 m/s
Latent heat , H_f	271 kJ/kg
Thermal conductivity, k_{steel}	30 W/m-K
Density, ρ_{steel}	7400 kg/m^3
Specific heat, C_{psteel}	760 J/kg-K
Thickness of the slab, L_x	100 mm
Width of the slab, L_y	1500 mm
Length of the mold, L_z	1000 mm

Numerical coefficients of the second and third terms on the right hand of the equation are negligible compared to the first term. Thus, the change of temperature with respect to y and z directions can be treated as negligible in the continuous casting of steel. Neglecting the third term due to the high Pe number of the process, enables the treatment of the system as a transient system with a moving slice domain in a Lagrangian reference frame.

Thus the simplified governing equation in the solidifying steel slice is

$$\rho C_p \frac{\partial T}{\partial t} = k \frac{\partial^2 T}{\partial x^2} + \frac{\partial k}{\partial T}\left(\frac{\partial T}{\partial x}\right)^2 + \rho H_f \frac{\partial f_s}{\partial t} \tag{29}$$

3.2.3. Analytical solution

An analytical solution to the above governing equation, as given in Appendix C, can be obtained by solving conduction equations in each phase, and in the mold, by employing the Stefan Condition [64] and furthermore assuming constant properties, which further allows the temperature-dependent thermal conductivity term to be neglected from Equation 29:

$$\left(\emptyset \exp(\emptyset^2) + \frac{c_{p_s}(T_m - T_\infty)}{L_f\sqrt{\pi}} \frac{\exp\left[\left(1 - \frac{\alpha_s}{\alpha_l}\right)\emptyset^2\right]}{\left[\operatorname{erfc}\left(\emptyset\sqrt{\frac{\alpha_s}{\alpha_l}} - 1\right)\right]} \sqrt{\frac{k_l \rho_l c_{p_l}}{k_s \rho_s c_{p_s}}} \right) \cdot \left(\operatorname{erf}(\emptyset) + \sqrt{\frac{k_s \rho_s c_{p_s}}{k_m \rho_m c_{p_m}}} \right) = \frac{c_{p_s}(T_m - T_o)}{L_f\sqrt{\pi}} \tag{30}$$

where $\emptyset$ is the parameter for calculating solution, k is thermal conductivity (W/m-k), ρ is density (kg/m^3), and $\mathbf{C_p}$ is specific heat (J/kg-K) with subscripts s, l, m for solid steel, liquid steel and mold respectively, L_f is latent heat of steel (J/kg), q is heat flux (W/m^2), T_s is steel shell surface temperature (°C), T_o is cold face temperature of the mold (°C), T_m is melting temperature of steel (°C) and $\mathbf{T}_\infty$ is pour temperature (°C).

The interface surface temperature is given by

$$T_s = \frac{T_o\sqrt{k_m \rho_m c_{p_m}}\operatorname{erf}(\emptyset) + T_m\sqrt{k_s \rho_s c_{p_s}}}{\sqrt{k_m \rho_m c_{p_m}}\operatorname{erf}(\emptyset) + \sqrt{k_s \rho_s c_{p_s}}} \tag{31}$$

The shell thickness as a function of time can be obtained from

$$\delta(t) = 2\emptyset\sqrt{\alpha_s t} \tag{32}$$

3.2.4. CON1D

CON1D is a Fortran program which models heat transfer and solidification in continuous casting. It includes 1-D transient finite-difference calculation of heat conduction within the solidifying shell coupled with 2-D steady-state heat conduction in the mold wall, or radiation, convection, and roll-conduction heat losses from the strand surface when below the mold in the spray cooling zones.

The governing equation for determining the temperature in the solidifying steel shell moving down along the length of the caster is the 1-D transient heat conduction equation.

$$\rho_{steel} {C_p}^*_{steel} \frac{\partial T}{\partial t} = k_{steel} \frac{\partial^2 T}{\partial x^2} + \frac{\partial k_{steel}}{\partial t}\left(\frac{\partial T}{\partial x}\right)^2 \tag{33}$$

where ρ_{steel} is density (kg/m^3), $\mathbf{C_p}^*_{\mathbf{steel}}$(J/kg-K) is the effective specific heat for the solidifying steel which includes both sensible heat and latent heat defined as follows and k_{steel} is thermal conductivity (W/m-k).

$${C_p}^* = \frac{dH}{dT} = C_p - L_f \frac{\partial f_s}{\partial t} \tag{34}$$

In the CON1D model [14], the Lagrangian frame of reference is adopted which takes advantage of the high Peclet number of the continuous casting process rendering axial heat conduction negligible that was presented in the previous section. The effect of non-uniform distribution of superheat is incorporated using the results from 3-D turbulent fluid flow calculations within the liquid pool. The material properties varying with temperature according to composition-dependent phase fractions are inherently programmed in the CON1D [65]. The latent heat of solidification is incorporated using an efficient enthalpy method and a post-time-step correction. Microsegregation effects are included via a modified Clyne-Kurz model [66].

Boundary conditions:

The simulation domain is the solidifying steel slice through the liquid steel and solid shell moving down the caster at casting speed, V_c. The boundary conditions for the solidifying strand are as follows:

- q_{sh} is the heatflux due to superheat on the innerside of the strand.
- $-k\frac{\partial T}{\partial z} = h_{int}(T_s - T_{int})$ in the mold considering interface.
- $-k\frac{\partial T}{\partial z} = (h_{spray} + h_{rad_spray} + h_{conv} + h_{roll})(T_s - T_{amb})$ in the secondary cooling spray zones.

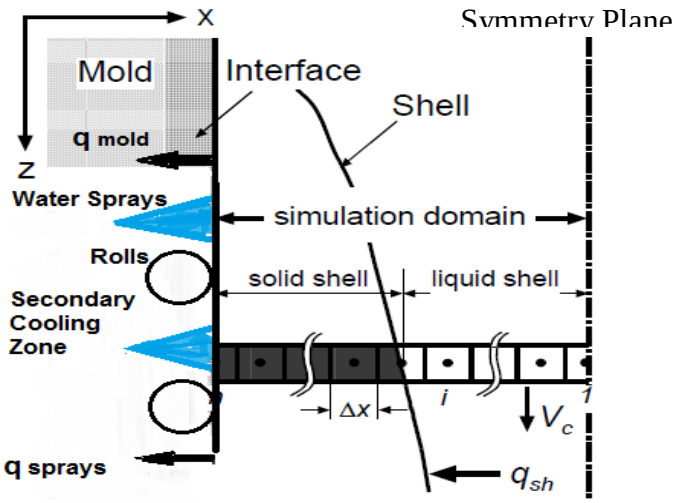

Figure 3.2 Simulation domain: Solidifying slice moving along the length of the caster from meniscus to the torch cut off point

Heat transfer in mold:

All of the equations governing the various complex phenomena involving the heat extraction in the mold region are clearly explained in the work by Ya Meng [14] et al. In the current parametric study using CON1D, average mold heat flux is considered which is calculated from the following empirical correlation.

$$Q = 3.128 \cdot 10^5 \cdot V_c^{0.620} \cdot T_{melt}^{-1.845} \cdot W^{0.072} \cdot \mu^{-0.017} \cdot \left(1 - 0.152 \cdot \exp\left(-0.021 \cdot \left(\frac{\frac{C_A + C_B}{2} - \%C}{(C_B - C_A)} \right)^2 \right) \right) \quad (35)$$

where Q is the mold heat flux (MW/m^2). The measured variables that are needed for the prediction, are casting speed V_c (m/min), mold slag viscosity μ (Pa-s), break point temperature of the powder T_{break} (°C), width of the slab W (mm) , carbon content of the steel: %C (weight %), C_A and C_B for determining the range of peritectic steels.

Heat transfer in secondary cooling zones:

In continuous casting of steel, heat transfer in the secondary cooling zones is a complex phenomenon. From the schematic of the heat transfer in the spray zones region as shown in Figure 3.3, heat extraction is a maximum directly beneath the spray nozzle assuming centered between the rolls followed by the roll and shell contact region [67]. The relative size of these maxima is governed by the fraction of heat leaving through the rolls relative to that removed by spray cooling water. Thus the surface temperatures are comparatively less at these regions compared to the rest of the strand where the heat extraction is only by natural convection and radiation.

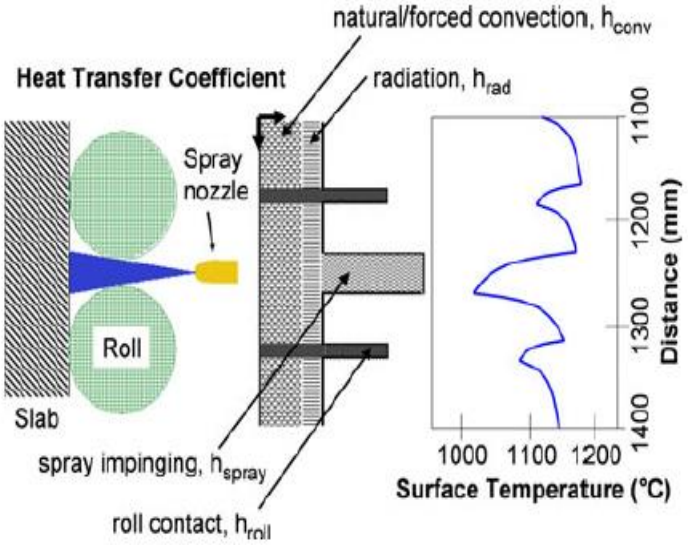

Figure 3.3 Schematic of heat transfer in spray zones

In the secondary cooling zones, heat flux from the strand surface varies greatly between each pair of support rolls according to spray nozzle cooling (based on water flux), h_{spray}; radiation, h_{rad_spray}; natural convection, h_{conv}; and heat conduction to the rolls, h_{roll} [68]. Heat transfer is governed mainly by the spray heat transfer coefficient which is calculated from the average spray water flow rate from the nozzle at each spray zone. Various parameters for spray cooling heat extraction are based on several previous experimental studies. Heat extraction by sprays, h_{spray} (W/m^2-K), is obtained from the work of Nozaki et al[53]

$$h_{spray} = A * Q_{water}^{c} * (1 - b * T_{spray}) \quad (36)$$

where Q_{water} (L/m^{2}s) is water flux in spray zones and T_{spray} is the temperature of the spray cooling water (°C). Nozaki's correlation employs A = 0.3925, c = 0.55 and b = 0.0075. Beyond the spray zones, heat transfer simplifies to radiation and natural convection.

Heat transfer coefficient for radiation, $\mathbf{h_{rad_spray}}$ (W/m^2-K), is calculated as,

$$h_{rad_spray} = \sigma \cdot \varepsilon_{steel}(T_{sK} + T_{ambK})(T^2{}_{sK} + T^2{}_{ambK}) \quad (37)$$

Where T_{sK} and T_{ambK} are strand surface and ambient temperatures respectively expressed in Kelvin. Heat transfer coefficient (h_{conv}) for natural convection is treated as a constant of 8.7W/m^{2}K everywhere. The heat extraction into the rolls is obtained from:

$$h_{roll} = \left(\frac{(h_{rad_spray} + h_{conv} + h_{spray}) \cdot L_{spray} + (h_{rad_spray} + h_{conv}) \cdot (L_{spray\ pitch} - L_{sp}}{L_{roll\ contact} \cdot (1 - f_{roll})} \right. \cdot f_{roll} \quad (38)$$

Heat extraction into the rolls is calculated based on the fraction of heat extraction to the rolls, f_{roll}, which is calibrated for each spray zone.

It is easy to calibrate CON1D model with mold thermocouples as the model outputs temperatures of mold thermocouples at locations as desired by the user. CON1D is quite helpful

in determining various output parameters like shell thickness, strand temperatures, heat flux leaving the shell etc., which otherwise is very difficult to measure. It is known for its user friendly features and less computational time to run.

In this work, shell thickness is defined by a liquid fraction of 0.3. Good accuracy is achieved using a grid spacing of approximately 0.05 mm and finite difference time-stepping size of 0.03S. With this grid spacing and time step, CON1D solves the equations using explicit central finite-difference algorithm which takes approximately 10 sec for each run.

3.2.5. Validation of CON1D with analytical solution and plant results

Validation of the numerical solution from CON1D model is performed using analytical solution [64]. A test problem for 1D transient heat conduction in the solidifying strand is defined for a 100 mm thick slab over a total mold length of 5000mm. Since analytical solution is for pure material, almost pure iron with 0.005% carbon with no other alloying elements is considered in CON1D. Constant material properties including density, thermal conductivity, specific heat, melting temperature, latent heat in steel and corresponding properties in the mold are listed in Table VIII.

A constant shell surface temperature of 1000°C is considered in the analytical solution. To maintain similar conditions in the numerical model, CON1D, the heat flux profile from the analytical solution is provided as input to CON1D shown in Figure 3.4 and Figure 3.5. Then surface temperature and shell thickness of the strand between the two solutions are compared.

Table VIII Input parameters for validation of CON1D solution with analytical solution

Property	Value
Melting temperature, T_m	1535.6 ^{o}C
Pour temperature, T_{pour} / T_{∞}	1550 ^{o}C
Mold temperature at other end of copper mold, T_o	683.71 ^{o}C
Surface temperature, $T_{surface}$	1000.08 ^{o}C
Casting speed, V_c	2 m/min
Latent heat , L_f	243 kJ/kg
Thermal conductivity, k_s / k_l	34.5 W/m-K
Density, ρ_s / ρ_l	7400 kg/m^3
Specific heat, C_{ps} / C_{pl}	760 J/kg-K
Thermal conductivity, k_m	315 W/m-K
Density, ρ_m	8960 kg/m^3
Specific heat, C_{pm}	386 J/kg-K

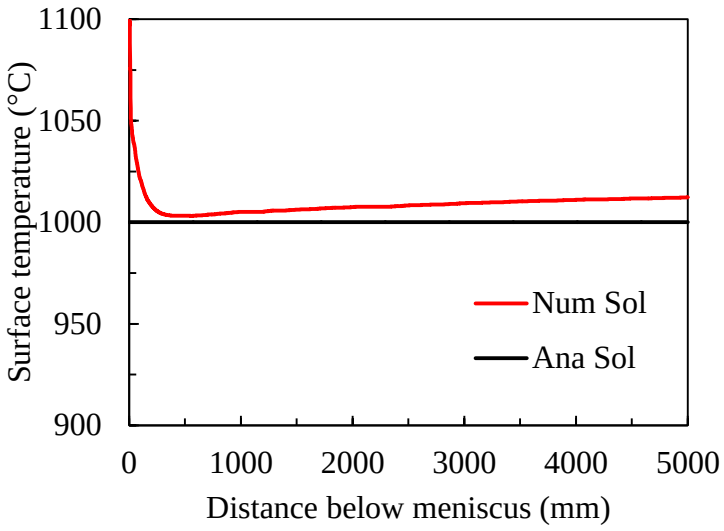

Figure 3.4 Validation of CON1D solution with analytical solution: Surface temperature of 1000°C is given as input

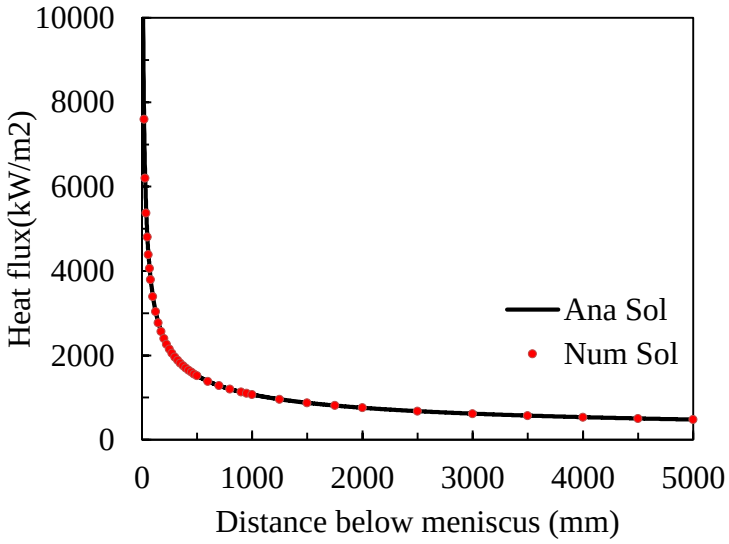

Figure 3.5 Validation of CON1D solution with analytical solution: Heat flux for a surface temperature of 1000°C as input

Figure 3.6 shows the growth of shell thickness down the mold for CON1D solution and analytical solution. Assuming symmetry at the center of 100 mm thickness, the RMS error for the shell thickness over a length of 5000 mm for a thickness of 50 mm is 0.950 mm. The numerical model roughly agrees with the analytical solution.

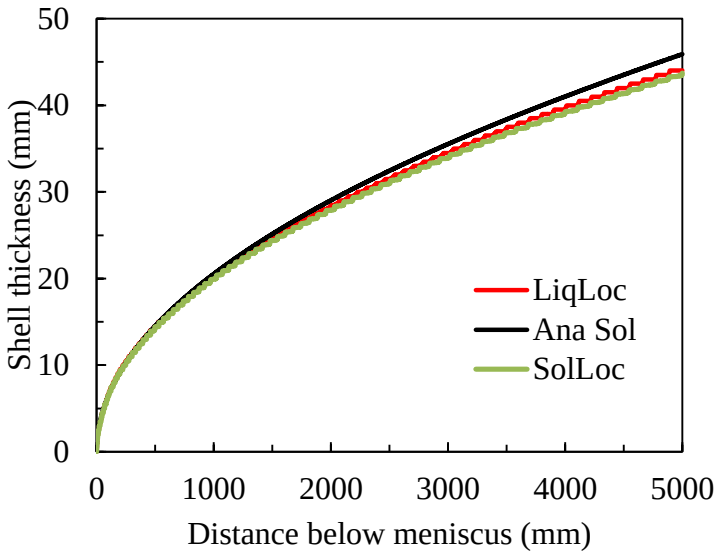

Figure 3.6 Validation of CON1D solution with analytical solution: Shell thickness of strand as output

Model validation with plant results

Before applying it to optimize a real caster, the CON1D model must be validated with actual plant measurements from that caster. CON1D was able to predict the two whale defect incidents which occurred in 2004 and 2006 at the Nucor Decatur steel mill of interest in this work [67]. The input conditions for these two events with complete details of the input files are run in CON1D.

The results in Figure 3.7 and Figure 3.8 indicate that CON1D correctly predicts the whale cases where the metallurgical length is shown beyond the exit of the last roll. Thus, before actual operation, CON1D results can be very insightful in preventing whales in avoiding accidents and in saving cost and time.

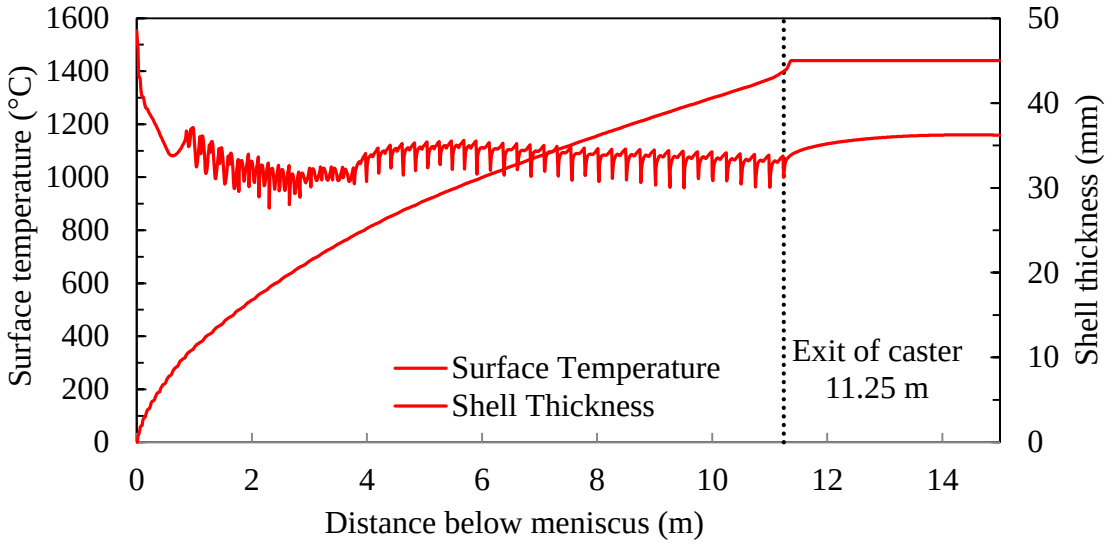

Figure 3.7 2004 whale case: CON1D predicting metallurgical length beyond the end of caster

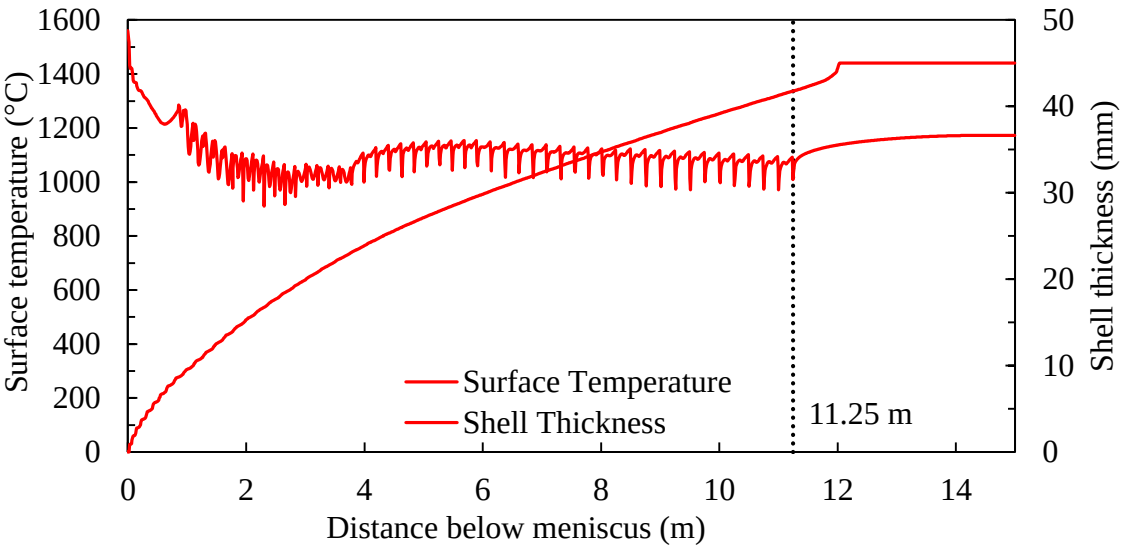

Figure 3.8 2006 whale case: CON1D predicting metallurgical length much beyond the end of caster

3.2.6. Thin slab caster at Nucor Decatur

Secondary cooling systems are designed based on the amount of heat to be extracted from the surface of the solidifying strand as it passes down the casting machine. The caster contains a

number of spray zones with specific nozzle arrangements and water flow rates in each zone. These are highly specific to a particular casting machine and are operated based on casting speed, grade of the slab etc., to regulate surface temperature of the strand.

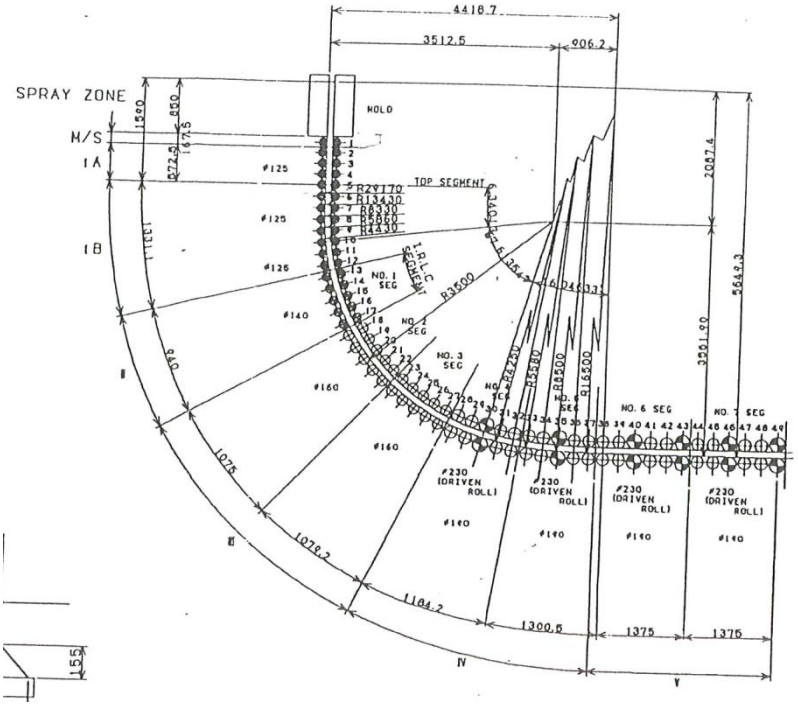

Figure 3.9 Schematic of Nucor Decatur caster

The nozzle layout design in the secondary cooling zones at Nucor Steel mill in Decatur is shown in Figure 3.9. The entire spray region is divided into 7 different zones namely M/S, IA, IB, II, III, IV and V with the foremost starting at the exit of the mold. Each zone has a specified nozzle quantity, row arrangement, and maximum and minimum water flow rates per nozzle (l/min) as given in the above Figure 3.9. For the first two zones, namely M/S and IA, there are spray zones on the narrow side, for enhancing cooling at the mold exit. These are not accounted for in the model for simplification and since the domain is a line that moves down the centerline symmetry plane of the casting machine, these may not have much effect. The zones IA, IB and II have a central spray system followed by two outer spray systems that are different from the rest of the zones. In practice, depending on the width of the slab, inner nozzles are operated initially followed by the outer nozzles depending on the requirement. In the current work, spray cooling is optimized to determine feasible casting speed ranges considering only the inner nozzles which affect the centerline.

3.2.7. Procedure

CON1D is employed to determine the feasible range of casting speeds and critical speed for a critical super heat with optimum water flow rates in the secondary cooling zones for a thin slab caster satisfying the following sets of constraints.

- Constraint set 1: Maintain metallurgical length (ML) between straightener and end of containment.

- Constraint set 2: Maintain ML (satisfy constraint 1) and also keep surface temperature (T_s) above the ductility trough (T_s > 900 °C)

If the strand is fully solidified before the exit of the straightener, unbending the solid strand is difficult and can result in stress-related cracks. This also causes damage to machine affecting the alignment of rolls. Thus, constraint set 1 suggests maintaining metallurgical length beyond the straightener. Also, if the strand contains solidifying liquid inside and is not fully solidified by the exit of the caster, then bulging of the strand occurs and results in the major catastrophic defect called a whale. To avoid this, metallurgical length is to be maintained before the exit of the caster which comprises the second part of constraint 1.

In steels which contain high levels of soluble aluminum, niobium and / or vanadium precipitates, the ductility of the solidifying steel decreases significantly between 700°C and 900°C leading to the formation of transverse cracks [57] if also subjected to excessive tensile stress. Although this phenomenon is most predominant in the bender and straightener, constraint 2 suggests avoiding the ductility region between 700 °C and 900 °C until the exit of the straightener in secondary cooling zones.

The strand outer surface temperature and shell thickness are predicted for a 90 mm thick and 1396 mm wide slab for three different compositions of steel as given below in Table IX.

Table IX Different compositions considered in the study

Grade	Liquidus Temperature (°C)	Solidus Temperature (°C)
Low Carbon Steel (0.03%) 0.03%C, 0.08%Mn, 0.01%S, 0.015%P, 0.005%Si, 0.01%Cr, 0.01%Ni, 0.01%Cu, 0.00%Mo, 0.05%Ti, 0.04%Al, 0.000%V, 0.00%N, 0.00%Nb)	1531.5	1509.7
Peritectic (0.1011%) (0.1011%C, 2.0666%Mn, 0.0027%S, 0.0102%P, 0.0722%Si, 0.0096%Cr, 0.00%Ni, 0.00%Cu, 0.2985%Mo, 0.0046%Ti, 0.644%Al, 0.000%V, 0.0058%N, 0.00%Nb)	1515.5	1474.7
High Carbon Steel (0.24%) 0.24%C, 1.09%Mn, 0.0019%S, 0.014%P, 0.175%Si, 0.04%Cr, 0.04%Ni, 0.087%Cu, 0.01%Mo, 0.002%Ti, 0.039%Al, 0.001%V, 0.0076%N, 0.035%Nb	1508.5	1453.5

All the temperature-dependent material properties are calculated by CON1D using inbuilt programs. An ambient temperature of 298 K (25°C) is considered. Natural convection is treated as a constant of 8.7 W/m^{2}K. In the secondary cooling zones, optimum water flow rates in the range of maximum and minimum water flow rates as provided in the nozzle layout drawing are considered satisfying the constraints considered. In practice, for the three spray zones in the secondary cooling namely IA, IB and II, only central spray systems are employed at first and then the outer spray systems depending on the strand width and other conditions. In this work, which considers only the centerplane, only the spray-zone widths of central spray

systems and the corresponding water flow rates for the nozzles in those central zones are considered. All other input parameters and conditions considered in this study are to be provided as input files to CON1D. Mold heat removal which is a function of casting speed, % carbon and mold powder properties is calculated using empirical equation (35) given above.

Next, the feasibility of changing strand patterns is explored by changing water flow rates in secondary cooling zones alone satisfying given constraint sets using this CON1D model.

3.3. Results and Discussion

3.3.1. Feasible range of casting speeds

The validated CON1D model was first applied to determine the maximum feasible range of casting speeds which satisfy constraint set 1, for a fixed set of typical operating conditions, including superheat of 40.3^{o}C. With increasing casting speed, the strand remains in the casting machine for shorter time period, so the time for solidification and heat extraction reduces. For the same cooling conditions, this increases metallurgical length. So, to maintan metallurgical length within roll containment, increasing water flow rates to their maximum levels to maximize surface heat extraction enables slight extra increase in maximum castging speed.

As casting speed decreases, residence time of strand inside the caster increases, which raises total heat removed for the same cooling conditions. This results in faster solidification of the strand and reduced metallurgical length. To maintain metallurgical length beyond the straightener exit to avoid stress related cracks, decreasing water flow rate to their minimum levels to decrease the solidfication rate enables slightly lower minimum casting speed and still satisfies constraint set 1.

Thus, to satisfy constraint set 1 by keeping metallurgical length in the desired range, Table X shows the maximum water flow rates, applied at maximum casting speed, and the minimum water flow rates employed at the minimum speed. For the Nucor thin slab caster with high carbon steel, the casting speed can be varied from 2.45 to 4.0 m/min at these extreme conditions and satisfying constraint set 1. The corresponding temperature profiles and shell thickness profiles are shown in Figure 3.10. Even though the casting speed is higher, the temperature

profile at the upper limit of 4.0m/min is colder than at the lower speed, owing to the smaller water flow rates.

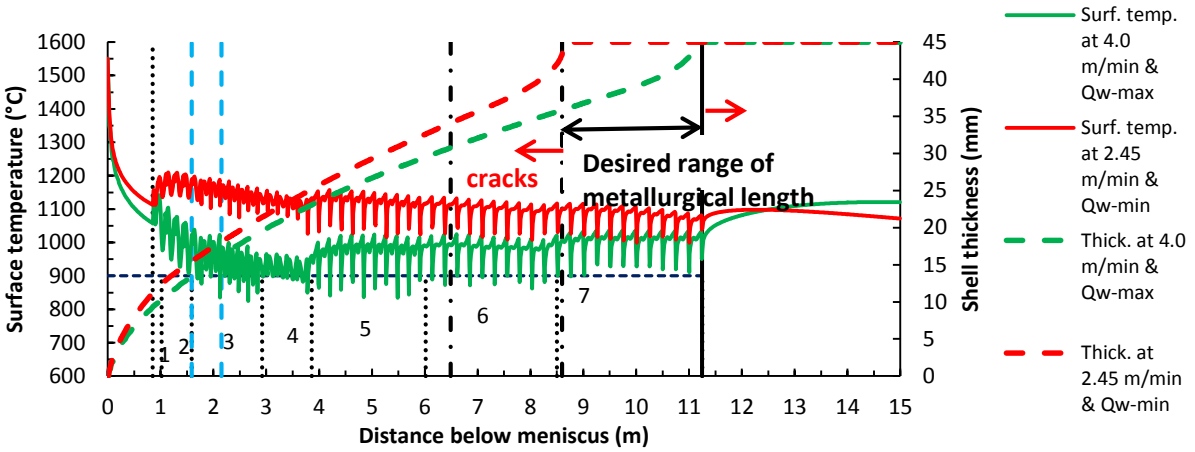

Figure 3.10 Profiles at limits of feasible casting speed range of 2.4 to 4.0 m/min with constraint 1 (metallurgical length in the desired range)

When operating at the calculated maximum casting speed with maximum water flow rate, a slight decrease in water flow rate will raise surface temperatures of the strand resulting in metallurgical length beyond 11.246 m causing liquid core beyond containment. Similarly, when operating at the calculated minimum casting speed, a slight increase in water flow rates will enhance heat flux leading to metallurgical length shorter than 8.5 m, moving some fully solid strand into the straightener, causing stress related cracks.

As shown in Figure 3.10, the surface temperatures of the strand are falling below 900°C in zones 3,4,5 and 6. This could cause transverse cracks, which could be avoided by satisfying constraint set 2. Simply lowering the water flow rates in these spray zones to raise the surface temperatures would result in increased metallurgical length beyond the caster exit. So, the maximum casting speed has to be reduced and the spray pattern optimized according to the flow rates in Table X, to simultaneously decrease the metallurgical length while maintaing temperatures above ductility trough (ie above 900 °C). On the other hand, the minimum casting speed for constraint set 1 produces temperatures well above the ductility trough, so also satisfies constraint set 2. Thus, to satisfy both sets of constraints, the casting speed can be varied

in the range of 2.45 to 3.75 m/min for high carbon steel. The resulting temperature and shell thickness profiles down the caster for these two extremens are shown in Figure 3.11.

Table X Optimum water flow rates in secondary cooling zone

Zone	Optimum water flow rates (L/min/row)				
	Constraint set 1 (All %C)		Constraint set 2		
	Max.	Min.	High Carbon	Peritectic	Low Carbon
MS	120	50	120	120	120
Z1A	240	30	210	230	240
Z1B	150	18	80	70	100
ZII	60	9	40	50	50
ZIII	60	9	30	30	30
ZIV	40	6	30	30	30
ZV	24	4	24	24	24

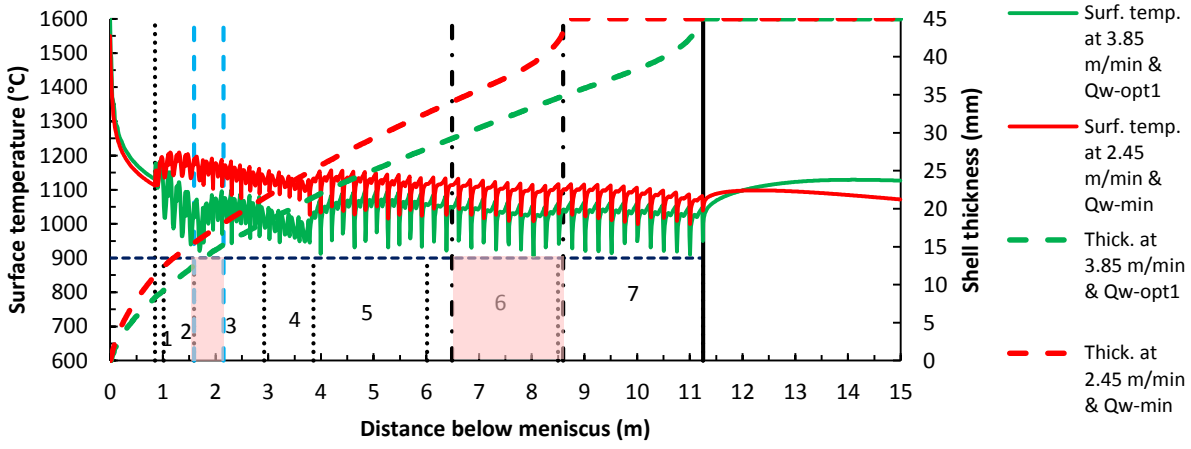

Figure 3.11 Casting speed can be varied from 3.75 to 2.45 m/min satisfying 2 constraints

The above analysis has been repeated for peritectic and low carbon steel grades, satisfying constraint set 1 and both constraint sets, with optimum flow water flow rates. The calculated

maximum and minimum casting speeds for all the three grades of steel for the Nucor thin slab caster is shown in Figure 3.12. The results indicate that range of casting speeds for high carbon steel is higher compared to low and peritectic steel grades by 3.7 % for the caster studied. The results also showed that the range of casting speeds for satisfying constraint set 2 is smaller by at least 11.11% than for constraint set 1as less water flow rates are employed to avoid ductility troughs in the earlier case.

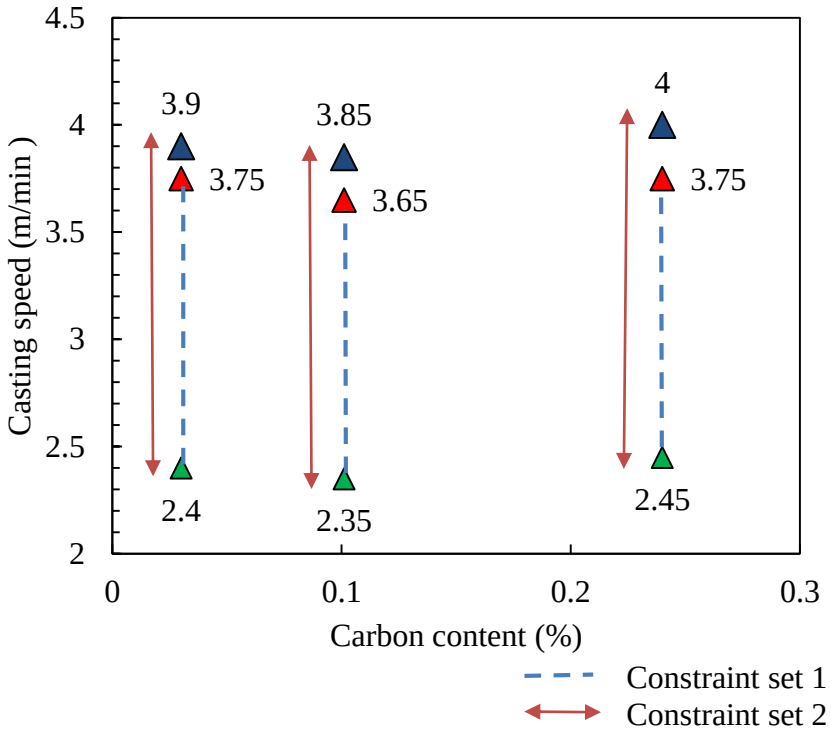

Figure 3.12 Range of casting speeds for low, peritectic and high carbon steels

3.3.2. Critical casting speeds for critical super heats

During casting, higher casting speeds are usually preferred to increase production rate, so determing the critical maximum casting speed for a given super heat is very useful to maximize production of good quality steel slabs. Thus, in this section the model analysis using CON1D that was presented in the previous section is extended for the range of superheats experienced in typical operation.

Increase in either casting speed or super heat will result in higher heat content rate to extract from the solidifying strand. Thus, to determine critical casting speeds for a given superheat, maximum water flow rates are employed when satisfying only constraint 1.

But, with maximum water flow rates, any further increase in casting speed or superheat will result in metallurgical length beyond the caster which would produce a whale event. As described in the previous section, with maximum water flow rates, the surface temperatures of the strand fall in the undesired ductility trough zone. Thus, for satisfying both the constraints, (constraint set 2), optimum water flowrates are found by numerical investigation.

For higher carbon steel, critical casting speeds for typical superheats are presented in Figure 3.13, satisfying constraint set 1 only, and constraint set 2 (both constraints).

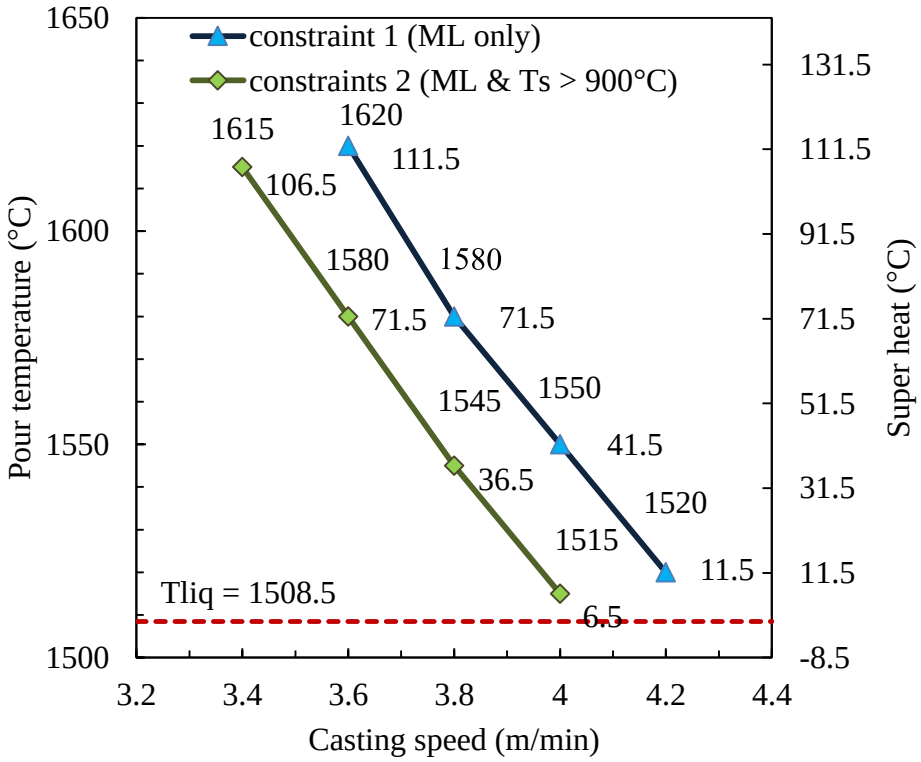

Figure 3.13 Maximum casting speed at different superheats satisfying given constraints

Figure 3.13 shows that the maximum feasible superheat decreases with casting speed for both sets of constraints (1 or 2). Maximum casting speeds further decrease for 2 constraints, because

less water (compared to constraint1) must be used to keep temperatures above the ductility trough.

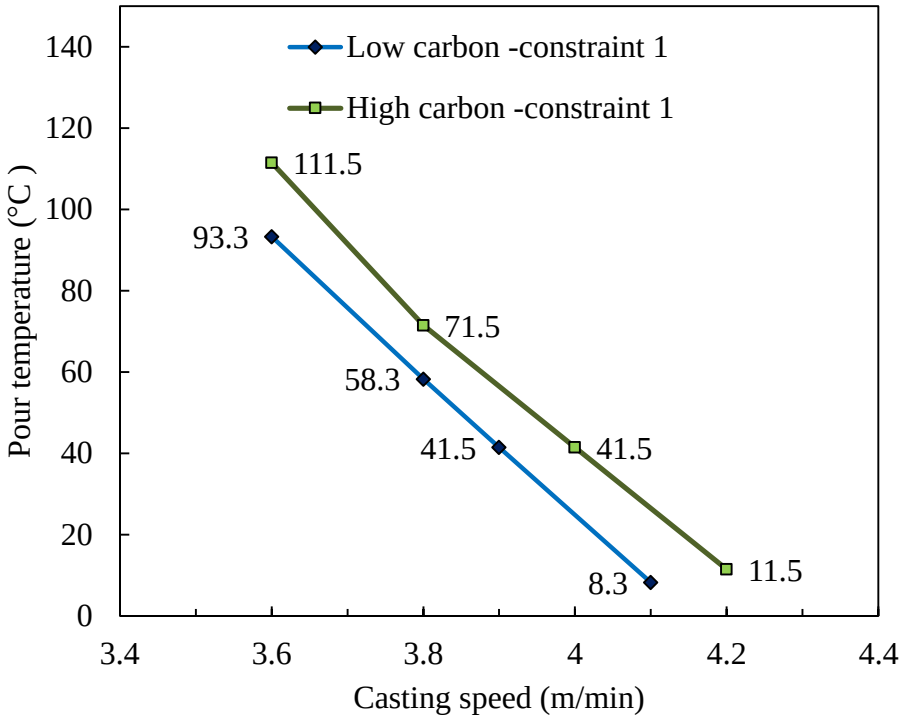

Figure 3.14 At a given casting speed, higher pour temperatures can be employed for high carbon steels compared to low carbon steels

Similarly, this analysis was repeated for low carbon steel satisfying constraint 1. Figure 3.14 compares the results with the two carbon contents. This shows that for a given super heat, the high carbon steels can be cast at greater speeds compared to those of low carbon. This is because of lower melting temperatures of high carbon steels compared to low carbon steels.

3.3.3. Investigating feasible secondary water spray patterns

The model is next applied to explore the importance of the spray pattern (relative flow rates in different zones) on the results presented in the previous sections. The different spray patterns employed at Nucor Decatur are developed as a function of casting speed. In this section, the

thin slab caster with high carbon steel operating at a speed of 3.3 m/min and super heat of 61.5^{o}C is investigated for spray pattern 1 as given in Table XI. The water flow rates are modified using one of the following two methods to adjust the flow rates in other spray zones for a given change in zone 2, as depicted in Figure 3.15.

- Method 1: For a given change in water flow rate in zone 2; zone 1 changes by half and other zones are kept constant.

- Method 2: For a given change in water flow rate in zone 2; zone 1 changes by half and other zones change in proportion to zone 2 (ie same percentage change in flow rate).

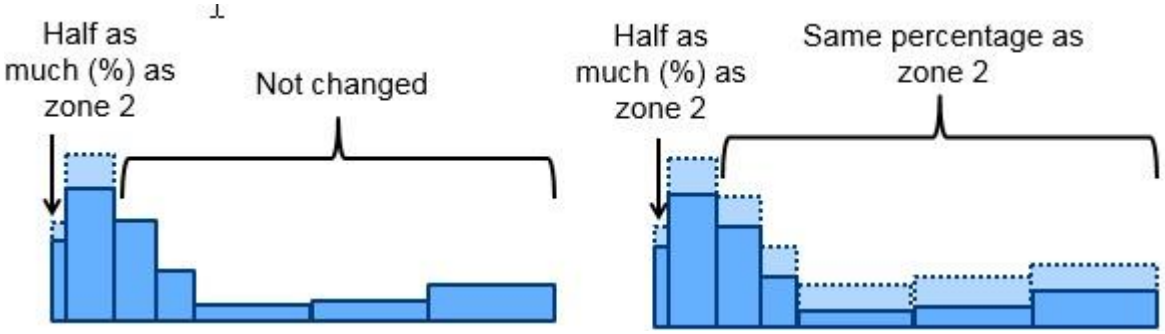

Figure 3.15 Two methods to change spray patterns in the secondary cooling zones

Table XI Spray pattern 1 for a casting speed of 3.3 m/min at Nucor Decatur caster

Zone No.	Zone starts (mm)	Water flow rate (l/min/row)
1	850	120
2	1017.5	180
3	1590	170
4	2921.1	60
5	3861.1	60
6	6015.3	40
7	8500	24

For the thin slab caster at Nucor Decatur, shell thickness and surface temperature profiles down the caster for the standard spray pattern 1 are shown in Figure 3.16. Using method 1 to adjust the spray pattern, the effect of increasing the flow rates to their maximum values (limited by zone 2) is shown in Figure 3.17. The corresponding effect of decreasing to minimum flow rates is shown in Figure 3.18. In both cases, the effect on metallurgical length is very small. And, although constraint set 1 remains satisfied, constraint set 2 is not.

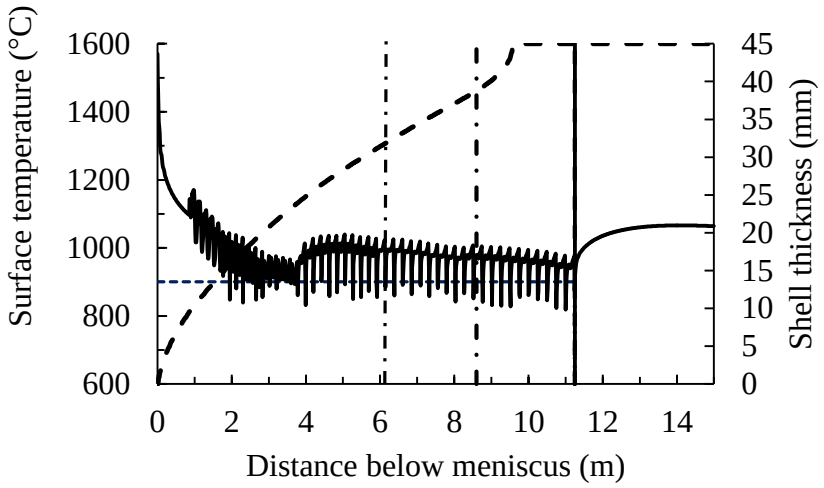

Figure 3.16 Caster profiles with spray pattern 1 at a casting speed of 3.3 m/min

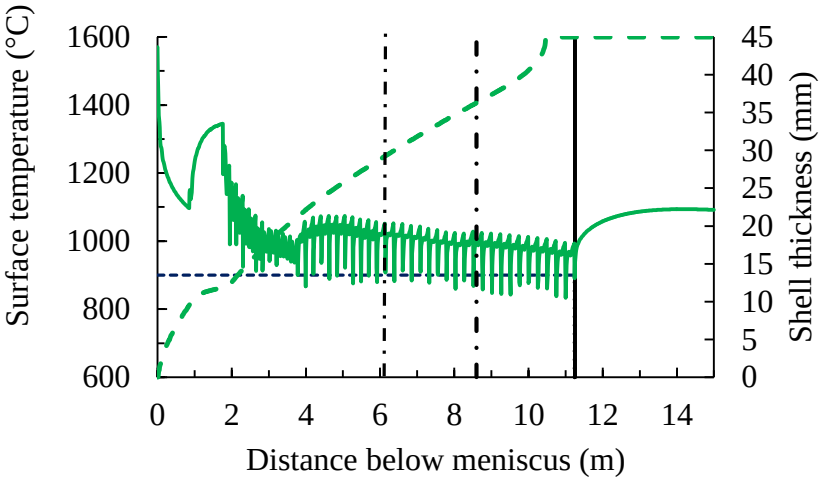

Figure 3.17 Caster profiles with spray pattern 1 modified using Method 1, with minimum water flow rate in zone 2

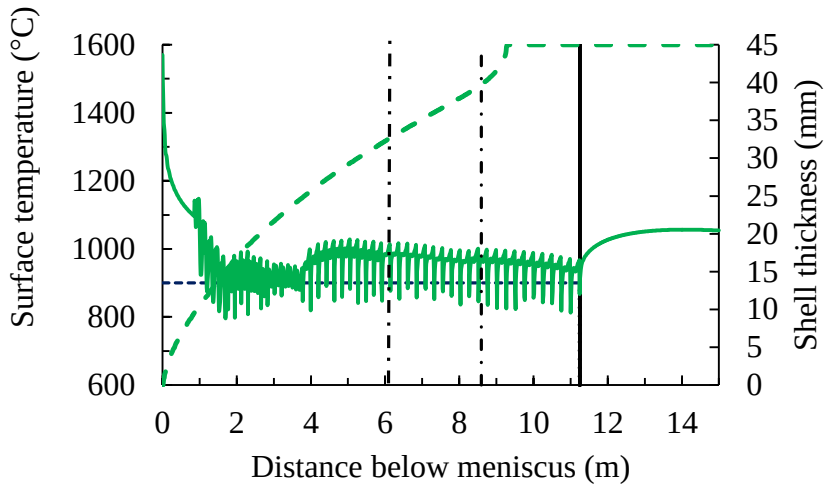

Figure 3.18 Caster profiles with spray pattern 1 modified using Method 1, with maximum water flow rate in zone 2

Using method 2 to adjust the spray pattern, the effect of decreasing the flow rates to their minimum values is shown in Figure 3.19. Water flow rate is reduced by 60% in every zone except the first. This is the greatest reduction in water flow rate that still satisfies both constraints (set 2).

Any further decrease in water flow rate will extend the metallurgical length beyond containment, causing whale defects, such as shown in Figure 3.20 for the minimum flow rates.

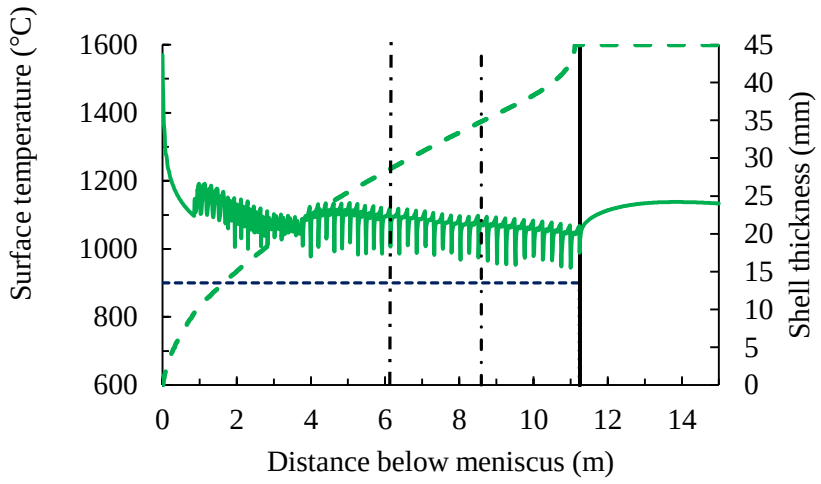

Figure 3.19 Caster profiles with spray pattern 1 modified using Method 2, with water flow rate in zone 2 as 40% of that of standard in zone 2

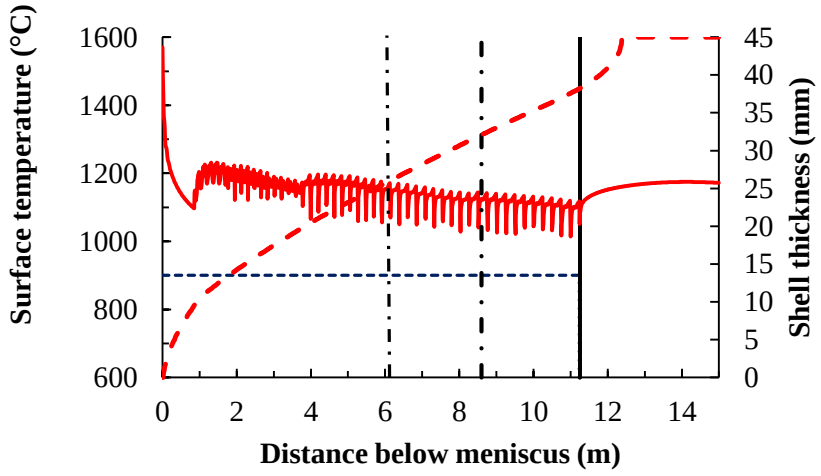

Figure 3.20 Caster profiles with spray pattern 1 modified using Method 2, with minimum water flow rate in zone 2

Next, method 2 was used to increase spray pattern 1 to the maximum water flow rate in zone 2 with corresponding changes in other zones. The results in Figure 3.21 show that this increment of water flow rate at this speed is still satisfies constraint set 1, but drops temperatures into the ductility trough so violates constraint set 2.

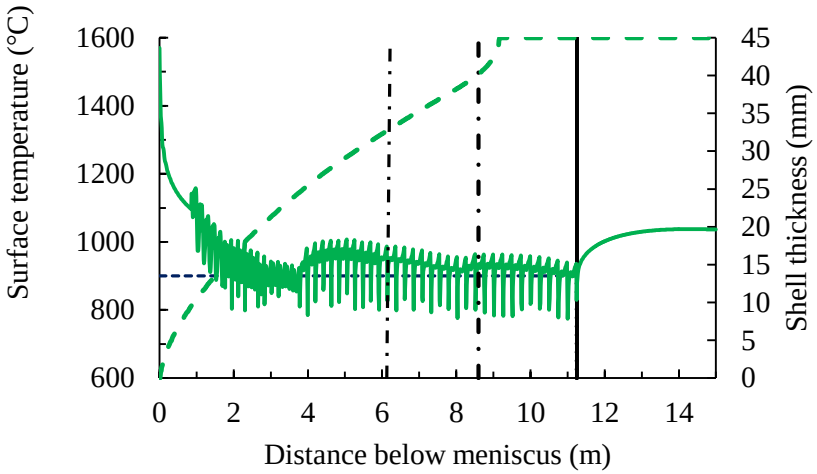

Figure 3.21 Caster profiles with spray pattern 1 modified using Method 2, with maximum water flow rate in zone 2

Further increasing water flow rate in zone 2 to 200% of the maximum water flow rate, the shell thickness results in Figure 3.22 show that even for this impossible situation, the metallurgical length would stay within the desired region, so constraint 1 is satisfied. Of course, constraint set 2 would be violated.

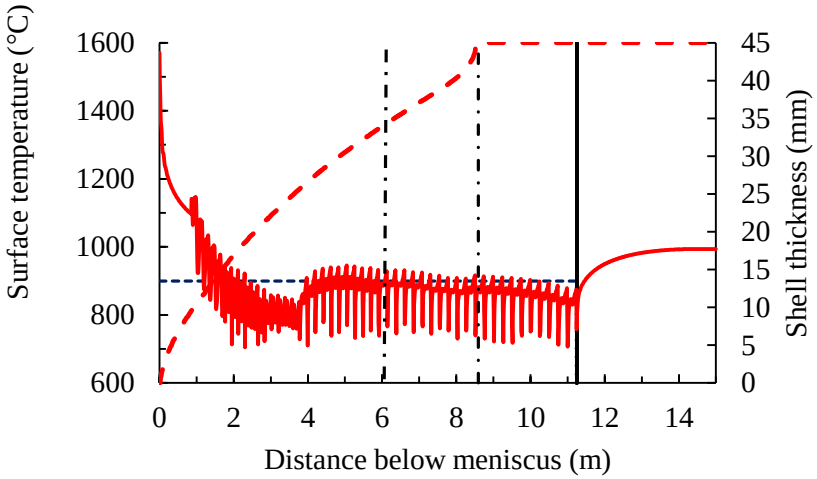

Figure 3.22 Caster profiles with spray pattern 1 modified using Method 2, with 200% of maximum water flow rate in zone 2

These results show that the constraints are relatively insensitive to water flow rates. Method 2 adjustment is preferred over method 1, because it has more effect on the metallurgical length, while making it easier to adjust flow rates and still satisfy the constraint sets.

3.4. Conclusions

To optimize the continuous casting process, it is essential to possess quantitative knowledge of how the various input parameters affect the production of high quality slabs. To accomplish this, two constraints are imposed in this work – one to maintain metallurgical length in the region between straightener to the caster exit; the other to regulate strand surface temperature profile avoiding ductility trough (700°c to 900°C). This work provides insights into the determination of range of casting speeds and combination of critical super heat with critical casting speed for the thin slab caster at Nucor steel mill for three different grades of the steel using CON1D program satisfying the given constraints sets. The results show that the range of casting speeds is wider for high carbon steels than for peritectic and low carbon steels by 3.7 %. The results showed that the range of casting speeds is smaller by at least 11.11% for satisfying constraint set 2 than satisfying 1 constraint as less water flow rates are employed to avoid ductility troughs in the earlier case. Irrespective of the grades of steel, as casting speed increases, corresponding critical superheat decreases and vice-versa as both result in higher heat content of the steel. This work further explores the feasibility of changing water flow rates with respect to standard patterns in the secondary cooling zones.

CHAPTER 4: CONCLUSIONS AND FUTURE WORK

This work has performed numerical analysis for controlling heat transfer in mold and secondary cooling zones in thin slab continuous casting machines. In the first part of the work, statistical analysis is carried out based on the wide database of plant measurements to determine correlation equations to predict mold heat flux. In the second part, numerical analysis is performed from CON1D simulations to determine feasible operating conditions by controlling secondary cooling sprays for high quality slabs in safe environment.

In the first part, average mold heat flux over the wide face of thin slab casting molds is investigated using measurements of eight casting variables. The analysis is performed for two different thin slab casters at Nucor steel mills. The effect of individual casting variables on mold heat flux is analyzed independently for both the casters. Then non-linear regression analysis is performed in MATLAB combining all the measurements of both casters. Different correlation equations to predict mold heat flux are determined as a function of casting variables in different combinations. Owing to lack of variety of data with respect to steel composition and powder properties, recommended simple equation is the model with casting speed alone based on entire Nucor data. The developed Nucor equation as a function of 5 casting variables comprising measurements from both Nucor and Tuscaloosa casters is predicting better for both the casters rather than individual models on different caster. This combined Nucor model is predicting better than the Cicutti equation, which was originally developed for a thick slab caster. Though characteristic to the plant, the developed model is expected to behave well on other casters. This work from plant measurements provide a greater understanding of mold thermal behavior.

In the future, the methodology presented here can be further applied to evaluate other important relationships and to extract other useful correlations from the “big data” that is continuously being collected and available in most casting operations. Analysis of casters with measurements on peritectic grades and additional mold powders is needed to develop a better, more general, correlation for mold heat flux. The developed correlation is ready to be evaluated at other casters, and the methodology to improve it can be extended easily to other casters.

In the second part of this work, feasible operating windows of casting speed are determined for a thin slab caster at Nucor Decatur for three grades by controlling secondary cooling sprays satisfying the given constraints. High productivity without comprising quality or safety is always an objective of the steel industry, which is applied in choosing conditions for the real process of continuous casting of steel. To optimize this process, it is essential to possess quantitative knowledge of how the various input parameters affect the production of high quality slabs. To achieve this, two constraints pertaining to controlling metallurgical length and surface temperature profile are considered. Sometimes desired exit temperature of the strand can also be a constraint as per the requirement of rolling operations to avoid reheating for saving energy. Also, feasibility of changing water flow rates corresponding to standard patterns in the secondary cooling zones are explored.

This work introduces the idea of using validated computational models to explore the production capabilities of real commercial casters, by determining the feasibile ranges of casting speeds combined with superheats and spray cooling rates to avoid different quality and production constraints, such as bending cracks and whale defects. The methodology should be extended to explore feasible operating windows for other caster operations, such as involving different slab thicknesses, secondary cooling configurations, and defect constraints.

The results of this work provide deeper insight for understanding different process parameters and their influence on heat transfer and solidification for optimizing the process of steel continuous casting for production of high quality slabs without defects.

REFERENCES

1. Thomas, B.G. Introduction to Continuous casting. Available from: http://ccc.illinois.edu/introduction/concast.html.
2. Mahapatra, R.B., et al., Mold Behavior and Its Influence on Quality in the Continuous-Casting of Steel Slabs .1. Industrial Trials, Mold Temperature-Measurements, and Mathematical-Modeling. Metallurgical Transactions B-Process Metallurgy, 1991. 22(6): p. 861-874.
3. Mahapatra, R.B., J.K. Brimacombe, and I.V. Samarasekera, Mold Behavior and Its Influence on Quality in the Continuous-Casting of Steel Slabs .2. Mold Heat-Transfer, Mold Flux Behavior, Formation of Oscillation Marks, Longitudinal Off-Corner Depressions, and Subsurface Cracks. Metallurgical Transactions B-Process Metallurgy, 1991. 22(6): p. 875-888.
4. Billany, T.J.H., et al., Surface Cracking in Continuously Cast Products. Ironmaking & Steelmaking, 1991. 18(6): p. 403-410.
5. Hiraki, S., et al., Influence of Mold Heat Fluxes on Longitudinal Surface Cracks during High Speed Continuous Casting of Steel Slab. 77th Steelmaking Conference, 1994. 77: p. 397-403.
6. Tada, K., IMPROVEMENT IN SERVICE LIFE OF CONTINUOUS CASTING MOLD. Kawasaki Steel technical report, 1987. 17: p. 26-33.
7. Takeuchi, E. and J.K. Brimacombe, The Formation of Oscillation Marks in the Continuous-Casting of Steel Slabs. Metallurgical Transactions B-Process Metallurgy, 1984. 15(3): p. 493-509.
8. Xia, G., et al., Investigation of mould thermal behaviour by means of mould instrumentation. Ironmaking & Steelmaking, 2004. 31(5): p. 364-370.
9. Hecht, M., et al., Mould investigations on a thick slab caster. Stahl Und Eisen, 2005. 125(11): p. S107-+.
10. Shin, H.J., et al., Measurement and prediction of lubrication, powder consumption, and oscillation mark profiles in ultra-low carbon steel slabs. Isij International, 2006. 46(11): p. 1635-1644.

11. Lee, G.G., et al., Prediction and control of subsurface hooks in continuous cast ultra-low-carbon steel slabs. Ironmaking & Steelmaking, 2009. 36(1): p. 39-49.

12. Wolf, M., Product Quality Considerations in Continuous Slab Casting. Iron and Steel International, 1977. 50(1): p. 19-23.

13. Kumar, S., et al., Development of intelligent mould for online detection of defects in steel billets. Ironmaking & Steelmaking, 1999. 26(4): p. 269-284.

14. Meng, Y.A. and B.G. Thomas, Heat-transfer and solidification model of continuous slab casting: CON1D. Metallurgical and Materials Transactions B-Process Metallurgy and Materials Processing Science, 2003. 34(5): p. 685-705.

15. Peng, X., J. Zhou, and Y. Qin, Improvement of the temperature distribution in continuous casting moulds through the rearrangement of the cooling water slots. Journal of Materials Processing Technology, 2005. 167(2-3): p. 508-514.

16. Ozgu, M.R., M.B. Perrine, and G.P. Buckley, Caster productivity, quality and cost improvements through mold modifications at Burns Harbor. 79th Steelmaking Conference Proceedings, 1996. 79: p. 195-202.

17. Oconnor, T.G. and J.A. Dantzig, Modeling the Thin-Slab Continuous-Casting Mold. Metallurgical and Materials Transactions B-Process Metallurgy and Materials Processing Science, 1994. 25(3): p. 443-457.

18. Park, J.K., et al., Thermal and mechanical Behavior of copper molds during thin-slab casting (II): Mold crack formation. Metallurgical and Materials Transactions B-Process Metallurgy and Materials Processing Science, 2002. 33(3): p. 437-449.

19. Emling, W.H. and S. Dawson, Mold Instrumentation for Breakout Detection and Control. Mold Operation for Quality and Productivity, 1991: p. 161-181.

20. Mukai, T., The Mechanism of Break-out during Continuous-Casting Operation. Tetsu to Hagane-Journal of the Iron and Steel Institute of Japan, 1985. 71: p. 1025-1025.

21. Jin, Y., H. Ding, and Z.B. Tian, Development of Slab Caster Break-out Alarm ANN System. Advanced Materials, Pts 1-3, 2012. 415-417: p. 321-324.

22. Bellomo, P., et al., On Line Detection of Mold Thermal Transfer Characteristics. 77th Steelmaking Conference, 1994. 77: p. 319-327.

23. Cicutti, C., et al., Mould thermal evaluation in a slab continuous casting machine. 85th Steelmaking Conference Proceedings, 2002. 85: p. 97-107.

24. Thomas, B.G., D. Lui, and B. Ho, Effect of transverse depressions and oscillation marks on heat transfer in the continuous casting mold. Sensors and Modeling in Materials Processing: Techniques and Applications, 1997: p. 117-142.

25. Ho, B., Characterization of Interfacial Heat Transfer in the Continuous Slab Casting Process in Mechanical Engineering. 1992, University of Illinos at Urbana-Champaign.

26. Thomas B.G , M.Y., CON1D Users Manual. 2002.

27. Santillana, B., et al., Heat Transfer in Funnel-mould Casting: Effect of Plate Thickness. Isij International, 2008. 48(10): p. 1380-1388.

28. Lait, J.E., J.K. Brimacombe, and F. Weinberg, MATHEMATICAL MODELLING OF HEAT FLOW IN THE CONTINUOUS CASTING OF STEEL. Ironmaking and Steelmaking, 1974. 1(2): p. 90-97.

29. Samarasekera, I.V. and J.K. Brimacombe, The Thermal Field in Continuous-Casting Molds. Canadian Metallurgical Quarterly, 1979. 18(3): p. 251-266.

30. Grill, A., J.K. Brimacombe, and F. Weinberg, MATHEMATICAL ANALYSIS OF STRESSES IN CONTINUOUS CASTING OF STEEL. Ironmaking and Steelmaking, 1976. 3(1): p. 38-47.

31. Sorimachi, K. and J.K. Brimacombe, IMPROVEMENTS IN MATHEMATICAL MODELLING OF STRESSES IN CONTINUOUS CASTING OF STEEL. Ironmaking and Steelmaking, 1977. 4(4): p. 240-245.

32. Kapaj, N., M. Pavlicevic, and A. Poloni. Exceeding the casting speed of bloom CC machines by three times. in 84 th Steelmaking Conference. 2001.

33. Wolf, M., Mold length in slab casting: a review. Iron & steelmaker, 1996. 23(2): p. 47-51.

34. Park, J.K., et al. Analysis of thermal and mechanical behavior of copper mould during thin slab casting. in Steelmaking Conference Proceedings. 2000.

35. Brimacombe, J.K., DESIGN OF CONTINUOUS CASTING MACHINES BASED ON A HEAT-FLOW ANALYSIS: STATE-OF-THE-ART REVIEW. Canadian Metallurgical Quarterly, 1976. 15(2): p. 163-175.

36. Li, C. and B. Thomas. Analysis of the potential productivity of continuous cast molds. in The Brimacombe Memorial Symposium. 2000.

37. Lorento, D.P., Beam blank mold for continuous casting. 2003, Google Patents.

38. Yang, W., et al. Study of Heat Flux in CSP Continuous Casting Mold. in 4th International Symposium on High Temperature Metallurgical Processing. 2013. John Wiley & Sons.

39. Blazek, K.E., Calculation of the peritectic range for steel alloys. Iron & steel technology, 2008. 5(7): p. 80-85.

40. Nelder, J.A. and R. Mead, A Simplex-Method for Function Minimization. Computer Journal, 1965. 7(4): p. 308-313.

41. Morgan, J.A. and J.F. Tatar, Calculation of Residual Sum of Squares for All Possible Regressions. Technometrics, 1972. 14(2): p. 317-&.

42. Sakamoto, Y., M. Ishiguro, and G. Kitagawa, Akaike information criterion statistics. Dordrecht, The Netherlands: D. Reidel, 1986.

43. Sadat, M., A.H. Gheysari, and S. Sadat, The effects of casting speed on steel continuous casting process. Heat and Mass Transfer, 2011. 47(12): p. 1601-1609.

44. Meng, X.N. and M.Y. Zhu, Effect of Casting Speed on Temperature Difference between Copper Plate and Solidifying Shell in Meniscus of Slab Continuous Casting Mold. Epd Congress 2011, 2011: p. 755-762.

45. Li, B.W., et al., Influences of casting speed and sen depth on fluid flow in the funnel type mold of a thin slab caster. Acta Metallurgica Sinica, 2007. 20(1): p. 15-26.

46. Chow, C., et al., High speed continuous casting of steel billets - Part 2: Mould heat transfer and mould design. Ironmaking & Steelmaking, 2002. 29(1): p. 61-69.

47. Hecht, M., et al., Mould investigations on a thick slab caster. Revue De Metallurgie-Cahiers D Informations Techniques, 2005. 102(11): p. S107-+.

48. Meng, X.N. and M.Y. Zhu, Thermal Behavior of Hot Copper Plates for Slab Continuous Casting Mold with High Casting Speed. Isij International, 2009. 49(9): p. 1356-1361.

49. Singh, S.N. and K.E. Blazek, Heat-Transfer and Skin Formation in a Continuous-Casting Mold as a Function of Steel Carbon Content. Jom-Journal of Metals, 1974. 26(10): p. 17-&.

50. Wolf, M. and W. Kurz, The Effect of Carbon Content on Solidification of Steel in the Continuous-Casting Mold. Metallurgical Transactions B-Process Metallurgy, 1981. 12(1): p. 85-93.

51. Watanabe, K., et al., The effect of crystallization of mold powder on the heat transfer in continuous casting mold. Tetsu to Hagane-Journal of the Iron and Steel Institute of Japan, 1997. 83(2): p. 115-120.

52. Brimacombe, J.K., et al., Spray Cooling in Continuous Casting. Continuous Casting, 1984. 2: p. 105-123.

53. Nozaki, T., et al., Secondary Cooling Pattern for Preventing Surface Cracks of Continuous-Casting Slab. Transactions of the Iron and Steel Institute of Japan, 1978. 18(6): p. 330-338.

54. Petrus, B., et al., Real-time, model-based spray-cooling control system for steel continuous casting. Metallurgical and materials transactions B, 2011. 42(1): p. 87-103.

55. Thomas, B., J. Brimacombe, and I. Samarasekera, The Formation of Panel Cracks in Steel Ingots, A State of the Art Review, Part II--Mid-Face and Off-Corner Cracks. Transactions of the Iron and Steel Society, 1986. 7: p. 21-29.

56. Thomas, B., J. Brimacombe, and I. Samarasekera, The formation of panel cracks in steel ingots, A state of the art review, Part I: Hot ductility of steel. Transactions of the Iron and Steel Society, 1986. 7: p. 7-20.

57. Brimacombe, J.K. and K. Sorimachi, Crack Formation in Continuous-Casting of Steel. Metallurgical Transactions B-Process Metallurgy, 1977. 8(3): p. 489-505.

58. Sengupta, J., B.G. Thomas, and M.A. Wells, The use of water cooling during the continuous casting of steel and aluminum alloys. Metallurgical and Materials Transactions a-Physical Metallurgy and Materials Science, 2005. 36A(1): p. 187-204.

59. Yamasaki, N., et al., Particle-Based Numerical Analysis of Spray Water Flow in Secondary Cooling of Continuous Casting Machines. Tetsu to Hagane-Journal of the Iron and Steel Institute of Japan, 2013. 99(10): p. 1-8.

60. Stetina, J., et al., Operational Experiences with the Secondary Cooling Modification of Continuous Slab Casting. Metal 2013: 22nd International Conference on Metallurgy and Materials, 2013: p. 62-67.

61. Uehara, M., I.V. Samarasekera, and J.K. Brimacombe, Mathematical-Modeling of Unbending of Continuously Cast Steel Slabs. Ironmaking & Steelmaking, 1986. 13(3): p. 138-153.

62. Li, C.S. and B.G. Thomas, Thermomechanical finite-element model of shell behavior in continuous casting of steel\. Metallurgical and Materials Transactions B-Process Metallurgy and Materials Processing Science, 2004. 35(6): p. 1151-1172.

63. Li, H. and B.G. Thomas, Validation of CON1D Slab Surface Temperature Prediction Using Goodrich Pyrometer Measurements at Mittal Riverdale. Continuous Casting Consortium 2007, 2007.

64. Dantzig, J.A., C.L. Tucker, and Safari Books Online (Firm), Modeling in materials processing. 2001, Cambridge University Press,: Cambridge, U.K. ; New York. p. 1 online resource.

65. Thomas, B.G., CON1D Users Manual Version 10.10.01. 2010.

66. Won, Y.M. and B.G. Thomas, Simple model of microsegregation during solidification of steels. Metallurgical and Materials Transactions a-Physical Metallurgy and Materials Science, 2001. 32(7): p. 1755-1767.

67. Petrus, B., et al., Implementation of a Real-Time Model-Based Spray-Cooling Control System for Steel Continuous Casting. Sensors, Sampling, and Simulation for Process Control, 2011: p. 76-83.

APPENDIX A: MATLAB CODE FOR REGRESSION ANALYSIS

```
%***MATLAB CODE FOR PERFORMING NONLINEAR MULITIPLE REGRESSION ANALYSIS***
%***To determine correlations between heat flux and casting variables***
% Step 1: Validation - Test problem - Sanity Check
% Step 2: Initial plots-scatter,boxplot etc.,for determining filters (Input1)
% Step 3: Development of models and selection of best model
% Step 4: Testing the model
% Challenges:  Initial guess,..
clc;
clear all;
close all;

fs=16; Font size
fn='Times New Roman'; Font name

 % **********Step 1: Validation - Test problem - Sanity Check**********
 [Testset]=xlsread('Sanitycheck-Nucornorth');  Reading Data set from excel sheet
 n=length(Testset);
 G=Testset(:,2);
 dT=Testset(:,3);
 W=Testset(:,4);
 Z=Testset(:,5);
 ActQ=Testset(:,6);

 % Validating method of using fminsearch with known function
 Q = @(x,data)x(1)*(G.^x(2)).*(dT.^x(3)).*(W.^x(4)); Structure of the proposed equation
 reseqn = @(x) (Q(x)-ActQ)'*(Q(x)-ActQ);
 x0=[0.00005 0.9 0.9 -0.9];  % Initial guess
 options=optimset('TolFun',1e-10,'TolX',1e-10,'MaxFunEvals',40000,'MaxIter', 10000, 'Display',' off');
 [x,fval,exitflag]=fminsearch(reseqn,x0,options);  % Determining the coefficients using fminsearch function
```

```
PredQ=x(1)*G.^x(2).*dT.^x(3).*W.^x(4);

%  Calculating statistical estimates
TSS=0;
RSS=0;
p=length(x);
for i=1:n
   TSS=TSS+(ActQ(i)-mean(ActQ))^2;
   RSS=RSS+(PredQ(i)-ActQ(i))^2;
end

R2=1-(RSS/TSS)
aR2=1-(1-R2)*(n-1)/(n-p-1);
mle=-(n/2)*log(RSS/n);
AIC=-2*mle+2*p
BIC=-2*mle+p*log(n)

% Plot
figure(1)
Min=1.5; Max=3; xp=Min:0.1:Max; yp=xp; % defining limits of the graph
plot(ActQ,PredQ,'ko','markersize',8),xlim([Min Max]),ylim([Min Max]),xlabel('Actual heat flux (MW/m^2)','FontSize',fs,'FontName',fn),ylabel('Predicted heat flux (MW/m^2)','FontSize',fs,'FontName',fn);
hold all
plot(xp,yp,'r-');  plotting a diagonal line
set(gca,'TickLength',3*get(gca,'ticklength'));
set(gca,'XMinorTick','on','YMinorTick','on','FontSize',fs);
axis square;
lg=legend('1000 heats');
set(lg,'location','northwest');
legend('boxoff','FontSize',fs,'FontName',fn);

*******Step 2: Initial plots - scatter, boxplot etc.,**********
```

```
% Reading Data set from excel sheet - All data with primary filters - input for regression analysis
% Plot box plots and histograms - To determine secondary filters - to study individual variables
[dataset,txt]=xlsread('Tusc+Decatur_input');
len=length(dataset);  Total length
%  Reading variables in each column of the entire data set
vc=dataset(:,1);            % casting speed (m/min)
mu=dataset(:,2);            % viscosity (pa.s)
T=dataset(:,3);             % Break point temperature (°C)
s=dataset(:,4);             % Superheat (°C)
w=dataset(:,5);             % Width (mm)
t_f=dataset(:,6);           % Fixed plate thickness (mm)
l=dataset(:,7);             % Standard level deviation (mm)
c=dataset(:,8);             % Carbon (wt )
Heatflux_f=dataset(:,9);    % Heat flux fixed face(MW/m2)
ca=dataset(:,10);           % Ca from composition for determining peritectic range
cb=dataset(:,11);           % Cb from composition for determining peritectic range
b=dataset(:,12);            % Basicity
hm=dataset(:,13);           % Heats on mold
sl=dataset(:,14);           % Mold oscillation stroke Length (mm)
sf=dataset(:,15);           % Mold oscillation Frequency (cps)
t_l=dataset(:,16);          % Loose plate thickness (mm)
Heatflux_l=dataset(:,17);   % Heat flux loose face (MW/m2)
t_hf_f=dataset(:,18);       % Fixed plate hot face thickness(mm)
t_hf_l=dataset(:,19);       % Loose plate hot face thickness(mm) – some variables for future work

 % Scatter plot - Not enough resolution - difficult to read -so R can be used
figure(2)
plotmatrix(dataset(:,1:9))
% Histograms and Box plots
i=8 ;  Give a value to i
```

```
variables={'Casting speed (m/min)','Viscosity (Pa.s)','Break point temp. (^oC)','Super heat (^oC)','Mold width (mm)','Fixed plt. thk. (mm)', 'Mold lvl. st. dev. (mm)','Carbon ()','9','10','11','Basicity','13','Oscillation stroke length (mm)', 'Ocsillation frequency(cps)','Loose plt. thk. (mm)','17','Fixed plt. hot face thk.(mm)','Loose plt. hot face thk.(mm)','Fixed plt. hot face temp. (^oC)','Loose plt. hot face temp. (^oC)','water flowrate(^oC)'};

figure(3)
hist(dataset(:,i),50)
 % Select appropriate limits for corresponding plots
 xlim([0,2]);ylim([0,3000]); set(gca,'XTick',[0 0.5 1.0 1.5 2.0],'YTick',[0 500 1000 1500 2000 2500 3000])  Casting speed limits
 xlim([0,0.4]); ylim([0,3000]);set(gca,'XTick',[0 0.1 0.2 0.3 0.4],'YTick',[0 500 1000 1500 2000 2500 3000])  viscosity limits
 xlim([900,1200]); ylim([0,3000]);set(gca,'XTick',[900 1000 1100 1200],'YTick',[0 500 1000 1500 2000 2500 3000])  Break point temperature limits
 xlim([0,50]);ylim([0,1000]); set(gca,'XTick',[0 10 20 30 40 50],'YTick',[0 200 400 600 800 1000])  super heat limits
 xlim([1000,2600]); ylim([0,5000]);set(gca,'XTick',[1000 1400 1800 2200 2600],'YTick',[0 1000 2000 3000 4000 5000])  Mold width limits
 xlim([35,45]); ylim([0,2000]);set(gca,'XTick',[35 37 39 41 43 45],'YTick',[0 500 1000 1500 2000])  Fixed face plt thk. limits
 xlim([0,2]);ylim([0,1000]); set(gca,'XTick',[0 0.5 1 1.5 2],'YTick',[0 250 500 750 1000]) lvl deviation limits
xlim([0,0.5]);ylim([0,2000]); set(gca,'XTick',[0 0.1 0.2 0.3 0.4 0.5],'YTick',[0 500 1000 1500 2000])  carbon limits
 xlim([0.5,1.5]); ylim([0,8000]);set(gca,'XTick',[0.5 0.75 1 1.25 1.5],'YTick',[0 2000 4000 6000 8000])  basicity limits
 xlim([80,100]);ylim([0,5000]); set(gca,'XTick',[80 85 90 95 100],'YTick',[0 1000 2000 3000 4000 5000])  Mold oscillation stroke length limits
 xlim([0,25]);ylim([0,3000]); set(gca,'XTick',[0 5 10 15 20 25],'YTick',[0 1000 2000 3000]) Mold frequency limits
```

```
 xlim([30,38]);  ylim([0,2000]);set(gca,'XTick',[30 32 34 36 38],'YTick',[0 500 1000 1500 2000])  Loose face plt thk. limits
 xlim([15,22]); ylim([0,2000]);set(gca,'XTick',[15 17 19 21],'YTick',[0 500 1000 1500 2000]) Hot face thk. limits
 xlim([150,290]);  ylim([0,2000]);set(gca,'XTick',[150 170 190 210 230 250 270 290],'YTick',[0 500 1000 1500 2000])  Hot face temp. limits

h = findobj(gca,'Type','patch');
set(h,'FaceColor',[0.5 0.5 0.5],'EdgeColor','k')
set(gca,'XMinorTick','on','YMinorTick','on','FontSize',fs,'FontWeight','bold');
xlabel(variables(i),'FontSize',fs),ylabel('No.of heats','FontSize',fs,'FontWeight','bold')

figure(4)
bplot= boxplot(dataset(:,i),'orientation','horizontal','symbol','k+','outliersize',10);
 % Select appropriate limits for corresponding plots
 xlim([0,2]); set(gca,'XTick',[0 0.5 1.0 1.5 2.0])   Casting speed limits
 xlim([0,0.4]); set(gca,'XTick',[0 0.1 0.2 0.3 0.4])  viscosity limits
 xlim([900,1200]); set(gca,'XTick',[900 1000 1100 1200])  Break point temperature limits
 xlim([0,50]); set(gca,'XTick',[0 10 20 30 40 50])  super heat limits
 xlim([1000,2600]); set(gca,'XTick',[1000 1400 1800 2200 2600])  Mold width limits
 xlim([35,45]); set(gca,'XTick',[35 37 39 41 43 45])   Plate thickness limits
 xlim([0,2]); set(gca,'XTick',[0 0.5 1 1.5 2]) lvl deviation limits
xlim([0,0.5]); set(gca,'XTick',[0 0.1 0.2 0.3 0.4 0.5])  carbon limits
 xlim([0.5,1.5]); set(gca,'XTick',[0.5 0.75 1 1.25 1.5])  basicity limits
 xlim([80,100]); set(gca,'XTick',[80 85 90 95 100])  Mold stroke length limits
 xlim([0,25]); set(gca,'XTick',[0 5 10 15 20 25])  Mold frequency limits
 xlim([15,21]); set(gca,'XTick',[15 17 19 21])   Hot face thickness limits
 xlim([150,290]); set(gca,'XTick',[150 170 190 210 230 250 270 290])  Hot face temperature limits

set(gca,'XMinorTick','on','YMinorTick','on','FontSize',fs,'FontWeight','bold');
ylabel(variables(i),'FontSize',fs,'FontWeight','bold')
axis square
```

```
% To get the range of variables in data from whisker values of box plots
h = findobj(gcf,'tag','Lower Whisker');
Lower_whis = get(h,'XData')
g = findobj(gcf,'tag','Upper Whisker');
Upper_whis = get(g,'XData')
m = findobj(gcf,'tag','Median');
median = get(m,'XData')
quantile(dataset(:,i),[.25 .5 .75])
range=[min(dataset(:,i)) max(dataset(:,i))]
% Extra statiscal data visualization and data analysis techniques
%     boxplot(zscore(dataset(:,1:8)),'orientation','horizontal','symbol','ko','outliersize',4,'labels',
variables1(1:8));
% Pearson Correlation coefficient Matrix - Same for data & normalized data
[corr_mat,Pvalues]=corr(zscore(dataset))
% PCA - followed by Backward selection for significant variables
 % [coeff,score, latent, tsquare]=princomp(zscore(dataset));
% Manual selection of variables after discarding variables
********** Step 3: Development of models and selection of best model******
 for k=1
      for j=1:100  To make sure global minima from different initial guesses
            guess_range = 100;
           Initial guesses from previous work knowledge
            x0i(j) = randsample(linspace(0.9,1.5,guess_range),1);  intercept - greatly varies with
only vc term and all terms
            x0i2(j) = randsample(linspace(100000,700000,guess_range),1);  intercept - more
than vc term
            x0v(j) = randsample(linspace(0.45,0.9,guess_range),1);  casting speed
            x0c(j) = randsample(linspace(0.1,0.4,guess_range),1);  coefficient in exponent of
carbon term
            x0mt(j) = randsample(linspace(-2.0,-1.0,guess_range),1);  break point Temperature
            x0mu(j) = randsample(linspace(-0.055,0.055,guess_range),1);  viscosity
            x0w(j) = randsample(linspace(0.001,0.2,guess_range),1);  width
            x0s(j) = randsample(linspace(0.001,0.04,guess_range),1);  superheat
```

```
x0t(j) = randsample(linspace(-0.01,0.01,guess_range),1);  thickness of mold plate
x0ld(j) = randsample(linspace(0.001,0.02,guess_range),1);  sd of mold level fluctuations
x0b(j) = randsample(linspace(-0.15,0.15,guess_range),1);  basicity

options=optimset('TolFun',1e-10,'TolX',1e-10,'MaxFunEvals',40000,'MaxIter', 10000, 'Display','off');
 case 1 - Vc
Q = @(x) (x(1).*(vc.^x(2)));
x0=[x0i(j) x0v(j)];
% case 2 - Vc,c
 % Though effect of carbon is little due to insufficient data of peritectics, for general application of model, c term is included in all the following models (can do with out c in the eqns also)
Q = @(x,trainingset) (x(1).*(vc.^x(2))).*(1-0.152.*exp(-(x(3).*((((ca+cb)/2)-c)./(cb-ca))).^2));
x0=[x0i(j) x0v(j) x0c(j)];
% case 3 - Vc,c,T
Q = @(x,trainingset) (x(1).*(vc.^x(2))).*(1-0.152.*exp(-(x(3).*((((ca+cb)/2)-c)./(cb-ca))).^2)).*(T.^x(4));
x0=[x0i2(j) x0v(j) x0c(j) x0mt(j)];
 %  case 4 - Vc,c,T,mu
Q = @(x,trainingset)(x(1).*(vc.^x(2))).*(1-0.152.*exp(-(x(3).*((((ca+cb)/2)-c)./(cb-ca))).^2)).*(T.^x(4)).*(mu.^x(5));
x0=[x0i2(j) x0v(j) x0c(j) x0mt(j) x0mu(j)];
 % The process can be repeated for any combination as given in other code .Due to repetition & length of the code - only models of interest are dealt in this code.
 % case 5 - Vc,c,T,mu,w
Q = @(x,trainingset) (x(1).*(vc.^x(2))).*(1-0.152.*exp(-(x(3).*((((ca+cb)/2)-c)./(cb-ca))).^2)).*(T.^x(4)).*(mu.^x(5)).*(w.^x(6));
x0=[x0i2(j) x0v(j) x0c(j) x0mt(j) x0mu(j) x0w(j)];
 % case 6 - Vc,c,T,mu,w,l
```

```
Q = @(x,trainingset) (x(1).*(vc.^x(2))).*(1-0.152.*exp(-(x(3).*((((ca+cb)/2)-c)./(cb-
ca))).^2)).*(T.^x(4)).*(mu.^x(5)).*(w.^x(6)).*(l.^x(7));
x0=[x0i2(j) x0v(j) x0c(j) x0mt(j) x0mu(j) x0w(j) x0ld(j)];
  % case 7 - Vc,c,T,mu,w,l,t
Q = @(x,trainingset) (x(1).*(vc.^x(2))).*(1-0.152.*exp(-(x(3).*((((ca+cb)/2)-c)./(cb-
ca))).^2)).*(T.^x(4)).*(mu.^x(5)).*(w.^x(6)).*(l.^x(7)).*(t_f.^x(8));
x0=[x0i2(j) x0v(j) x0c(j) x0mt(j) x0mu(j) x0w(j) x0ld(j) x0t(j)];
  % case 8 - Vc,c,T,mu,w,l,t,s
Q = @(x,trainingset) (x(1).*(vc.^x(2))).*(1-0.152.*exp(-(x(3).*((((ca+cb)/2)-
c)./(cb-ca))).^2)).*(T.^x(4)).*(mu.^x(5)).*(w.^x(6)).*(l.^x(7)).*(t_f.^x(8)).*(s.^x(9));
x0=[x0i2(j) x0v(j) x0c(j) x0mt(j) x0mu(j) x0w(j) x0ld(j) x0t(j) x0s(j)];
  reseqn = @(x) (Q(x)-Heatflux_f)'*(Q(x)-Heatflux_f);
[x,fval,exitflag]=fminsearch(reseqn,x0,options);

case 1 - Vc
PredQ = (x(1).*(vc.^x(2)));

%  case 2 - Vc,c
PredQ = (x(1).*(vc.^x(2))).*(1-0.152.*exp(-(x(3).*((((ca+cb)/2)-c)./(cb-ca))).^2));
%  case 3 - Vc,c,T
PredQ = (x(1).*(vc.^x(2))).*(1-0.152.*exp(-(x(3).*((((ca+cb)/2)-c)./(cb-
ca))).^2)).*(T.^x(4));
% case 4 - Vc,c,T,mu
 PredQ = (x(1).*(vc.^x(2))).*(1-0.152.*exp(-(x(3).*((((ca+cb)/2)-c)./(cb-
ca))).^2)).*(T.^x(4)).*(mu.^x(5));
% case 5 - Vc,c,mu,T,w
PredQ = (x(1).*(vc.^x(2))).*(1-0.152.*exp(-(x(3).*((((ca+cb)/2)-c)./(cb-
ca))).^2)).*(T.^x(4)).*(mu.^x(5)).*(w.^x(6));
%  case 6 - Vc,c,T,mu,w,l
PredQ = (x(1).*(vc.^x(2))).*(1-0.152.*exp(-(x(3).*((((ca+cb)/2)-c)./(cb-
ca))).^2)).*(T.^x(4)).*(mu.^x(5)).*(w.^x(6)).*(l.^x(7));
%  case 7 - Vc,c,T,mu,w,l,t
```

```
            PredQ          =          (x(1).*(vc.^x(2))).*(1-0.152.*exp(-(x(3).*((((ca+cb)/2)-c)./(cb-
ca))).^2)).*(T.^x(4)).*(mu.^x(5)).*(w.^x(6)).*(l.^x(7)).*(t_f.^x(8));
          % case 8 - Vc,c,T,mu,w,l,t,s
            PredQ          =          (x(1).*(vc.^x(2))).*(1-0.152.*exp(-(x(3).*((((ca+cb)/2)-c)./(cb-
ca))).^2)).*(T.^x(4)).*(mu.^x(5)).*(w.^x(6)).*(l.^x(7)).*(t_f.^x(8)).*(s.^x(9));
                RSS=0;
                   for i=1:len
                      RSS=RSS+(PredQ(i)-Heatflux_f(i))^2;
                   end

                   RSS_k(j,:)=[RSS x];
                j
       end
   [leastRSS,idx]= min(RSS_k(:,1));  global minima RSS is selected
   RSS_x_opt(k,:) = RSS_k(idx,:)
   MLE_opt(k)=-(len/2)*(log(leastRSS/len));  Maximum likelihood
   AIC_opt(k)=-2*MLE_opt(k)+2*length(x);  Akaike Information criterion
   BIC_opt(k)=-2*MLE_opt(k)+length(x)*log(len);  Bayesian Informaiton criterion
  end
 final_ans = [RSS_x_opt AIC_opt(k) BIC_opt(k)]

   *******Step 4: Testing the model ********
    Testing best model and Cicuitti equation for same caster and a different caster

   % Second data set - Other caster
   [dataset,txt]=xlsread('Nucorsouth_fnldata','inputdata');
   len=length(dataset);  Total length
    % Reading variables in each column of the entire data set
  vc=dataset(:,1);            % casting speed ( m/min)
  mu=dataset(:,2);             % viscosity ( pa.s)
  T=dataset(:,3);             % Break point temperature (°C)
  s=dataset(:,4);             % Superheat (°C)
  w=dataset(:,5);             % Width (mm)
```

```
t_f=dataset(:,6);          % Fixed plate thickness (mm)
l=dataset(:,7);            % Standard level deviation (mm)
c=dataset(:,8);            % Carbon (wt )
Heatflux_f=dataset(:,9);   %  Heat flux fixed face(MW/m2)
ca=dataset(:,10);          % Ca from composition for determining peritectic range
cb=dataset(:,11);          % Cb from composition for determining peritectic range
b=dataset(:,12);           % Basicity
hm=dataset(:,13);          % Heats on mold
sl=dataset(:,14);          % Mold Stroke Length (mm)
sf=dataset(:,15);          % Mold Stroke Frequency (cps)
t_l=dataset(:,16);         % Loose plate thickness (mm)
Heatflux_l=dataset(:,17);  % Heat flux loose face (MW/m2)
t_hf_f=dataset(:,18);      % Fixed plate hot face thickness(mm)
t_hf_l=dataset(:,19);      %  Loose plate hot face thickness(mm)
T_hf_f=dataset(:,20);      % Fixed plate hot face temperature (°C)
T_hf_l=dataset(:,21);      % Loose plate hot face temperature (°C)
v_water=dataset(:,22);     % Water flowrate (lpm)

% Select an optimum case from step 3 - with corresponding x and predQ
   **********New equation - Nucor Equation**********
  x=[312778.80367524300000.61957031366670.0205067304677-
1.84458279408530.0720252053257-0.0167107940032];
  PredQ          =          (x(1).*(vc.^x(2))).*(1-0.152.*exp(-(x(3).*((((ca+cb)/2)-c)./(cb-
ca))).^2)).*(T.^x(4)).*(w.^x(5)).*(mu.^x(6));
v_RSS =0;
v_TSS=0;
for i=1:len
    v_RSS=v_RSS+(PredQ(i)-Heatflux_f(i))^2;
end
v_R2=1-(double(v_RSS)/double(v_TSS)); R2
v_MLE=-(len/2)*(log(v_RSS/len));  Maximum likelihood
v_AIC=-2*v_MLE+2*(length(x)-1);  Akaike Information criterion
v_BIC=-2*v_MLE+(length(x)-1)*log(len);  Bayesian Informaiton criterion
```

```
fnl_tusc =[v_RSS v_AIC v_BIC]

  ******************Cicutti equation**************
v_PredQc=   4.63*(10)^3.*(vc.^0.47).*(mu.^(-0.09)).*(T.^(-1.19)).*(1-0.152.*exp(-(((0.107-
c)./0.027).^2)));
 v_RSSc =0;
for i=1:len
    v_RSSc=v_RSSc+(v_PredQc(i)-Heatflux_f(i))^2;
end
v_MLEc=-(len/2)*(log(v_RSSc/len));
v_AICc=-2*v_MLEc+2*4;
v_BICc=-2*v_MLEc+4*log(len);
fnl_cic =[v_RSSc v_AICc]


  ****************** Decatur equation***********
x_o=[312778.80367524300000.61957031366670.0205067304677-
1.84458279408530.0720252053257-0.0167107940032];
v_PredQo        =        (x_o(1).*(vc.^x_o(2))).*(1-0.152.*exp(-(x_o(3).*((((ca+cb)/2)-c)./(cb-
ca))).^2)).*(T.^x_o(4)).*(w.^x_o(5)).*(mu.^x_o(6));

v_RSSo =0;
for i=1:len
    v_RSSo=v_RSSo+(v_PredQo(i)-Heatflux_f(i))^2;
end
v_MLEo=-(len/2)*(log(v_RSSo/len));
v_AICo=-2*v_MLEo+2*(length(x_o)-1);
v_BICo=-2*v_MLEo+(length(x_o)-1)*log(len);
fnl_dec =[v_RSSo v_AICo]
%  Plotting results
Min=1.5; Max=3; Decatur
Min=0.5; Max=2; Tuscaloosa
xp=Min:0.1:Max; yp=xp;  defining limits of the graph
```

```
figure(12)
plot(Heatflux_f,PredQ,'ko','linewidth',1.2,'MarkerSize',6),xlabel('Measured heatflux
(MW/m^2)','FontSize', fs,'FontName',fn),ylabel('Predicted heatflux
(MW/m^2)','FontSize',fs,'FontName',fn)
hold on
plot(xp,yp,'r-','linewidth',1.5)
set(gca,'TickLength',3*get(gca,'ticklength'));
set(gca,'XMinorTick','on','YMinorTick','on','FontSize',fs);
axis square;
xlim([Min Max]);ylim([Min Max])
lg1=legend('Tuscaloosa equation');
set(lg1,'location','southeast')
legend('boxoff','FontSize',16,'FontName','Times New Roman')

figure(13)  Cicuitti equation
plot(Heatflux_f,v_PredQc,'bo','linewidth',1.2,'MarkerSize',6),xlabel('Actual heatflux
(MW/m^2)','FontSize', fs,'FontName',fn)
hold on
plot(xp,yp,'r-','linewidth',1.5)
set(gca,'TickLength',3*get(gca,'ticklength'));
set(gca,'XMinorTick','on','YMinorTick','on','FontSize',fs);
axis square;
xlim([Min Max]);ylim([Min Max])
 lg2=legend('Cicutti equation');
set(lg2,'location','southeast')
legend('boxoff','FontSize',16,'FontName','Times New Roman')
```

APPENDIX B: SIGNIFICANT DIGITS OF THE FITTING PARAMETERS FROM REGRESSION ANALYSIS

The fitting values with significant digits for all the equations developed in this work determined through non-linear regression analysis are as follows,

Model No.	Constant	Casting speed	Carbon (Grade)	Tbreak	Width	Viscosity	Thickness	Mold. Level. Standard dev.	Superheat
Nucor 1	1.058820456	0.645665241							
Nucor 2	1.247095678	0.645286677	0.114646757						
Nucor 3	28271.59873	0.569733635	8.19E-09	-1.414093623					
Nucor 4	15285.15114	0.608767337	1.68E-08	-1.402814062	0.067862296				
Nucor 5	37593.54575	0.589913261	-1.77E-08	-1.529444004	0.065739358	-0.010156027			
Nucor 6	39263.8762	0.588225389	-1.85E-08	-1.529395855	0.065283208	-0.010045335	-0.010846556		
Nucor 7	35261.82857	0.585987110	0.000432999	-1.497520491	0.061219739	-0.007985337	-0.031728776	0.011645537	
Nucor 8	30070.38712	0.590766525	0.061428674	-1.491618666	0.062490253	-0.008123694	-0.002721266	0.012483084	8.21E-05
Decatur	312778.80367	0.619570314	0.020506730	-1.844582794	0.072025205	-0.016710794			
Tuscaloosa	3645.028739	0.727729679	-1.58E-08	-1.240751567	0.085171926	-0.005990985			

APPENDIX C: ANALYTICAL SOLUTION OF THE CON1D GOVERNING EQUATION

(J. Dantzig and C. Tucker, Modeling in Materials Processing, Chapter. 4.3)

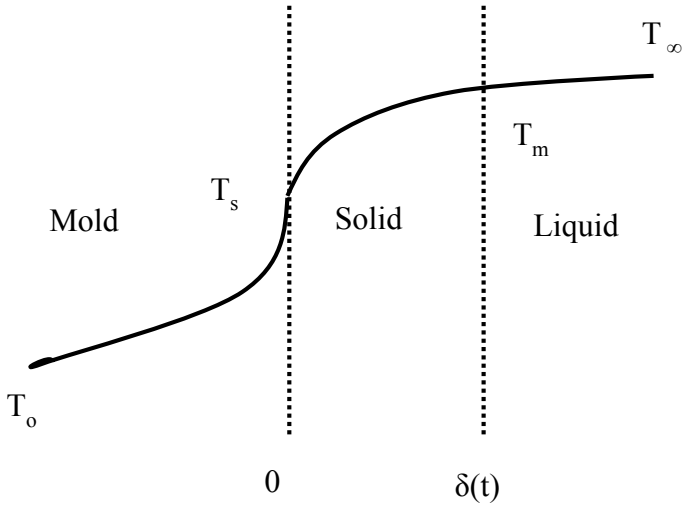

Figure A. Schematic drawing of one-dimensional solidification of a pure substance in a thick mold, with no interfacial resistance to heat flow

The heat transfer across the solidifying steel involves phase change and this is accounted in the form of Latent heat of fusion, L_f (J/kg), the heat that must be removed during the transformation of the liquid into solid steel at melting temperature.

Following assumptions are made in developing the solution:

1. Pure substance which solidifies at a single temperature
2. One dimensional model
3. No heat sources
4. Material properties are constant in each phase (Mold, Liquid and Solid)
5. Mold-solid interface has negligible thermal resistance
6. Stefan Condition: The position of the boundary at the liquid-solid interface is a part of the solution becoming a moving boundary problem. So, the temperature at the each point on the boundary at this interface is assumed as melting temperature. To consider this boundary condition, Stefan condition states that the heat conducted from the liquid across the interface must conduct through solid also and is accounted in the form of heat of fusion applying energy balance for the control volume at the interface as follows.

$$k_s \left.\frac{\partial T}{\partial x}\right|_s - k_l \left.\frac{\partial T}{\partial x}\right|_l = \rho_s L_f \frac{d\delta}{dt}$$

The conduction equation in each phase is solved and the unknown constant in the solution is determined by matching the boundary conditions between the two solutions.

- In the mold, the energy equation and the boundary conditions are as follows:

$$\frac{\partial T}{\partial t} = \alpha_m \frac{\partial^2 T}{\partial x^2}, -\infty < x \leq 0,\ T = T_o, x \to -\infty, T = T_s, x = 0$$

Though the surface temperature T_s is not known, it is assumed as a constant for ease in simplification of equations. The solution to the above equations is given by

$$T = T_s + (T_o - T_s)\mathbf{erf}\left(\frac{-x}{2\sqrt{\alpha_m t}}\right), -\infty < x \leq 0$$

Heat flux at the surface of the mold is,

$$k_m \left.\frac{\partial T}{\partial x}\right|_{x=0} = \frac{(T_s - T_o)\sqrt{k_m \rho_m c_{p_m}}}{\sqrt{\pi t}}$$

- The differential equations and boundary conditions for the solid which lies between $x = 0$ and $x = \delta(t)$ are as follows:

$$\frac{\partial T}{\partial t} = \alpha_s \frac{\partial^2 T}{\partial x^2}, 0 \leq x \leq \delta(t), T = T_s, x = 0, T = T_m, x = \delta(t)$$

Assuming the temperature follows an error function solution in the solid,

$$T = c_1 + c_2\, erf\left(\frac{x}{2\sqrt{\alpha_s t}}\right)$$

The boundary condition at $x = 0$ gives $c_1 = T_s$. Substituting the boundary condition at $= \delta(t)$,

$$T_m = T_s + c_2\, erf\left(\frac{\delta(t)}{2\sqrt{\alpha_s t}}\right)$$

As the left hand side of the above equation is a constant, as is T_s , so either $\delta(t)$ is proportional to $\sqrt{t}$, or there is no solution. Accordingly, we choose, $\delta(t) = 2\emptyset\sqrt{\alpha_s t}$

Where $\emptyset$ is a constant to be determined in the analysis. Then the corresponding interface velocity is then

$$\frac{d\delta}{dt} = \frac{\emptyset\sqrt{\alpha_s}}{\sqrt{t}} = \frac{2\emptyset^2 \alpha_s}{\delta}$$

And solving for c_2 from $T_m = T_s + c_2\, erf(\emptyset)$,

The temperature in the solid is then

$$\boldsymbol{T = T_s + \frac{T_m - T_s}{\mathrm{erf}(\emptyset)}\, erf\left(\frac{x}{2\sqrt{\alpha_s t}}\right), 0 \le x \le \delta(t)}$$

Heat fluxes at both solid interfaces,

$$\boldsymbol{k_s \frac{\partial T}{\partial x}\Big|_{x=0} = \frac{(T_m - T_s)\sqrt{k_s \rho_s c_{p_s}}}{\mathrm{erf}(\emptyset)\sqrt{\pi t}}}$$

$$\boldsymbol{k_s \frac{\partial T}{\partial x}\Big|_{x=\delta} = \frac{(T_m - T_s)\sqrt{k_s \rho_s c_{p_s}}}{\mathrm{erf}(\emptyset)\sqrt{\pi t}} \exp(-\emptyset^2)}$$

- The temperature in the liquid, must satisfy the following equations:

$$\boldsymbol{\frac{\partial T}{\partial t} = \alpha_l \frac{\partial^2 T}{\partial x^2}, \delta(t) \le x < \infty, T = T_m, x = \delta(t), T = T_\infty, x \to \infty}$$

This set of equations also has an error-function-type solution for $\boldsymbol{\delta(t) \le x < \infty}$, given by

$$\boldsymbol{T - T_m = \frac{1}{erf\left(\emptyset\sqrt{\frac{\alpha_s}{\alpha_l}}\right) - 1}\left[T_\infty erf\left(\emptyset\sqrt{\frac{\alpha_s}{\alpha_l}}\right) - T_m + (T_m - T_\infty)\mathrm{erf}\left(\frac{x}{2\sqrt{\alpha_l t}}\right)\right]}$$

The heat flux at the liquid-solid interface, is given by

$$\boldsymbol{k_l \frac{\partial T}{\partial x}\Big|_{x=\delta} = \frac{(T_\infty - T_m)\sqrt{k_l \rho_l c_{p_l}}}{\left[erf\left(\emptyset\sqrt{\frac{\alpha_s}{\alpha_l}}\right) - 1\right]\sqrt{\pi t}} \exp\left(-\emptyset^2 \frac{\alpha_s}{\alpha_l}\right)}$$

Now the constants $\emptyset$ and $\boldsymbol{T_s}$ are determined by matching the heat fluxes in the mold and solid at $\boldsymbol{x = 0}$ and by enforcing the Stefan condition at $\boldsymbol{x = \delta(t)}$. At the mold-solid interface, equating the heat flux results,

$$\boldsymbol{\frac{(T_o - T_s)\sqrt{k_m \rho_m c_{p_m}}}{\sqrt{\pi t}} = \frac{(T_m - T_s)\sqrt{k_s \rho_s c_{p_s}}}{\mathrm{erf}(\emptyset)\sqrt{\pi t}}}$$

The time dependence of $\frac{1}{\sqrt{t}}$ on both sides can be cancelled and tells us the assumption of a constant interface temperature is correct. The interface temperature is

$$\boldsymbol{T_s = \frac{T_o\sqrt{k_m \rho_m c_{p_m}}\,\mathrm{erf}(\emptyset) + T_m\sqrt{k_s \rho_s c_{p_s}}}{\sqrt{k_m \rho_m c_{p_m}}\,\mathrm{erf}(\emptyset) + \sqrt{k_s \rho_s c_{p_s}}}}$$

Finally equating the fluxes at the liquid-solid interface in the Stefan condition, we obtain,

$$\frac{(\boldsymbol{T_m - T_s})\sqrt{\boldsymbol{k_s\rho_s c_{p_s}}}}{\mathbf{erf}(\emptyset)\sqrt{\boldsymbol{\pi t}}}\mathbf{exp}(-\emptyset^2) - \frac{(\boldsymbol{T_m - T_\infty})\sqrt{\boldsymbol{k_l\rho_l c_{p_l}}}}{\left[\boldsymbol{erf}\left(\emptyset\sqrt{\frac{\boldsymbol{\alpha_s}}{\boldsymbol{\alpha_l}}}\right)-\mathbf{1}\right]\sqrt{\boldsymbol{\pi t}}}\mathbf{exp}\left(-\emptyset^2\frac{\boldsymbol{\alpha_s}}{\boldsymbol{\alpha_l}}\right)$$

$$= \boldsymbol{\rho_s L_f \emptyset}\sqrt{\frac{\boldsymbol{\alpha_s}}{\boldsymbol{t}}}$$

Now substituting T_s results in a transcendental equation for $\emptyset$:

$$\left(\emptyset\exp(\emptyset^2) + \frac{c_{p_s}(T_m - T_\infty)}{L_f\sqrt{\pi}}\frac{exp\left[\left(1-\frac{\alpha_s}{\alpha_l}\right)\emptyset^2\right]}{\left[erfc\left(\emptyset\sqrt{\frac{\alpha_s}{\alpha_l}}-1\right)\right]}\sqrt{\frac{k_l\rho_l c_{p_l}}{k_s\rho_s c_{p_s}}}\right)$$

$$\cdot\left(\text{erf}(\emptyset) + \sqrt{\frac{k_s\rho_s c_{p_s}}{k_m\rho_m c_{p_m}}}\right) = \frac{c_{p_s}(T_m - T_o)}{L_f\sqrt{\pi}}$$

The above equation is the general solution. Now a special case of casting with no superheat $T_\infty = T_m$, the equation reduces to

$$\emptyset\exp(\emptyset^2)\left(\text{erf}(\emptyset) + \sqrt{\frac{k_s\rho_s c_{p_s}}{k_m\rho_m c_{p_m}}}\right) = \frac{c_{p_s}(T_m - T_o)}{L_f\sqrt{\pi}}$$

The above equation is especially important because it can be used to estimate the solidification time of a section with finite thickness. If there is no superheat, then the solution for the temperature in the liquid is a constant temperature at the melting point. There is no heat flux into the liquid and the solidification time for a slab of total thickness 2H can be found from the expression for the interface position.

$$t_f = \frac{H^2}{4\,\emptyset^2\alpha_s}$$

It is important to note that the solution with superheat cannot be used to find the solidification time of a finite-thickness section. The temperature solution underlying this equation extends into the liquid and involves a temperature reduction from $T_\infty\ to\ T_m$over a distance of the order of $\sqrt{\alpha_l t}$ ahead of the solid-liquid interface. For a finite thickness slab the temperature solutions growing from the two sides collide in the center will before the center of the slab is solid, and the solutions are not valid from that point onward.

With superheat, the solidification time for a finite thickness slab can be found with enhanced latent heat of fusion given by

$$L_f{}' = L_f + c_{p_l}(T_\infty - T_m)$$

Thus the extra sensible heat associated with the superheat has been added to the latent heat.